Chapter 5

RESEARCH ACTIVITIES

5.1 Nuclear physics

R. P. Singh, A. Jhingan and S. Nath

Nuclear structure as well as heavy ion reaction dynamics were investigated using the Indian National Gamma detector Array (INGA) by various groups. In nuclear structure studies, the focus was on transitional nuclei and evolution of their shapes as a function of excitation energy and angular momentum. Ancillary devices like light charge particle detector array (CPDA(CsI)), LaBr detectors and plunger device were also used for many of these studies. Several nuclei were found to exhibit wobbling (transverse as well as longitudinal) bands. This points to their shapes becoming triaxially-deformed even at low to moderate spins. Some of these nuclei also showed signatures of strong octupole correlations almost simultaneously with enhanced electric dipole transitions between opposite parity bands.

Nuclei with nucleon numbers close to the magic numbers were another important area of study with the possibility of testing spherical shell model with different residual interactions using large basis calculations. This was possible with the advent of the high performance computing facilities available now.

Detectors of the INGA array were also used for studies of nuclear reaction mechanisms with heavy ions. Incomplete fusion (ICF) reactions formed a large part of such studies. Many systematic studies investigated the effect of projectile-target structure, target-projectile mass-asymmetry and α-cluster structure of projectile on ICF reactions. ICF reaction was also used to study the production of some medically relevant isotopes and the INGA detectors were also used to characterize some of the medical isotopes produced at the Institute of Nuclear Medicine and Allied Sciences (INMAS). More than 15 research papers were published in leading scientific journals by various groups using the INGA setup in the last academic year. More than 50 contributions were presented in various national and international conferences.

Five experiments were carried out using the GPSC and the NAND facilities using the Pelletron beam in the last year. The physics problems addressed could be classified into two broad categories. The first one was fission studies, wherein the effects of entrance channel properties in fusion-fission reactions were studied by measuring the fission fragment mass distribution. The study carried out in mass ~ 200 nuclei is important for the recently observed phenomenon of asymmetric fission in neutron-deficient nuclei in the mercury-lead region. The second type of studies were on direct reactions. The angular distributions of elastic, inelastic and transfer products were measured to understand the underlying reaction mechanism. In addition, the quasielastic measurements were also measured to get the fusion barrier distribution, an important parameter to understand heavy ion-induced nuclear reaction dynamics.

Results from some of the previous studies were published recently, emphasizing the importance of fission studies in the mass ~ 200 region. The studies on the fission of ^{186}Pt showed the presence of asymmetric fission from the fragment mass distribution measurements. It was conjectured that the quadrupole deformed shell gaps played a crucial role in deciding the fate of the disintegration of the compound nucleus. Nevertheless, the presence of slow quasifission in the fission could not be ruled out in this mass region, as indicated by the mass-angle and the mass-total kinetic energy distribution studies of the Pt compound nucleus. The studies carried out in the actinide region, in ^{249}Bk and ^{257}Md nuclei, recommended the consideration of the interplay

between K-relaxation time, dynamic dissipation and their influence on shell correction to understand the fusion-fission dynamics.

The group was also involved in the development of the facility for low-energy nuclear reactions relevant to nuclear astrophysics research. This facility consists of a cylindrical scattering chamber, made of stainless steel (60 cm diameter and 45 cm height). It has provisions to carry out angular distribution studies using charged particle detectors. The re-entrant cup provided to keep a Clover HPGe detector close to the target position will enable the particle-γ coincidence measurements, to suppress the background in the studies of rare events. The production cross section of some of the nuclei of importance in nucleosynthesis can be carried out using activation techniques. An in-vacuum target transfer facility is incorporated for such measurements.

In addition to performing user experiments, the NAND group is also involved in the development of customized detectors. Keeping in view the availability of high beam current from the HCI facility in the near future, a new hybrid telescope has been fabricated and tested with gas (ΔE) and CsI-photodiode (E) configurations. In the existing telescopes, we were using a 300 μm-thick silicon detector as the E detector, which was prone to radiation damage. In the future, an array of these new telescopes will be made for angular distribution studies in nuclear astrophysics experiments with low-energy, high-intensity beams from the HCI facility.

The radioactive beam production facility, using the HIRA, was revived after a long gap. All the hardware add-ons were refurbished and tested offline. A new stepper motor controller was used for the rotary / linear motion device used for holding the target (polypropylene foil). This facility was made ready for a beam test to be scheduled in the beginning of the next academic year.

Several user experiments were carried out in the HIRA beam line. The focus was to study channel-coupling effects, particularly the role of positive Q-value neutron transfer channels, in near barrier fusion dynamics. A newly-installed deep ionization chamber at the focal plane on the HIRA significantly enhanced the detection system. Multi-nucleon transfer channels (neutron pick up and proton stripping) could be unambiguously identified at the focal plane for the system ^{28}Si+^{62}Ni. This decetctor was also helpful in extending fusion measurements deeper below the barrier for ^{28}Si+^{58,62}Ni reactions to look for fusion hindrance.

The first stage of the HYRA, used in gas-filled mode, has been in operation since 2010. The complete layout, to be used in vacuum mode, will open up new possibilities for the user community. Two large-bore quadrupole magnets, along with matching high-current power supplies, are required in the second stage of the HYRA. A Technical Committee was constituted to look into the options for fabrication / procurement of these components. Further developments is expected in this project next year.

A five-day school on detectors and Geant4 simulations were conducted by the NAND group to enable young researchers to carry out Monte Carlo simulations of the detector systems independently. A three-day international workshop on physics studies with recoil separators and large neutron arrays was jointly organized by the HIRA-HYRA and the NAND groups. This meeting provided a platform for the users to present their recent results in nuclear reaction studies using IUAC facilities and discuss further research possibilities.

5.1.1 Measurements of mass-angle and mass-TKE distributions for ^{28}Si+^{160}Gd and ^{12}C+^{178}Hf reaction systems

Vikas[1], Kavita[1], K. S. Golda[2], A. Jhingan[2], P. Sugathan[2], A. Chatterjee[2], N. Saneesh[2], Mohit[2], Abhishek Yadav[2], C. Yadav[2], B. R. Behera[3], Ashok Kumar[3], A. Banerjee[3], S. K. Duggi[4], Rakesh Kumar[1], Kajal[1], Rakesh Dubey[5], Neeraj Kumar[6], Anjali[6], Kavita Rani[3], Shoaib Noor[7], Jaimin Acharya[8] and Hardev Singh[1]

[1] *Department of Physics, Kurukshetra University, Kurukshetra, Haryana 136119, India*
[2] *Inter-University Accelerator Centre, Aruna Asaf Ali Marg, New Delhi 110067, India*
[3] *Department of Physics, Panjab University, Chandigarh 160014, India*
[4] *Department of Nuclear Physics, Andhra University, Visakhapatnam 530003, India*
[5] *iThemba LABS, National Research Foundation, Somerset West, South Africa*
[6] *Department of Physics and Astrophysics, University of Delhi, Delhi 110007, India*
[7] *Department of Physics, Thapar University, Patiala, Punjab 147004, India*
[8] *Department of Physics, M. S. University of Baroda, Vadodara, Gujarat 390002, India*

Since the last few decades, a large number of experimental studies have been performed to understand the fusion-fission dynamics of heavy-ion induced reactions in the $A \sim 200$ mass region [1,2,3]. Fission fragment mass distribution, mass-angle, and mass-energy correlations are the key probes to examine the dynamics of fusion-fission and quasi-fission (QF) processes in a given reaction.

In the present work, we have carried out measurements of mass-angle and mass-energy distributions of fission fragments produced in the reactions ^{28}Si + ^{160}Gd and ^{12}C + ^{178}Hf, populating ^{188,190}Pt compound nuclei, respectively, at various excitation energies. The experiment was performed using the General Purpose Scattering Chamber (GPSC) facility at the Inter University Accelerator Centre (IUAC), New Delhi. Pulsed beams of ^{28}Si and ^{12}C from the Pelletron accelerator, in the laboratory energy ranges of 120–140 MeV and 60–88.2 MeV, respectively, were used. ^{160}Gd and ^{178}Hf targets with thicknesses of 220 μg/cm^2 and 260 μg/cm^2, respectively, and carbon backings of 20 μg/cm^2 and 30 μg/cm^2 were fabricated in the target laboratory of IUAC, New Delhi.

Fission fragments were detected using two large area (16 cm × 11 cm) multiwire proportional counters (MWPCs), mounted on each arm of the chamber. The calibrated position and time-of-flight (TOF) information from the two MWPCs were used to determine the emission angles of the fission fragments. The velocity ratio method was employed to obtain the masses of complementary fission fragments [4].

No mass-angle correlation was observed for the ^{12}C + ^{178}Hf reaction system, indicating the absence of any QF contribution at all studied energies. In contrast, a significant correlation between mass and angle of fission fragments was observed in the ^{28}Si + ^{160}Gd reaction system [5]. For the ^{12}C + ^{178}Hf reaction system, the measured mass–TKE distributions revealed liquid-drop model (LDM) fission behaviour [4]. For the ^{28}Si + ^{160}Gd reaction, the mass–TKE distributions showed clear signatures of the presence of slow quasi-fission events along with fusion–fission [5].

Our findings from the experimentally measured mass-angle and mass–TKE distributions are consistent with previously reported mass distribution measurements [1] for the fission of ^{188,190}Pt compound nuclei populated via the ^{28}Si + ^{160}Gd and ^{12}C + ^{178}Hf reaction systems, respectively.

References:

1. Kavita *et al.*, Phys. Rev. C **100**, 024626 (2019).
2. G. N. Knyazheva *et al.*, Phys. Rev. C **75**, 064602 (2007).
3. S. Gupta *et al.*, Phys. Lett. B **803**, 135297 (2020).
4. Vikas *et al.*, J. Phys. G: Nucl. Part. Phys. **51**, 035103 (2024).
5. Vikas *et al.*, Eur. Phys. J. A **60**, 202 (2024).

5.1.2 A study of fusion and transfer reactions in the ^{28}Si+^{58,62}Ni systems

Rajesh K. Sahoo[1], Dharmendra Singh[1], Amritraj Mahato[1,2], Pankaj K. Giri[1], Nitin Sharma[1], Lupteindu Chhura[1], Rahul Mahato[1], Chandra Kumar[3], Rishabh Kumar[3], Anjali Merin[4], Komal[5], Alankar Singh[3], Monuj Gogoi[6], Gonika[3], J. Gehlot[3] and S. Nath[3]

[1] *Department of Physics, Central University of Jharkhand, Ranchi 835222, India*
[2] *Dr. Shyama Prasad Mukherjee University, Ranchi 8354008, India*
[3] *Inter-University Accelerator Centre, Aruna Asaf Ali Marg, New Delhi 110067, India*
[4] *Department of Physics, Central University of Kerala, Kasaragod 671316, India*
[5] *Department of Physics, Panjab University, Chandigarh 160014, India*
[6] *Department of Physics, Cotton University, Guwahati 781001, India*

The study of fusion reaction dynamics below and above the fusion barrier has received significant attention in recent years. The observed enhancement in fusion cross sections below the fusion barrier, as compared to the predictions from one-dimensional barrier penetration models, highlights the influence of additional coupling effects [1]. Among these mechanisms, nucleon transfer with positive Q values plays an important role in the fusion process [2]. Consequently, investigating transfer channels and their correlation with evaporation residues (ERs) formation offers valuable insights into the underlying dynamics of sub-barrier fusion.

In this respect, excitation functions of the ERs and transfer reaction measurements in the ^{28}Si + ^{58,62}Ni system were carried out using the Heavy-ion Reaction Analyser (HIRA) [3] facility at IUAC, New Delhi, India. A pulsed ^{28}Si^{6+} beam, with a pulse separation of 2 μs for ER and 1 μs for transfer measurements, was obtained from the 15UD Pelletron accelerator at IUAC and incident on ^{58}Ni and ^{62}Ni targets. Two self-supporting and isotopically enriched ^{58}Ni targets with enrichment ≈99.98% and 99.8%, with thicknesses ≈495 and ≈330 μg/cm^2 respectively, and one ^{62}Ni target with enrichment ≈98.45% and thickness ≈250 μg/cm^2 mounted on ^{12}C backing (≈20 μg/cm^2) were used to measure the excitation function of ER and transfer reactions. The beam energy ranged from $E_{\rm Lab} \approx$ 68–92 MeV.

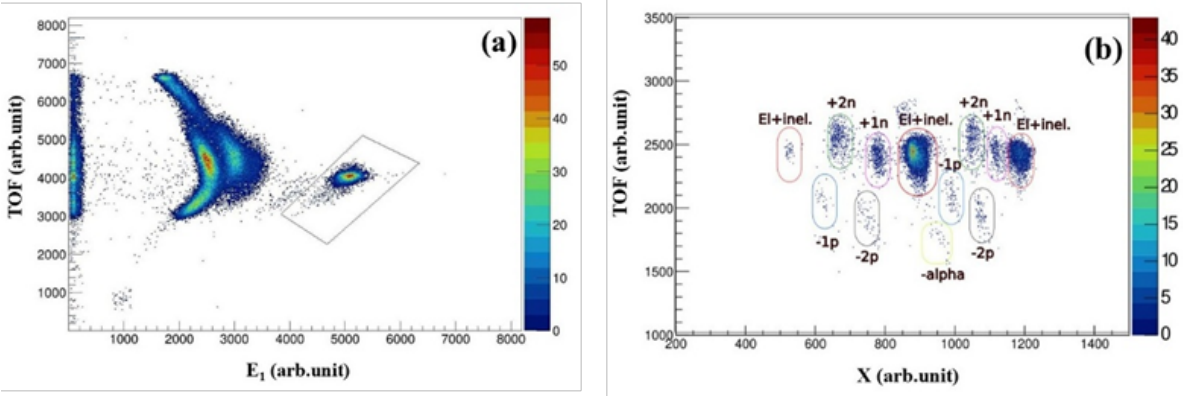

Figure 5.1: Two-dimensional scatter plots (a) E1–TOF and (b) X–TOF for ^{28}Si+^{62}Ni at projectile energy, $E_{\rm Lab} \approx 78$ MeV, when the HIRA was set for target-like events.

For ER cross-section measurements, the HIRA facility was operated at an angle of 0° with a solid angle acceptance of 5 msr. In transfer reaction measurements, HIRA was rotated to 10° with respect to the beam direction. It is important to note that data collection at the focal plane was associated with major concerns in separating the reaction products from the intense beam background. Due to the symmetric nature of the ^{28}Si + ^{58}Ni and ^{28}Si + ^{62}Ni systems, signals from the multi-wire proportional counter (MWPC) alone were insufficient to distinguish ER events (during fusion measurements) and target-like recoils (during transfer measurements) from other projectile-like fragments (PLFs). However, a clear separation was achieved using signals from the ionisation chamber (IC) [4] positioned behind the MWPC.

In both ER and transfer reaction measurements, four signals—E1, E2, E3 and E4—from the IC, corresponding to different segments, were recorded. For data acquisition, IUAC's in-house software NIAS-MARS, based on the ROOT framework, was employed in list mode. As a representative case, Fig. 1(a) shows a spectrum between E1 and time of flight (TOF), while Fig. 1(b) represents the corresponding X position and TOF spectrum of target-like ions for the system ^{28}Si + ^{62}Ni at $E_{\rm Lab} \simeq 78$ MeV. Further analysis is in progress.

References:

1. A. M. Stefanini *et al.*, J. Phys. G: Nucl. Part. Phys. **48**, 055101 (2021).
2. R. A. Broglia, C. H. Dasso, S. Landowne, and A. Winther, Phys. Rev. C **27**, 2433 (1983).
3. A. K. Sinha, N. Madhavan, J. J. Das, P. Sugathan *et al.*, Nucl. Instrum. Methods A **339**, 543 (1994).
4. J. Ghelot *et al.*, Proc. DAE-BRNS Symp. Nucl. Phys. **68** (2024).

5.1.3 Elastic and transfer reaction studies of ^{10,11}B+^{40}Ca systems at 50 MeV

Harun Al Rashid[1,2], K. Kalita[1], Lakhyajit Sarma[1], Amar Das[1,3], Nabendu K. Deb[4], P. Sugathan[5], Golda K.S.[5], A. Jhingan[5], N. Saneesh[5], Mohit Kumar[5], Anamika Parihari[6], Honey Arora[7] and J.J. Das[8]

[1] *Department of Physics, Gauhati University, Guwahati 781014, India*
[2] *Department of Physics, BBK College, Nagaon 781311, India*
[3] *Department of Physics, Suren Das College, Hajo 781102, India*
[4] *Department of Physics, Kamrup College, Chamata 781306, Assam, India*
[5] *Inter-University Accelerator Centre, New Delhi, 110067, India*
[6] *Rajdhani College, University of Delhi, Delhi 110015, India*
[7] *Department of Physics, Central Michigan University, Mt. Pleasant, Michigan, USA*
[8] *Department of Physics, Cotton University, Guwahati 781001, Assam, India*

An experimental study was carried out at IUAC, to investigate elastic and transfer reactions in ^{10,11}B + ^{40}Ca systems at 50 MeV using the GPSC facility. Elastic scattering angular distributions were analyzed using Woods-Saxon (WS), M3Y-Paris double-folding (DF) and Sao Paulo Potential (SPP2) potentials. Significant differences in real and imaginary potential strengths were observed, especially for WS. A hybrid model using M3Y-Paris (real) and WS (imaginary) best reproduced the data. The results showed strong absorption for both systems, with ^{10}B exhibiting a deeper, localized potential and ^{11}B a more diffuse, extended structure, consistent with its loosely bound nature. SPP2 analysis confirmed enhanced radii in ^{11}B, supporting its

broader density distribution. A new set of optical model parameters was extracted from the data, providing improved insight into the reaction mechanisms. The experimental results were also compared with earlier data by Glover *et al.* at 46.6 MeV and 51.5 MeV, showing good agreement and validating the present findings [1]. This work has been reported in detail in Ref. [2]. A comparative angular distribution using various potentials is shown in the left panel of Fig. 5.2.

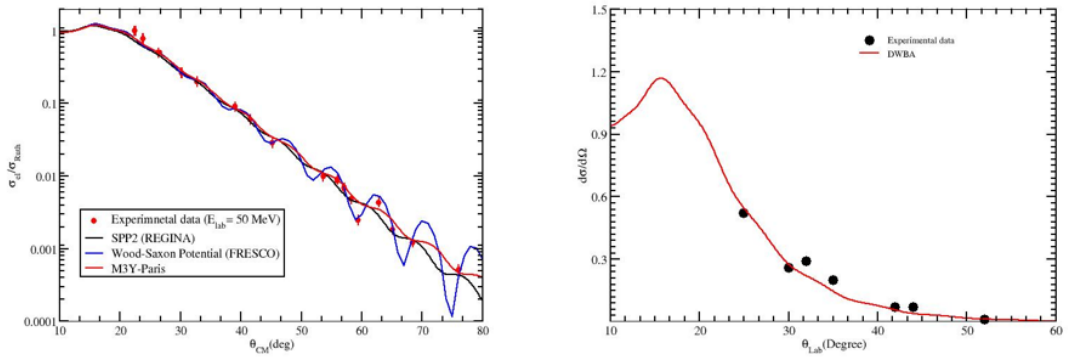

Figure 5.2: Left Panel: Ratio of elastic to Rutherford cross-section for ^{10}B + ^{40}Ca at 50 MeV using various potentials. **Right panel:** A preliminary result on the experimental cross-section along with DWBA analysis for the reaction ^{40}Ca(^{10}B,^{7} Be)^{43}Sc is presented.

In addition to elastic scattering, various transfer reactions were investigated. One-proton (1p) stripping reaction ^{40}Ca(^{10}B,^{9}Be)^{41}Sc was studied to examine proton binding and spectroscopic factors. Additionally, transfer reactions like ^{40}Ca(^{11}B,^{9}Be)^{42}Sc and ^{40}Ca(^{10}B,^{7}Be)^{43}Sc were being analyzed to investigate multi-nucleon transfer and the role of clustering. These transfer reactions are particularly significant for ^{11}B, known to exhibit strong α-cluster and 2α + t structures. A primary result on experimental cross-section along with DWBA analysis for ^{40}Ca(^{10}B,^{7}Be)^{43}Sc is shown in the right panel of Fig. 5.2.

References:

1. C.W. Glover, K.W. Kemper, L.A. Parks *et al.*, Nucl. Phys. A **337**, 520 (1980).
2. H.A. Rashid, K. Kalita, A. Das *et al.*, Nucl. Phys. A **1059**, 123074 (2025).

5.1.4 Fusion studies around the barrier for the reactions ^{16}O+^{124}Sn,^{138}Ba

K. Prameela[1], S. Ramakrishna Reddy[1], Anjali Merin[2], K. V. Varsha[2], K. V. Jinu[3], Gonika[4], Alankar Singh[4], Rishabh Kumar[4], J. Gehlot[4], S. Nath[4], E. Prasad[2], A. M. Vinodkumar[3], P. V. Madhusudhana Rao[1] and S. Appannababu[1]

[1] *Department of Nuclear Physics, Andhra University, Vishakhapatnam 530003, India*
[2] *Department of Physics, Central University of Kerala, Kasaragod 671316, India*
[3] *Department of Physics, University of Calicut, Malappuram 673635, India*
[4] *Inter-University Accelerator Centre, Aruna Asaf Ali Marg, New Delhi 110067, India*

Understanding the heavy ion reaction dynamics in the vicinity of Coulomb barrier is a topic of great interest due to the observation of sub-barrier fusion enhancement, when compared with the the one-dimensional barrier penetration model (1D- BPM). The enhancement of sub-barrier fusion can be understood by considering the influence of intrinsic nuclear degrees of freedom, such as inelastic coupling channels and nuclear deformations etc [1]. It is observed that, in most of the cases the experimental sub barrier fusion data can be well reproduced by coupled-channels (CC) calculations, by including the nuclear structure effects, such as vibrations and deformations [2]. However, in few systems it is observed that including inelastic excitations alone in the CC code is not sufficient to explain the sub-barrier fusion enhancement [3]. In order to explore the channel-coupling effects on sub-barrier fusion enhancement with respect to 1D- BPM, we have performed the fusion cross-section measurements for the reactions ^{16}O+^{124}Sn, ^{138}Ba.

The experiment was carried out at the 15UD Pelletron accelerator facility of IUAC by using the Heavy Ion Reaction Analyzer (HIRA). A pulsed beam of ^{16}O with a pulse separation of 4 μs was bombarded on isotopically enriched thin targets of ^{124}Sn (thickness $\approx$ 100 μg/cm^2 on 20 μg/cm^2 carbon backing) and ^{138}Ba (thickness $\approx$ 150 μg/cm^2 on carbon backing and capping of 20 μg/cm^2). Fusion excitation functions were measured in the laboratory beam energy from 51 to 74 MeV in steps of 1 MeV. In order to monitor the beam flux on the center of the target and for absolute normalization of evaporation residue (ER) cross sections, two solid state silicon surface barrier detectors were mounted at $\theta_{\rm lab} = \pm 20^\circ$ with respect to the beam direction. The fusion cross-sections were extracted from the yield of evaporation residues (ERs) which were separated from the beam-like particles using HIRA [4]. To detect the ERs, a position sensitive Multi-Wire Proportional Counter (MWPC) with an active area of 150 $\times$ 50 mm^2 was mounted at the focal plane of HIRA. For the present experiment HIRA was kept at zero degrees with respect to the beam direction and solid angle of acceptance of HIRA is 5 msr. A two-dimensional spectrum of energy loss of the ERs (ΔE) versus TOF for the ^{16}O+^{124}Sn reaction at $E_{\rm lab}$ = 62 MeV is shown in Fig. 5.3. The region enclosed within rectangle indicates the evaporation residues reaching the focal plane detector MWPC. The data were acquired through the IUAC software NIAS-MARS and analyzed using the ROOT framework.

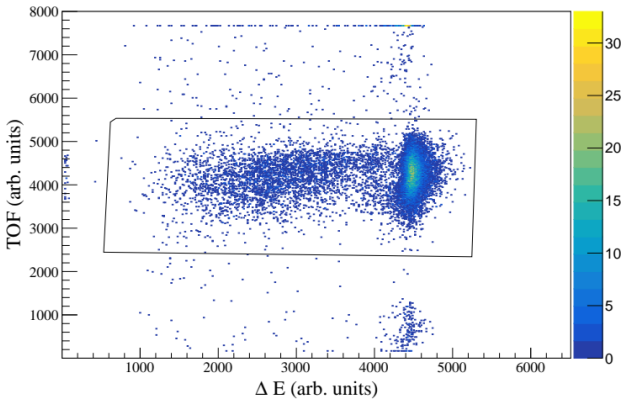

Figure 5.3: Two-dimensional spectrum of energy loss (ΔE) vs time of flight (TOF) for the ^{16}O+^{124}Sn system at $E_{\rm lab}$ = 62 MeV.

References:

1. J. R. Leigh *et al.*, Phys. Rev. C **52**, 3151 (1995).
2. J. D. Bierman *et al.*, Phys. Rev. Lett. **76**, 1587 (1996).
3. H. Timmers *et al.*, Nucl. Phys. A **633**, 421–445 (1998).
4. A. K. Sinha *et al.*, Nucl. Instrum. Methods A **339**, 543 (1994).

5.1.5 Role of neutron transfer in the sub-barrier fusion in ^{30}Si+^{124}Sn,^{138}Ba

K. Prameela[1], S. Ramakrishna Reddy[1], Anjali Merin[2], K. V. Varsha[2], K. V. Jinu[3], Gonika[4], Alankar Singh[4], Rishabh Kumar[4], J. Gehlot[4], S. Nath[4], E. Prasad[2], Hardev Singh[5], A. M. Vinodkumar[3], P.V. Madhusudhana Rao[1] and S. Appannababu[1]

[1] *Department of Nuclear Physics, Andhra University, Vishakhapatnam 530003, India*
[2] *Department of Physics, Central University of Kerala, Kasaragod 671316, India*
[3] *Department of Physics, University of Calicut, Malappuram 673635, India*
[4] *Inter-University Accelerator Centre, Aruna Asaf Ali Marg, New Delhi 110067, India*
[5] *Department of Physics, Kurukshetra University, Kurukshetra, Haryana 136119, India*

Heavy-ion fusion reactions at sub-barrier energies offer crucial and valuable information for understanding the fundamental aspects of quantum tunnelling. Significant enhancement in the fusion cross-sections are observed at sub-barrier energies when compared to one-dimensional barrier penetration model (1D-BPM). This enhancement can be attributed to the projectile/target coupling of internal degrees of freedom such as collective vibrations, nucleon transfer channels, and static deformation etc [1]. Although the impact of inelastic excitations on sub-barrier fusion enhancement is quite well established within the framework of coupled-channels calculations [2], but the exact contribution of nucleon transfer channels with positive Q-value is yet to be understand clearly [3]. In order to investigate the role of neutron transfers with positive Q-value, we measured the fusion cross-sections for the reactions ^{30}Si+^{124}Sn, ^{138}Ba.

The experiment was performed with a ^{30}Si pulsed beam of 2 μs repetition rate delivered from the 15UD Pelletron accelerator facility at IUAC. ^{30}Si beam was bombarded on isotopically enriched thin ^{124}Sn (thickness $\approx$ 100 μg/cm^2 on 20 μg/cm^2 carbon backing) and ^{138}Ba (thickness $\approx$ 150 μg/cm^2 on carbon backing and capping of 20 μg/cm^2) targets. These measurements were carried out around the Coulomb barrier energies $E_{\rm lab}$ = 94 to 125 MeV in steps of 1.5 MeV. In order to monitor the beam flux on the center of the target and for absolute normalization of evaporation residue (ER) cross sections, two solid state silicon surface barrier detectors were mounted at $\theta_{\rm lab} = \pm 20^\circ$ with respect to the beam direction. The

fusion cross-sections were extracted from the yield of evaporation residues (ERs) which were separated from the beam-like particles by using Heavy Ion Reaction Analyzer (HIRA) [4]. In the present experiment HIRA was kept at zero degrees with respect to the beam direction and the acceptance of HIRA is $\sim$ 5 mSr. In order to detect the ERs, a position sensitive Multi-Wire Proportional Counter (MWPC) with an active area of 150 $\times$ 50 mm^2 followed by a segmented ionization chamber (IC) with an equivalent area to that of the preceding MWPC, were used at the focal plane of HIRA. The isobutane gas pressure in the MWPC was maintained at $\approx$ 5 mbar and in the IC was $\approx$ 8 mbar maintained during the experiment. A two-dimensional spectrum of energy loss of the ERs (ΔE from MWPC) versus TOF and $E_{\rm Total}$ (from IC) versus TOF for the ^{30}Si+^{124}Sn reaction at $E_{\rm lab}$ = 108 MeV is shown in Fig. 5.4. Fig. 5.4(b) shows a clear indication that using IC effectively separates the ERs from the beam-like particles that reach the focal plane detector. The data was acquired through the IUAC software NIAS-MARS and analysed using the ROOT framework.

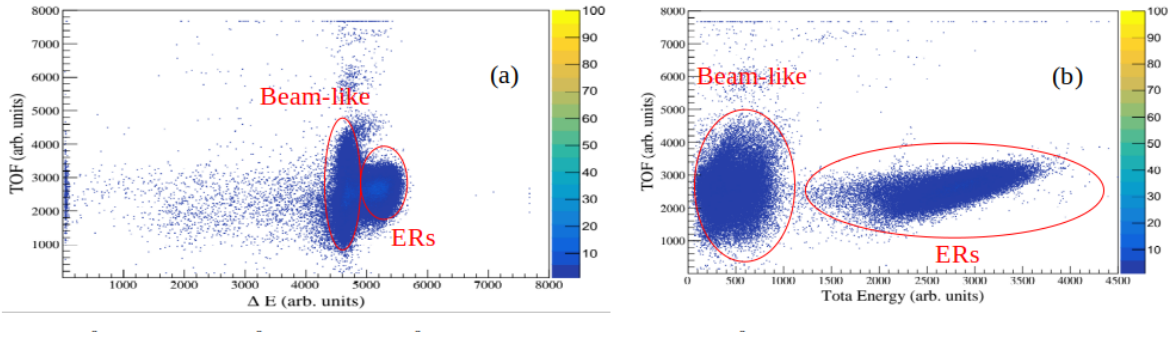

Figure 5.4: Two-dimensional spectrum of (a) ΔE (from MWPC) vs. TOF spectra and (b) $E_{\rm Total}$ (from IC) vs. TOF for the reaction ^{30}Si+^{124}Sn at $E_{\rm lab}$ = 108 MeV.

References:

1. V. I. Zagrebaev, Phys. Rev. C **67**, 061601 (2003).
2. K. Hagino, N. Takigawa, M. Dasgupta, D. J. Hinde and J. Leigh, Phys. Rev. C **55**, 276 (1997).
3. Z. Kohley *et al.*, Phys. Rev. Lett. **107**, 202701 (2011).
4. A. K. Sinha *et al.*, Nucl. Instrum. Methods A **339**, 543 (1994).

5.1.6 Study of fission fragment mass distribution in the reaction ^{14}N+^{193}Ir

Lakhyajit Sarma[1], K. Kalita[1,*], Harun Al Rashid[1,2], Amar Das[1,3], Nabendu Kumar Deb[4], M. Bhuyan[5], Taniya M. Sonowal[1], Gyandeep Narzary[1], Avitesh Agrawal[6], Neha Dhanda[7], A. Jhingan[8], K. S. Golda[8], N. Saneesh[8], M. Kumar[8] and P. Sugathan[8]

[1] *Department of Physics, Gauhati University, Guwahati 781014, Assam, India*
[2] *Department of Physics, BBK College, Nagaon, Barpeta 781311, Assam, India*
[3] *Department of Physics, Suren Das College, Hajo 781102, Assam, India*
[4] *Department of Physics, Kamrup College, Chamata, Nalbari 781306, Assam, India*
[5] *Department of Physics, Rangia College, Rangia 781354, Assam, India*
[6] *Department of Physics & Astrophysics, Central University of Haryana, Mahendergarh 123029, India*
[7] *Department of Physics, Panjab University, Chandigarh 160014, India*
[8] *Inter-University Accelerator Centre, Aruna Asaf Ali Marg, New Delhi 110067, India*

The systematic study of the fusion-fission process is very important to understand the complex dynamical evolution of the composite system formed via heavy-ion induced reactions at energies near the Coulomb barrier [1]. To understand the fission dynamics in the pre-actinide region, we populate ^{207}Po via the reaction ^{14}N + ^{193}Ir. The experiments were performed at IUAC, New Delhi, with the 15 UD Pelletron accelerator using the NAND facility at $E_{\rm lab}$ = 65 to 80 MeV. Pure enriched isotopic targets of ^{193}Ir were fabricated at the target laboratory of IUAC for performing the experiment. Two larger area MWPCs (20 $\times$ 10 cm^2) were mounted at the folding angles 40° and 125° with respect to the beam axis to collect the fission fragments in coincidence. The fission events are separated from elastic events using the timing correlation of the MWPCs by applying a gate as shown in Fig. 5.5(a).

For the analysis of the data, time and position calibration were done, and from the calibrated timing and position information, folding angles and the velocities of the fission fragments were reconstructed. Finally, the mass distribution of the fission fragments of the reaction ^{14}N + ^{193}Ir is compared with the mass distribution

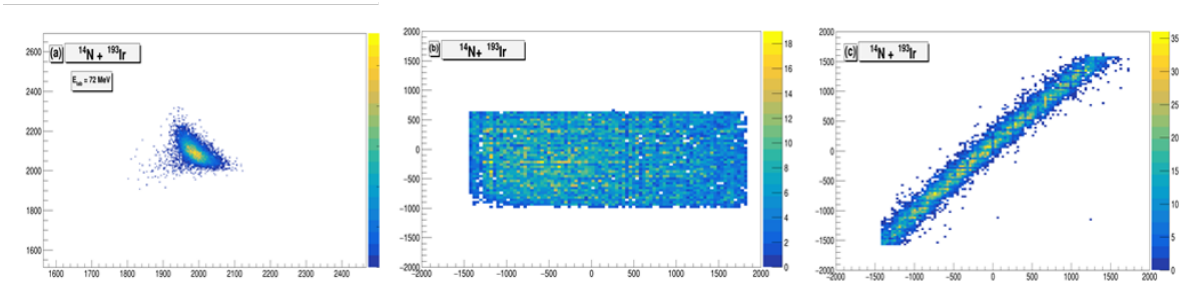

Figure 5.5: For the reaction ^{14}N +^{193} Ir: (a) TOF correlation spectra of MWPC1 and MWPC2, (b) X and Y position spectra of MWPC1 and MWPC2 at $E_{\rm lab}$ = 72 MeV, and (c) X position spectra of MWPC1 and MWPC2 at $E_{\rm lab}$ = 72 MeV.

of the same and nearby nuclei formed via different entrance channels to understand the influence of entrance channel parameters on nuclear fission mass distribution. In Fig. 5.6, the mass distribution for the previously measured reaction ^{30}Si + ^{176}Yb [2] at $E_{\rm lab}$ = 137 MeV is shown. It is found to be symmetric (peaked at $A_{\rm CN}/2$, where $A_{\rm CN}$ is the compound nucleus mass) and fitted with a single Gaussian function to extract the width of the mass distribution (σ_m).

Further data analysis of the ^{14}N + ^{193}Ir system is in progress and details will be reported soon. As the two reactions under study have different entrance channel properties and are populated with around similar excitation energies, the dynamical evolution [3] of the composite system after capture can be compared to understand the onset of quasifission and the influence of entrance channel parameters on compound nucleus and non-compound nucleus fission.

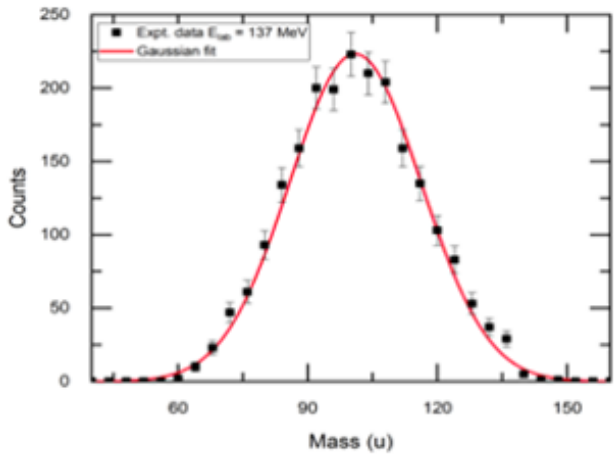

Figure 5.6: FFs mass distribution for the reaction ^{30}Si+^{176}Yb at $E_{\rm lab}$ = 137 MeV.

References:

1. T. K. Ghosh *et al.*, Phys. Rev. C **79**, 054607 (2009).
2. L. Sarma *et al.*, Phys. Rev. C **111**, 024606 (2025).
3. D. Hinde *et al.*, Phys. Rev. C **53**, 1290 (1996).

5.1.7 Evaporation residue cross-section measurement of ^{16}O+^{170,172}Yb reactions

K. V. Jinu[1], A. M. Vinodkumar[1], B. R. S. Babu[1], S. Nath[2], J. Gehlot[2], Gonika[2], P. V. Madhusudhana Rao[3], E. Prasad[4], B. Ashna[4], K. V. Varsha[4], P. P. Panchami[4], Shiva Prasad Nayak[4], Rishabh Kumar[2], Alankar Singh[2], Rajesh K. Sahoo[5] and Monuj Gogoi[6]

[1] *Department of Physics, University of Calicut, Kerala 673635, India*
[2] *Nuclear Physics Group, Inter-University Accelerator Centre, New Delhi 110007, India*
[3] *Department of Nuclear Physics, Andhra University, Andhra Pradesh 530003, India*

[4] *Department of Physics, Central University of Kerala, Kerala 671316, India*
[5] *Department of Physics, Central University of Jharkhand, Jharkhand 835222, India*
[6] *Department of Physics, Cotton University, Guwahati, Assam 781001, India*

The measurement of fusion-fission, fusion-evaporation residue, and quasi-fission provides a quantitative measure of total capture cross-sections for medium heavy ion reactions forming compound nuclei $A \sim 200$. A major challenge in super heavy element production is the presence of non-equilibrium processes such as Quasi-fission (QF) [1]. Theoretically, QF is predicted when the charge product $Z_1Z_2 > 1400$. Recent studies on many systems with Z_1Z_2 even less than 1000 revealed the onset of the quasi-fission events near and around the Coulomb barrier energies [2]. The quasi-fission process is found to have a very strong entrance channel dependence such as entrance channel mass asymmetry, nuclear deformation and orientation [3]. The presence of QF can be understood from the fission cross-section, fission mass distribution, ER measurements, etc.

In fusion reactions, the composite system, after capture, follows a long dynamical path, during which it equilibrates in all degrees of freedom and forms a compound nucleus (CN) or reseparates into fission-like fragments. The isotopes of Pt and Hg nuclei with $A \sim 170$–190 show structural changes as they move from neutron-poor to neutron-rich nuclei. The fission, fusion, and ER cross-sections may be affected by it.

The cross-sections for the sub-barrier fusion of ^{32}S with the isotopes of Sm and ^{16}O+^{170}Yb are measured and compared [4]. They observed that the fusion-fission cross-section increases with nuclear deformation. Both reactions ^{32}S+Sm and ^{16}O+^{170}Yb showed that the fission of Pt systems has a strong dependence on the target deformation. They also measured the total kinetic energy and fragment mass distributions, and excitation functions were analyzed using a model that allows for the effects of static target deformations. These calculations show that the target deformation effects are also important for the fusion-fission cross-sections. The inclusion of the centrifugal contribution in the total kinetic energy gives an excellent reproduction of the data for the ^{32}S+^{154}Sm reaction; however, for ^{16}O+^{170}Yb reaction, the agreement is not so good. In comparison with the coupled channels calculation, measured cross-section showed a significant role of hexadecapole deformation of ^{174,176}Yb targets [5].

We have measured evaporation residues for ^{16}O+^{170,172}Yb reactions forming ^{186,188}Pt compound nuclei to study the ERs, the deformation effects, and the presence of quasifission. The experiment was performed using the Heavy Ion Reaction Analyzer (HIRA) at IUAC. A 4 μs pulsed beam of ^{16}O with energy in the range 65 MeV to 100 MeV was provided by the 15UD Pelletron Accelerator Facility. Targets of ^{170,172}Yb with thickness ~ 200 μg/cm^2 on carbon backing of 22 μg/cm^2 and 20 μg/cm^2 respectively were bombarded.

Two silicon detectors were placed inside the target chamber to record Rutherford-scattered beam particles for absolute normalization of ER cross-sections. A multiwire proportional counter (MWPC), with an active area of 150 mm $\times$ 50 mm, was placed at the focal plane of the HIRA to detect the ERs. A time-of-flight method is used to separate the beam-like particles from ERs. The analysis is in progress.

References:

1. D. J. Hinde, M. Dasgupta, J. R. Leigh, J. P. Lestone *et al.*, Phys. Rev. Lett. **74**, 1295 (1995).
2. S. Sanila, A. M. Vinodkumar, B. R. S. Babu, N. Madhavan *et al.*, Phys. Rev. C **106**, 024614 (2022).
3. E. Prasad, K. M. Varier, R. G. Thomas, P. Sugathan *et al.*, Phys. Rev. C **81**, 054608 (2010).
4. B. G. Glagola, B. B. Back and R. R. Betts, Phys. Rev. C **29**, 486 (1984).
5. T. Rajbongshi, K. Kalita, S. Nath, J. Gehlot *et al.*, Phys. Rev. C **93**, 054622 (2016).

5.1.8 Measurement of quasi-elastic excitation functions for ^{16}O+^{176}Yb

Amar Das[1,2], K. Kalita[1], Harun Al Rashid[1,3], Lakhyajit Sarma[1], Nabendu Kumar Deb[1,4], Taniya Sonowal[1], Anita Tamang[1], M. Bhuyan[5], Chandra Kumar[6], Rajesh Kumar Sahoo[7], Bhargav Baruah[8], Rasna Baruah[8], Anamika Parihari[9], Madhuchanda Swain[10], Gonika[6], J. Gahlot[6], S. Nath[6] and N. Madhavan[6]

[1] *Department of Physics, Gauhati University, Guwahati-781014, Assam, India*
[2] *Department of Physics, Suren Das College, Hajo, Assam, India*
[3] *Department of Physics, Baoci Banikanta Kakati College, Nagaon, Barpeta, Assam, India*
[4] *Department of Physics, Kamrup College, Chamata, Nalbari, Assam, India*
[5] *Department of Physics, Rangia College, Rangia-781354, Assam, India*
[6] *Inter University Accelerator Centre, New Delhi-110067, India*
[7] *Central University of Jharkhand, India*
[8] *Cotton University, Guwahati, Assam, India*
[9] *Rajdhani College, Delhi University, New Delhi, India*
[10] *Centurion University of Technology and Management, Odisha*

5. RESEARCH ACTIVITIES

Quasielastic scattering (QES) at backward angles and the extraction of barrier distributions (BD) provide critical insights into nuclear reaction dynamics, particularly the role of nuclear deformation and couplings. Motivated by this, we carried out an experiment for measurement of QES using spherical and deformed targets in the systems of ^{16}O +^{116} Sn, ^{176}Yb, and ^{178}Hf. The experiment was conducted at a backward angle of 138° and at a forward angle corresponding to 180°, using the HIRA setup at IUAC, New Delhi. QES excitation functions were measured over the energy range of $0.78V_c$ to $1.09V_c$ for ^{16}O +^{116} Sn and $0.78V_c$ to $1.10V_c$ for ^{16}O +^{176} Yb and ^{178}Hf, where V_c is the Coulomb barrier. The QES barrier distributions were extracted from these excitation functions using the three-point difference method. Our aim was to measure excitation functions for spherical and deformed targets such that effect of coupling and deformation can be seen on the BD. Preliminary study reveals that the hexadecapole deformation in ^{176}Yb has a considerable effect on the barrier distribution consistent with the reported deformation parameters ranging from 0.012 to -0.059 [1,2] Furthermore, given the scarcity of available data on the ^{16}O +^{178} Hf system, our study provides a valuable set of QES measurements for this system.

To measure QES events at a back angle, we employed two Si-back detectors at back angles of 150° and 138.5°, and the target-like particles were detected using a multi-wire proportional counter (MWPC) situated at the HIRA focal plane. Two monitor detectors were employed for normalizing purposes. R. Biswas et al. [3] used the same technique to measure the QES excitation function at the forward angle. Fig. 5.7(a) shows the QES events for ^{16}O+^{176}Yb at the focal plane of the HIRA, measured at $E_{\rm lab}$ = 77 MeV. Fig. 5.7(b) shows the x-TOF spectrum for QES events at the same energy. Fig. 5.7(c) and (d) show spectra show the QES excitation functions measured at the backward angles and the corresponding barrier distributions Detailed analysis of the data is in progress.

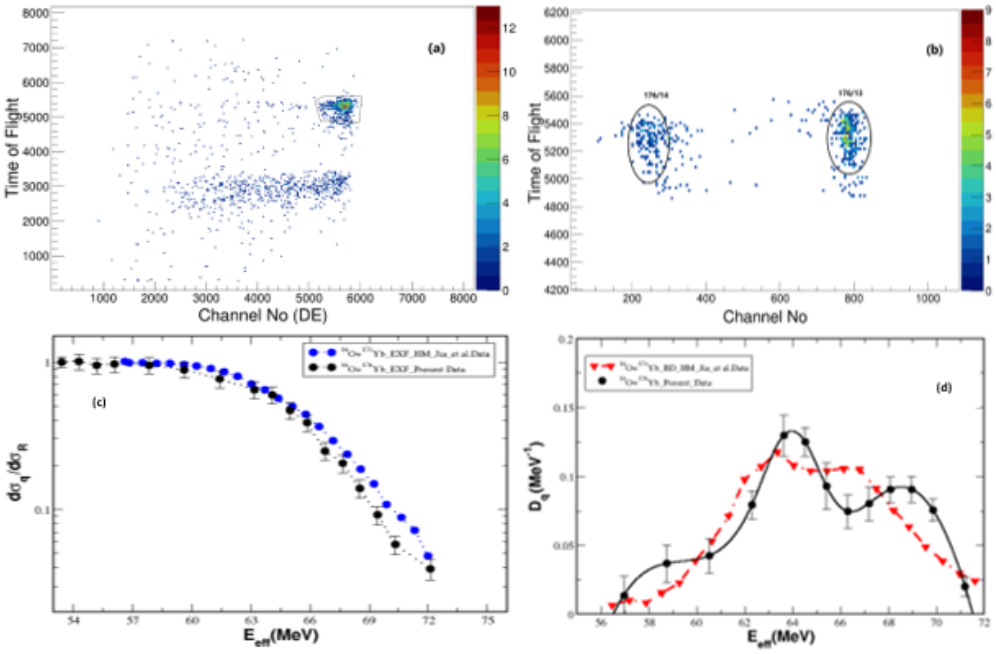

Figure 5.7: (a) Quasielastic events for ^{16}O+^{176}Yb detected at the focal plane of the HIRA, (b) x-TOF spectrum for the events shown in panel (a). Panels (c) and (d) show QES excitation functions and barrier distributions obtained from backward angle measurements, along with the results reported by Jia *et al.*

References:

1. H. J. Wollersheim, W. Wilcke, and T. W. Elze, Phys. Rev. C **11**, 2008 (1975).
2. P. Möller, Nucl. Phys. A **142**, 1 (1970).
3. Rohan Biswas and S. Nath, Eur. Phys. J. A **56**, 1 (2020).
4. H. M. Jia, C. J. Lin, H. Q. Zhang, Z. H. Liu *et al.*, Phys. Rev. C **82**, 027602 (2010).

5.1.9 Back-angle quasi-elastic scattering measurements for ^{35}Cl+^{130}Te system

Abhishek Yadav[1], Md. Moin Shaikh[2], A. Jhingan[3], M. Kumar[3], N. Saneesh[3], Indu Bala[3], Unnati Gupta[1], K. S. Golda[3], Gobind Ram[4], Rishabh Prajapati[3], Rayees Ahmad[5], Amanjot Kaur[6], Aquib Siddique[7], Keshav Kapoor[4], S. Kalkal[5], M. K. Sharma[4] and B. P. Singh[7]

[1] *Amity Institute of Nuclear Science & Technology, Amity University Uttar Pradesh, Noida 201313, U.P., India*
[2] *Department of Physics, Chanchal College, Malda 732123, West Bengal, India*
[3] *Nuclear Physics Group, Inter-University Accelerator Centre, New Delhi 110067, India*
[4] *Department of Physics, University of Lucknow, Lucknow 226021, U.P., India*
[5] *Department of Physics, Thapar Institute of Engineering & Technology, Patiala 147004, Punjab, India*
[6] *Department of Physics, Indian Institute of Technology Ropar, Roopnagar 140001, Punjab, India*
[7] *Department of Physics, Aligarh Muslim University, Aligarh 202001, U.P., India*

Fusion reactions, especially sub-barrier fusion in heavy ion induced reactions, offer a unique opportunity to study both the static and dynamic properties of nuclei, as well as to explore tunneling phenomena, including the coupling of inelastic excitations and transfer channels [1, 2, 3, 4]. The understanding of the effect of coupling phenomenon on sub-barrier fusion reaction mechanisms is crucial for advancing the synthesis of superheavy elements and studying fusion reaction dynamics at deep sub-barrier energies [1, 2, 3, 4].

Recently, significant interest has developed in fusion barrier studies, as collisions near the Coulomb barrier are influenced by the coupling between relative motion and the internal degrees of freedom of colliding ions. This results in a barrier distribution (BD) rather than a single potential barrier ($B_{\rm fus}$). The BD can be experimentally extracted from the fusion excitation function $\sigma_{\rm fus}(E)$ using the relation $D_{\rm fus} = \frac{d^2(E\sigma_{\rm fus})}{dE^2}$, which reflects the reaction mechanism through the nature and strength of the couplings. Timmers et al. [5] also extracted the BD from quasi-elastic (QEL) scattering at backward angles, showing that the same information can be obtained from the QEL cross-section, as total flux is conserved.

The experiments have been planned and performed at the Inter-University Accelerator Centre, New Delhi using ^{35}Cl beam (energy from 114 MeV to 147 MeV, in steps of 3 MeV) on ^{130}Te target of thickness $\sim$ 170 μg/cm^2. The HYTAR detecting set-up in the General-Purpose Scattering Chamber has been used to detect the scattered particles [6]. In this experiment, the detector array was comprised of twelve telescope detectors placed at different angular positions (four at 173°, four at +100° to 160° with 20° angular separation, three at angles −154° to −114° and one at −74°) with respect to the incident beam direction.

The list mode data has been recorded and analyzed using NIASMARS software. The elastic, inelastic and transfer events are clearly separated out in the 2D E-ΔE spectrum. The quasi-elastic events have been extracted from the 2D plot for each angle and studied as a function of energy to obtain the excitation function and angular distribution of these events. The barrier distribution will be derived from the measured quasi-elastic excitation function.

Notably, the fusion barrier distribution for the ^{35}Cl+^{130}Te system, which has all positive neutron transfer channels, has already been studied in Ref. [7], making it an ideal system to compare quasi-elastic barrier distributions with fusion barrier distributions. Additionally, the transfer angular distributions measured in the present experiments will deepen our understanding of the role of transfer reactions in reaction dynamics. The detailed analysis is underway.

References:

1. B. B. Back *et al.*, Rev. Mod. Phys. **86**, 317 (2014), and the references therein.
2. A. M. Stefanini *et al.*, Phys. Rev. Lett. **74**, 864 (1995); *Phys. Rev. C* **96**, 014603 (2017).
3. A. Lemasson *et al.*, Phys. Rev. Lett. **103**, 232701 (2009).
4. L. Corradi, G. Pollarolo and S. Szilner, J. Phys. G: Nucl. Part. Phys. **36**, 113101 (2009).
5. H. Timmers *et al.*, J. Phys. G: Nucl. Part. Phys. **23**, 1175 (1997); *Nucl. Phys. A* **584**, 190 (1995).
6. A. Jhingan *et al.*, Nucl. Instrum. Methods A **903**, 326 (2018).
7. R. N. Sahoo *et al.*, Phys. Rev. C **102**, 024615 (2020).

5.1.10 Reaction measurements in the interactions of ^{28}Si with ^{64,68}Zn

Rayees Ahmad Yatoo[1], Sunil Kalkal[1], Akhil Jhingan[2], Gobind Ram[3], Anjali Merin[4], Taniya M Sonowal[5], Priyanka[6], Amit Jangra[7], Rishab Prajapati[2], Abhishek Yadav[8], Golda K.S.[2], Mohit Kumar[2] and N. Saneesh[2]

[1] *Department of Physics and Material Science, Thapar Institute of Engineering and Technology, Patiala-147004, India*
[2] *Inter University Accelerator Centre, New Delhi - 110067, India*
[3] *Department of Physics, University of Lucknow, U.P.-226007, India*
[4] *Department of Physics, Central University of Kerala, Kasaragod, Kerala-671320, India*
[5] *Department of Physics, Gauhati University, Assam-781014, India*

[6] *Department of Physics and Astrophysics, University of Delhi, Delhi-110007, India*
[7] *Department of Physics, Panjab University, Chandigarh-160014, India*
[8] *Department of Physics, Amity University Noida, Sector 125, U.P.-201313, India*

The reaction dynamics of heavy ion collisions at the bombarding energies near the Coulomb barrier are governed by the coupling to various reaction channels, including inelastic excitations, nuclear deformations, and particle transfer channels. To comprehend the fundamental reaction mechanism or the nuclear structure, it is essential to analyse the reaction mechanisms of these channels. The measurements of the elastic cross-section are beneficial for comprehending the interaction between the projectile and the target nucleus [1]. Transfer angular distribution measurements help us understand the dynamics of nuclear transfer reactions and the angular dependence of the transfer products, thus providing insights into reaction mechanisms [2]. In the present study, the elastic and transfer measurements were performed in the reaction of ^{28}Si with ^{64,68}Zn near the Coulomb barrier. The elastic and transfer angular distributions will be extracted from the experimental data. The experiment was performed by utilizing the HYTAR [3] detector set-up inside the General Purpose Scattering Chamber (GPSC) at IUAC, New Delhi. A DC beam of ^{28}Si available at the facility was used. Isotopically enriched targets of thickness $\sim 200\ \mu g/cm^{-2}$ were used for the measurements [4]. The transfer excitation measurements were performed in lab energy range of $64-114$ MeV with 2 MeV step. Two silicon monitor detectors were kept 10^o with respect to the beam axis for beam monitoring and the normalization of the cross-sections. Four hybrid $(\Delta E - E)$ detectors with angular spacing of 20^o were used on both arms of the GPSC chamber to cover the angular range. Four $\Delta E - E$ detectors were placed at the back angles $(\sim 173^o)$ to record the back-scattered quasielastic (QEL) events. $\Delta E - E$ detectors used are combination of a gas detector (ΔE) consisting iso-butane gas operating at $20-120$ mbar pressure and a E silicon detector with thickness $\sim 300\ \mu m$. The schematic of the detector set-up used is shown in figure 1.

The experimental data will be analyzed to extract the elastic and transfer angular distribution cross-sections at various energies. The transfer angular distribution cross-sections are obtained using the expres-

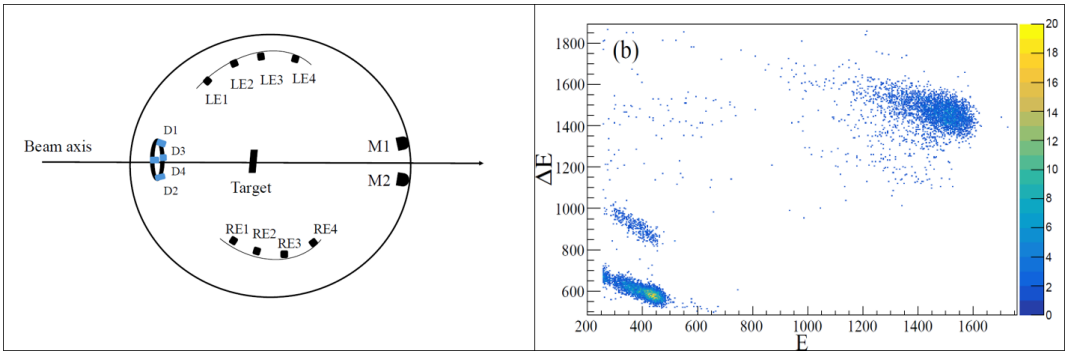

Figure 5.8: Left Panel: Schematic of the various detectors used in the experiment. RE1-RE4 and LE1-LE4 are the ΔE-E detectors on the right and left arms w.r.t. beam axis, respectively. D1-D4 are the fixed dome detectors, M1 and M2 are the monitor detectors. Right panel: $\Delta E - E$ spectrum of a) ^{28}Si + ^{64}Zn and b)^{28}Si + ^{68}Zn systems taken at $E_{lab} = 106$ MeV.

sion as:

$$\left[\left(\frac{d\sigma}{d\Omega}\right)_{tr}\right]_{tel} = \frac{(Y_{tel})_{tr}}{(Y_M)_R}\left[\left(\frac{d\sigma}{d\Omega}\right)_R\right]_M \frac{\Delta\Omega_M}{\Delta\Omega_{tel}} \tag{5.1}$$

where Y_{tel} is the yield of the transfer events at different angles in the telescopic detectors, Y_M is the geometric mean of the yield obtained from the two monitor detectors. $\frac{\Delta\Omega_M}{\Delta\Omega_{tel}}$ is the ratio of the solid angles of monitor and telescopic detector respectively. To precisely determine the solid angle subtended by the monitors and back angle detector, a low energy run (below barrier) was taken during the experiment by using ^{197}Au as the target. As this beam energy is well below the Coulomb barrier, thus elastic scattering at this bombarding energy is expected to be purely Rutherford.

References:

1. L. F. Canto *et al.*, Eur. Phys. J. A **56**, 1 (2020).
2. Zehong Liao *et al.* arXiv:2407.05395 (2024).
3. A. Jhingan *et al.*, Nucl. Instrum. Methods A **903**, 326 (2018).
4. Shoaib Noor *et al.*, Vacuum **193**, 110508 (2021).

5.1.11 Disentangling the role of different entrance channels on the transfer reaction mechanism

Gobind Ram[1], Manoj Kumar Sharma[1], Rayees Ahmed Ytoo[2], Abhishek Yadav[3], Aquib Siddique[4], Rishabh Prajaparti[5], Keshav Kapoor[1], Amanjot[6], Abhishek K. Mishra[1], Pariyanka[6], Subham Kumar[6], Tanmoy Bar[5], Akhil Jhingan[5], N. Saneesh[5], M. Kumar[5], B. P. Singh[2] and R. Prasad[2]

[1] *Department of Physics, University of Lucknow, Lucknow 226007, Uttar Pradesh, India*
[2] *Thapar Institute of Engineering & Technology, Patiala, Punjab 147004, India*
[3] *AINST, Amity University, Noida 201313, India*
[4] *Department of Physics, Aligarh Muslim University, Aligarh 202002, Uttar Pradesh, India*
[5] *Inter University Accelerator Centre, Aruna Asaf Ali Marg, New Delhi 110067, India*
[6] *Indian Institute of Technology Ropar, Rupnagar 140001, Punjab, India*

In recent years, there has been great interest in fusion barrier studies at energies around the Coulomb barrier. At these energies, the coupling between relative motion and internal degrees of freedom of colliding heavy ions is strongly affected, which results in a number of distributed barriers instead of a single barrier ($B_{\rm fus}$) [1, 2, 3, 4, 5, 6]. A barrier distribution (BD) can be extracted experimentally from the fusion excitation function $\{\sigma_{\rm fus}(E)\}$ using the relation $D_{\rm fus} = \frac{d^2}{dE^2}(E\sigma_{\rm fus})$ [3]. The extracted BD contains the fingerprint of the reaction dynamics. This is because the nature and strengths of the several couplings involved in the interaction give distinct peaks in the barrier distribution.

Further, it was suggested that the same information can also be extracted from the cross-section of quasi-elastic scattering (QE) (as the total flux is conserved), measured at large angles, using the prescription $D_{\rm qel} = \frac{d}{dE}\left(\frac{d\sigma_{\rm qel}}{d\sigma_R}\right)$, as an alternative representation of the fusion BD [5]. In the present work, the QE measurements have been performed for the ^{14}N+^{176}Hf,^{176}Yb systems, which will be translated into BD.

The experiment has been performed in the GPSC at the IUAC, New Delhi, employing the HYTAR detecting system, comprising 13 ΔE-E hybrid telescopes, where ΔE were gas ionization chambers and E detectors were passivated implanted planar silicon (PIPS) detectors [7]. Beam energy was varied in steps of 3 MeV ranging from 20% below to 20% above the barrier. Four telescope detectors, each at an angle of 173°, were arranged in a symmetrical cone geometry to measure the back-scattered quasi-elastic events. Two monitor detectors were placed at ±10° for beam monitoring and normalization purposes.

The ^{178}Hf and ^{176}Yb targets were bombarded with a ^{14}N beam of energies typically ranging from 15% below to 12% above the Coulomb barrier, with 3 MeV energy steps. Transfer angular distributions were measured at two or three incident energies, alongside the quasi-elastic excitation functions. These results will provide crucial insights into the reaction dynamics of these projectile-target interactions. Additionally, the transfer angular distributions measured in the present experiments will deepen our understanding of the role of transfer reactions in reaction dynamics. Analysis is currently underway.

References:

1. G. Kaur *et al.*, Phys. Rev. C **94**, 034613 (2016).
2. Md. Moin Shaikh *et al.*, Phys. Rev. C **91**, 034615 (2015).
3. N. Rowley, G.R. Satchler and P.H. Stelson, Phys. Lett. B **254**, 25 (1991).
4. M. Dasgupta *et al.*, Annu. Rev. Nucl. Part. Sci. **48**, 401 (1998).
5. H. Timmers *et al.*, Nucl. Phys. A **584**, 190 (1995).
6. K. Hagino, N. Rowley and A. T. Kruppa, Comp. Phys. Comm. **123**, 143 (1999).
7. A. Jhingan *et al.*, Nucl. Instrum. Methods **903**, 326 (2018).

5.1.12 Gamma-ray spectroscopy of neutron deficient Bi isotopes

Dhananjaya Sahoo[1], A. Y. Deo[1], Vijay Bangari[1], Gunjan Gaur[1], Careen A. Lakadong[1], Jinti Barman[1], Yashraj[2], Indu Bala[2], Mamta Jain[2], Khamosh Yadav[2], U. S. Ghosh[2], Rishabh Kumar[2], R. P. Singh[2], E. T. Subramaniam[2], Sachin Kumar Singh[3], Jay Kaushik[3], Ankit Rana[3], S. K. Tandel[3], P. S. Rawat[4], Nandini Patel[4], S. S. Ghugre[5] and R. Raut[5]

[1] *Department of Physics, Indian Institute of Technology Roorkee, Roorkee 247667, India*
[2] *Inter-University Accelerator Centre, Aruna Asaf Ali Marg, New Delhi 110067, India*
[3] *Department of Physics, School of Natural Sciences, Shiv Nadar Institution of Eminence, Gautam Buddha Nagar 201314, India*
[4] *Department of Physics and Astrophysics, University of Delhi, New Delhi 110007, India*
[5] *UGC-DAE CSR, Kolkata Centre, LB-8, LB Block, Sector III, Bidhannagar, Kolkata 700098, India*

Structure of atomic nuclei in the neutron deficient region around the $Z = 82$, $N = 126$ shell closure poses an inquisitive challenge due to the emergence of various structural phenomena such as shape coexistence, shears mechanism, presence of high- and low-spin isomers, α-clustering etc. In general, nuclei in the vicinity

of shell closures exhibit single-particle excitations, while collectivity is gradually built up as one moves away from the closed shells, leading to deformation in nuclei. However, the region lying between these two extremes shows an interplay between single-particle and collective modes of excitations. The observation of structural evolution with increasing angular momentum is particularly intriguing in the Pb isotopes near the $A \sim 200$ region. The low-lying states in these nuclides arise from the single-particle excitations, whereas the high-spin states exhibit a variety of collective rotational behaviors [1,2]. A similar structural evolution is also observed in Bi isotopes in the $A \sim 200$ region. Recently, five oblate bands consisting of the stretched magnetic dipole transitions have been observed in this mass region: one band each in ^{198}Bi, ^{199}Bi and ^{203}Bi and two in ^{200}Bi. These bands are tentatively assigned to the respective Bi isotopes based on their observed coincidence relationships with known low-lying transitions and the ratio of intensities of the strong γ-rays in each of the major populated channels at two different beam energies [2]. However, no such band structures have been reported in ^{201}Bi. In addition, the level structure of the doubly-odd ^{200}Bi is not fully understood due to the presence of very scanty information. Therefore, the ^{200,201}Bi isotopes, with one proton outside the $Z = 82$ shell closure, are interesting candidates to investigate the evolution of structure with increasing angular momentum.

Excited states in ^{200,201}Bi were populated using the ^{194}Pt(^{11}B,xn)^{200,201}Bi heavy-ion fusion-evaporation reaction. The ^{11}B beam (DC/Pulsed) in 57-72 MeV energy range, provided by the 15UD Pelletron accelerator at IUAC, was impinged on a self-supporting ^{194}Pt target of 17.1 mg/cm^2 thickness. The ^{11}B pulsed beam at 62 MeV with a repetition period of 1 μs (*i.e*, 1 ns ON and 1 μs OFF) was used to measure the half-lives of several isomeric states in ^{201}Bi. The Indian National Gamma Array, consisting of 11 Compton-suppressed Clover HPGe detectors, one Low Energy Photon Spectrometer (LEPS) and 4 $LaBr_3$(Ce) fast scintillators, was used for the detection of the emitted γ-rays. Singles and coincidence data were acquired using a VME-based data acquisition system.

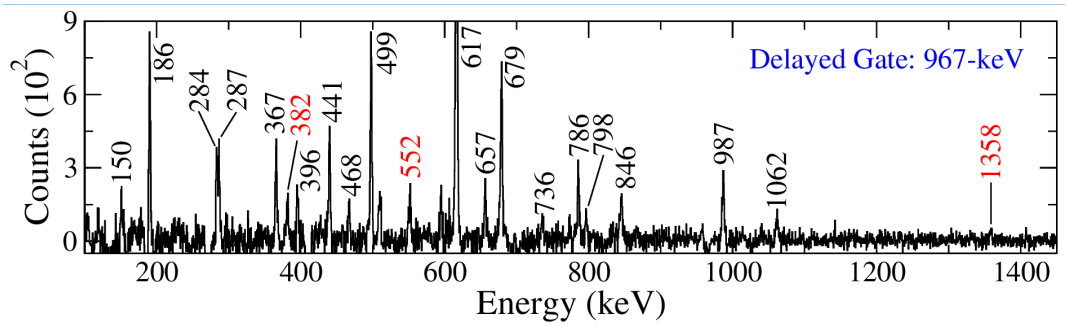

Figure 5.9: Coincidence γ-ray spectrum illustrating the transitions in the early coincidence with the 967 keV ground state transition of ^{201}Bi. The new transitions are marked with red color.

Preliminary data analysis reveals the evidence of several new transitions in addition to the already known information in ^{200,201}Bi. Fig. 5.9 illustrates the transitions observed in early coincidence with the 967 keV ground state transition of ^{201}Bi. The transitions marked in red are the newly identified transitions in ^{201}Bi. A detailed analysis of the data, including the construction of level schemes and spin-parity assignments, is currently in progress.

References:

1. G. Baldsiefen *et al.*, Nucl. Phys. A **592**, 365 (1995).
2. P. J. Dagnall *et al.*, J. Phys. G: Nucl. Part. Phys. **20**, 1591 (1994).

5.1.13 Study of octupole collectivity and octupole (I = 3) isomers in mass A ∼ 200 region

P. S. Rawat[1], S. Kumar[1], Nandini Patel[1], Phurba Sherpa[1], Priyanka[1], Khirush Pegu[1], Mohammad Anser[2], Khushi Singh[3], Rupesh Kushwaha[3], Dhananjaya Sahoo[4], Renu Kumari[1], Anuj[1], Khamosh Yadav[5], Uday Shankar Ghosh[5], Yashraj[5], H. P. Sharma[2], T. Trivedi[3], Indu Bala[5] and R. P. Singh[5]

[1] *Department of Physics & Astrophysics, University of Delhi, New Delhi 110007, India*
[2] *Department of Physics, Banaras Hindu University, Varanasi, Uttar Pradesh 221005, India*
[3] *Department of Physics, Allahabad University, Prajagraj, Uttar Pradesh 211002, India*

[4] *Department of Physics, Indian Institute of Technology, Roorkee, Uttarakhand 247667, India*
[5] *Nuclear Physics Group, Inter-University Accelerator Centre, New Delhi 110067, India*

A variety of nuclear phenomena, from single-particle structure and collective excitations to exotic modes like magnetic rotation, can be explored in neutron-deficient nuclei close to the $N = 126$ shell closure. The nuclear isomerism [1] and decay trends in these nuclei provide important hints on the underlying shell evolution and structural dynamics. In the present work, the focus is on Po isotopes with $N = 120 - 124$ [2-5]. In order to investigate the level structure of these nuclei, the experiments were performed at the Indian National Gamma Array (INGA) facility [6] at IUAC. The INGA setup consisted of 11 HPGe Clover detectors- five detectors at 90^o and three detectors each at 148^o and 32^o. Additionally, one LEPS detector and four $LaBr_3$(Ce) detectors were used.

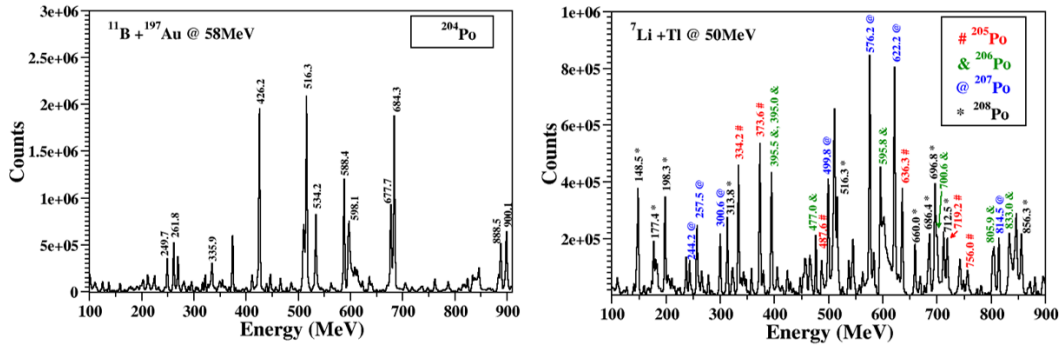

Figure 5.10: (Left) The projection spectrum indicating the γ-rays from ^{204}Po nucleus produced in reaction ^{11}B+^{197}Au at 58 MeV beam energy. (Right) The projection spectrum indicating the γ-rays from $^{205-208}$Po nuclei produced in reaction ^{7}Li+^{nat}Tl at 50 MeV beam energy.

In the first experiment, the ^{197}Au target with thickness $\sim$ 7 mg/cm^2 was irradiated by ^{11}B beam with 58 MeV energy, provided by the 15UD Pelletron tandem accelerator at IUAC, populating the excited levels in ^{204}Po. In the second experiment, a ^{7}Li beam with energy 50 MeV was used, populating $^{205-208}$Po as ERs from reactions with ^{203}Tl and ^{205}Tl present in the ^{nat}Tl foil of thickness $\sim$ 10 mg/cm^2. The events were recorded in singles as well as in $\gamma - \gamma$ coincidence mode using a VME-based data acquisition system [7]. Energy and efficiency calibrations were done by using the standard ^{152}Eu and ^{133}Ba sources. The projection spectrum from the symmetic $\gamma - \gamma$ matrix from the ^{11}B+^{197}Au reaction showed the several known γ-rays in ^{204}Po (shown in the left panel of Fig. 5.10). In the right panel of Fig. 5.10, the γ-rays belonging to $^{205-208}$Po isotopes are marked in the projection spectrum from ^{7}Li+Tl reaction. In order to identify the new γ-rays and extend the level structure of observed nuclei, further analysis of the data is in progress.

References:

1. Swati Garg *et al.*, At. Data and Nucl. Data Tables **150**, 101546 (2023).
2. B. Fant, T. Weckström and A. Källberg, Phys. Scr. **41**, 652 (1990).
3. V. Rahkonen *et al.*, Nucl. Phys. A **441**, 11 (1985).
4. A. M. Baxter *et al.*, Nucl. Phys. A **515**, 493 (1990).
5. A. R. Poletti *et al.*, Nucl. Phys. A **615**, 95 (1997).
6. S. Muralithar *et al.*, Nucl. Instrum. Methods A **622**, 281 (2010).
7. Mamta Jain *et al.*, Rev. Sci. Instrum. **94**, 013304 (2023).

5.1.14 Lifetime measurement of excited states of ^{76}Kr using the Doppler shift attenuation method

A. Choudhary[1], V. Kumar[1], Y. P. Singh[1], Gobind Ram[1], Samant Kumar Yadav[1], M. K. Sharma[1], Abhishek Yadav[2], Dhananjaya Sahoo[3], A. Y. Deo[3], Yashraj[4], U. S. Ghosh[4], Indu Bala[4] and R. P. Singh[4]

[1] *Department of Physics, University of Lucknow, Lucknow 226007, India*
[2] *Department of Nuclear Science and Technology, Amity University, Noida 201302, India*
[3] *Department of Physics, Indian Institute of Technology Roorkee, Roorkee 247667, India*
[4] *Nuclear Physics Group, Inter-University Accelerator Centre, Aruna Asaf Ali Marg, New Delhi 110067, India*

Excited States in ^{76}Kr have been populated via the ^{56}Fe(^{28}Si, 4p4n) reaction at a beam energy of 155 MeV. The mean lifetime of levels from the coincidence spectrum will be extracted [1], based on the Doppler

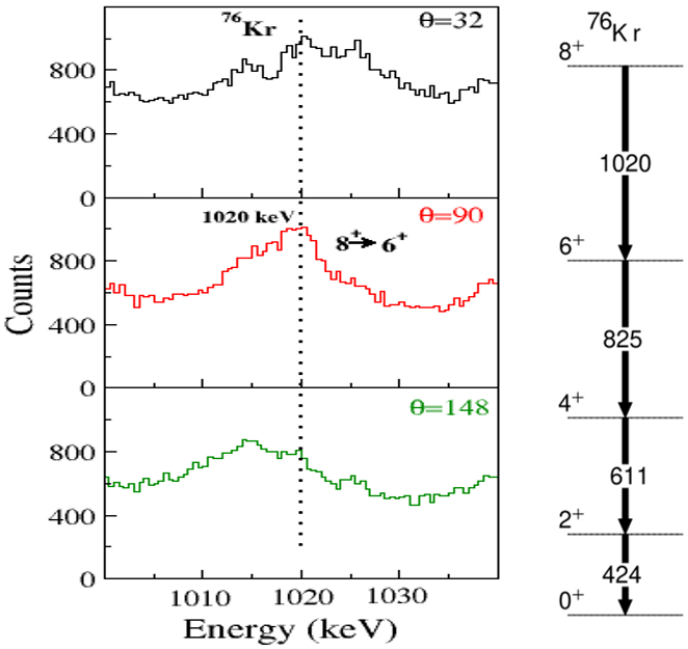

Figure 5.11: Gamma photo-peak of 1020 keV transition from detectors placed at 32^o, 90^o and 148^o. Partial level Scheme of ^{76}Kr is shown on the right.

Shift Attenuation Method (DSAM). The spectra of the shifted and the unshifted components for the 1020 keV γ-transition at detector angles of 32^o, 90^o and 148^o are shown in the Fig. 5.11.

References:

1. J. C. Wells and N. R. Johnson, ORNL-6689, p. 44 (1991).

5.2 Materials science

D. Kabiraj, V. V. Sivakumar and F. Singh

The materials science facilities support various research programs of users in collaborative manner on ion beam based research utilizing the online facilities and the facilities for materials characterizations. This year, a total of 115 shifts were utilized by the 34 users from various universities / institutes, including the users from abroad (USA, Japan and Algeria). A total of 11 thesis experiments were performed, involving 31 shifts. A total 21 shifts were utilized by the ISRO (Indian Space Research Organization) for testing their device performance under the irradiation conditions to check the single event upset. The testing was jointly performed by the ISRO Bangalore and the Semiconductor Laboratory, Mohali. As for the last few years, there was no beam time loss due to any major facility breakdown in the two beamlines for materials science experiments.

The materials science beamline in the BH-II is specifically designed and developed to perform the in-situ irradiation experiments, including in-situ X-ray diffraction, in-situ micro-Raman, in-situ high-temperature irradiation, and in-situ XRD in controlled gas environment. This year, three high-temperature irradiation experiments at $\sim$ 1000 K were performed by utilizing a total of 15 shifts of beam time. The first test experiment in association with Prof. S. V. S. Nageshwar Rao from Central University of Hyderabad, using the Ne (36 MeV) beam from the High Current injector in BH-II, was performed during January 17 - 19, 2025. This was to explore the feasibility of conducting materials science experiments using the HCI beam with and without acceleration by linac in the near future. The results of the experiments are under analysis.

Apart from ion beam facilities, the group also provides support to the users for characterization and analysis of the samples used for their studies on the effect of ion beam irradiation. The facilities in the Centre for Materials Characterization and Measurement, transmission electron microscope (TEM) laboratory

and the in-situ facilities of the Materials Science group are extensively used. The scheduling of the characterization requests are processed through Facility Utilization Request Form, available online. During this period, more than 1280 measurements on samples of users were performed using the structural (XRD: 150 samples of 30 users), optical (FTIR: 213 spectra of 13 users, UV-Vis-NIR: 222 spectra of 17 users, UV-Vis: 112 samples of 12 users), microscopy (SEM: 380 samples of 61 users, SPM: 52 samples of 11 users, TEM: 110 samples of 35 users) and transport (41 users) facilities, and contact angle measurement set-up (45 samples of 6 users). The TEM specimen preparation facility has been utilized to prepare approximately 50 TEM samples including 10 XTEM and 04 planar samples by various users. The radio-frequency (RF) sputtering system and electron-beam evaporation system were used for the growth of 75 thin films of 11 users.

There were more than 116 publications in reputed journals such as ACS Omega, Applied Surface Science, Applied Physics A, Journal of Physics D, Journal of Physical Chemistry C, Physica B, Ceramic International, Radiation Physics and Chemistry, Journal of Alloys and Compounds etc., where many interesting results in the various areas of research, including those on nanocomposites, track formation, DFT calculations, velocity and synergetic effects, band gap tuning, etc. are reported. A list of publications is given in Chapter 6.

A summary of the reports from the users is presented here. Structural and microscopic studies were performed to understand the effect of Au, Ag (100 MeV), and O (90 MeV) ion-irradiation on NASICON ($Na_3Zr_2Si_2PO_{12}$) ceramics. The XRD analysis shows no additional peak formation upon irradiation, excluding new phase formation. However, peak intensity decreases and broadening increases with increasing ion fluence. Au and Ag-irradiated samples exhibit amorphization above 5×10^{12} ions/cm^2, while the crystal structure remains intact for O irradiated samples. Au and Ag irradiation induces increasing strain with fluence, leading to amorphization. TEM micrographs of irradiated samples confirm damage through visible track formation in Au and Ag. $NaLi_2PO_4$:X OSL dosimetry materials (pellet and film forms) were irradiated with 80 MeV C and compared with that of gamma rays. Dosimetric evaluation using CW-OSL with blue light stimulation ($\lambda \approx 470$ nm) shows high sensitivity (6 times with gamma and 9 times with C^{6+} more sensitive than the commercially available Al_2O_3:C phosphor) in the linear dose range of (01 Gy – 01 kGy) when irradiated with gamma source and 1×10^{10} –1×10^{12} when irradiated with C^{6+} at 80 MeV. The high sensitivity and low Z_{eff} value make this material suitable for compact online dosimetry using optical fiber and small photodetectors in cancer radiotherapy applications involving gamma, proton, or hadron beams. The effects of 100 MeV Au^{8+} and Ni^{8+} ions irradiation of Se-Te-Sn-Ag thin films are studied. Remarkable structural phase transition has been observed with SHI irradiation by varying ion fluence and choice of ion. Surface topography was highly influenced by the choice of ion. The transport properties of SHI-irradiated samples infer that the material will be highly suitable for thermoelectric and phase-change memory applications. Irradiation of Sb and Sm doped Co_3O_4 thin films grown by PLD, was carried out by 140 MeV Ag 11^+ ions to study the effect of irradiation on structural and magnetic properties. The morphology of the thin film is drastically changed with irradiation. The irradiated samples show radiation-induced densification. The magnetoelectric coupling shows an increase with irradiation. The impact of SHI was observed in the ferrimagnetic properties of the thin film studied for different temperatures from 20 K to 300 K. The results indicate that the irradiation with Ag ions changes the properties. All the pristine and irradiated thin films show a ferromagnetic hysteresis loop at all the measured temperatures. However, the overall magnetism of the material changes with the SHI irradiation. $Ge_2Sb_2Te_5$ (GST) is a suitable material for energy harvesting as a thermoelectric. Ion irradiation of Te-based materials is a promising approach for improving the performance and stability of these materials. The crystal structure can be modified by bombarding these materials with ions, reducing thermal conductivity while maintaining high electrical conductivity. In this study GST thin films are irradiated with high-energy beam of Ag 11^+ ions of 140 MeV. The studies and analysis of structural, morphological, and electrical transport properties through these characterization techniques explore the possibility of optimizing GST thin films by means of regulated ion irradiation. PLD-grown NiO epitaxial films irradiated with 300 keV Ar-ions shows reduction in edge dislocation density and decrease of resistivity by more than three orders of magnitude when irradiated with ion fluence of 1×10^{15} ions/cm^2. Nanostructures of Au single-layer, Au/Ag bi-layer, and Au/Ag/Au/Ag four-layer thin films are irradiated with low energy Kr ions at fluences of 1×10^{15} and 3×10^{15} ions/cm^2. These nanostructured films were employed for dye molecule detection. Surface-Enhanced Raman Spectroscopy (SERS), due to their wide tunability of localized surface plasmon resonance across a broad wavelength range. The surface morphology and microstructural analysis indicated the formation of different nanostructures with different ion fluences by atomic force microscopy and field emission scanning electron microscopy. Rutherford backscattering spectrometry results indicate a considerable change in film thickness after ion irradiation, mainly due to the removal of surface atoms due to sputtering. Oxygen incorporation in iron pyrite thin film using

120 keV O implantation results in progressive broadening of the Raman peaks with increasing ion fluences suggesting crystal damage. The strain caused by the implantation also causes the blue shift of the A_{1g} mode. The Raman spectrum of the 1×10^{16} ions/cm^2 dose reveals the existence of the Fe_3O_4 phase. 100 keV Ag ions were implanted at different fluences to investigate their influence on the structural, optical properties, and photovoltaic device performance of irradiated TiO_2 films. Dye sensitized solar cell (DSSC) fabricated with Ag-irradiated TiO_2 exhibited a significant increase in power conversion efficiency compared to pristine TiO_2-based cells. This improvement is attributed to reduced charge recombination and enhanced electron mobility. These findings suggest that silver ion beam irradiation is a promising strategy for optimizing TiO_2 photoanodes in next-generation DSSCs. Argon ions with an energy of 150 keV were used CuCrZr alloy. The accumulation of heavy strain in the lattice due to energy deposition by ion irradiation is evidenced by the variation in FWHM of the XRD peaks with fluence. Post irradiation, scanning electron microscopy (SEM) analyses of CuCrZr alloy revealed significant surface modifications. Argon (120 keV), Helium (100 keV), and Nitrogen (220 keV) ions were irradiated to tune thermoelectric properties of metal chalcogenides based thin films of Bi_2Te_3 and Sb_2Te_3 having variable thicknesses (100–200 nm). XRD studies revealed that the thin films are polycrystalline and exhibit notable structural modifications upon irradiation. PM6 and PTB7-Th films were irradiated with Au ions at a fluence of 1×10^{13} ions/cm^2 at an energy of 70 keV. Upon irradiation it is observed that the absorption and photoluminescence spectra shifted closer to the UV region, which is beneficial for organic solar cells intended for space applications. The Raman spectra showed minimal shifts, and XPS spectra revealed that PTB7-Th has a more robust chemical structure, particularly due to the attachment of oxygen to a single carbon chain and the presence of only one fluorine atom. Tellurium (Te) thin films (16 nm) deposited on Si substrates are irradiated with a 400 keV Kr 2^+ ion beam of varying fluence of 1×10^{13}, 5×10^{13}, and 1×10^{14} ions/cm^2. The effect of irradiation shows rapid decrease in activation energy at both band-to-band conduction and nearest neighbour hopping (NNH) conduction. Hall measurements elucidate a reduction in carrier concentration and an increase in mobility due to irradiation. Highly c-axis oriented nanocrystalline ZnO thin films deposited on Si substrates using rf sputtering method were irradiated by 1.8 MeV Argon ion and implanted with 80 keV Silver (Ag) ion. The effect on the structural and optical properties were compared by utilizing XRD and UV-Vis spectrophotometry measurements performed on the pristine and implanted thin films.

The 8th International Conference on Ion Beams in Materials Engineering and Characterization (8th IBMEC-2024) was organized at IUAC during December 3-6, 2024. The International School on Microscopic Characterization Techniques (TEM/SEM/AFM) was held at IUAC during December 9-12, 2024. The details of which can be found in Chapter 6.

5.2.1 Effect of 300 keV Ar-ions irradiation on structural and electrical properties of PLD-grown NiO epitaxial films

Bhabani Prasad Sahu[1], Umakanta Patra[1], Monu Kataria[2], Debdulal Kabiraj[2], Subhabrata Dhar[1]

[1] *Department of Physics, Indian Institute of Technology Bombay, Mumbai-400076, India.*
[2] *Inter-University Accelerator Centre, Aruna Asaf Ali Marg, New Delhi, 110067, India.*

In this study, the effect of Ar-ions irradiation on structural and electrical properties of (111)NiO epitaxial films are investigated. The NiO films are grown on c-sapphire substrates using pulsed laser deposition (PLD) technique. Details of the growth process can be found elsewhere [1]. The Ar ions used during irradiation are in the charge state of +3 and beam energy of 300 keV. The ion fluences (F) are varied from 1×10^{14} to 1×10^{16} ions/cm^2. Structural properties of these layers are investigated by X-ray diffraction (XRD). The study reveals that the epitaxial nature of the layer remains intact after irradiations. Full width at half maximum (FWHM) of XRD rocking curves for (111)NiO and (2$\bar{2}$0)NiO reflections is plotted as a function of Ar ion fluence F [see Fig. 5.12(a)]. The decrease in FWHM of (2$\bar{2}$0)NiO reflection with increase in F suggests the reduction of edge dislocation density in the layers with Ar-ion irradiation. However, FWHM of (111) reflection of NiO is found to be maximum at $F = 1 \times 10^{15}$ ions/cm^2.

Two probe current-voltage characteristics are recorded for all samples. Ag contact is used as the contact metal for the measurement. Fig. 5.12(b) shows the variation of resistivity estimated in these layers with the fluence. Interestingly, resistivity is found to decrease by more than three orders of magnitude when irradiated with an Ar-ion fluence of 1×10^{15} ions/cm^2. Resistivity does not change much when F is further increased. This may suggest that the material has a limit of accommodating the Ni-vacancy-related defects. This sharp

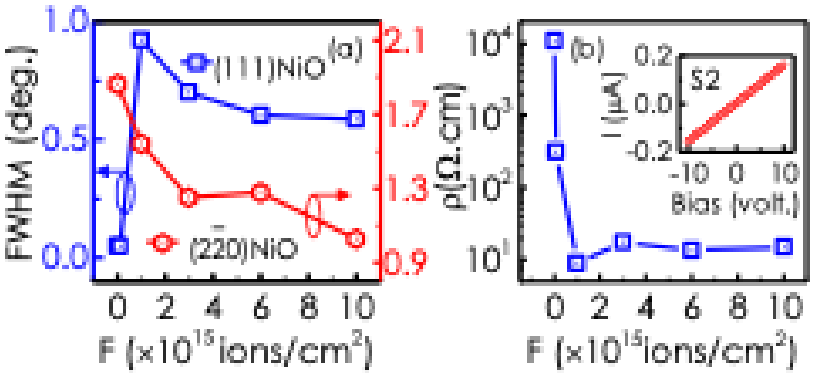

Figure 5.12: (a) Full width at half maximum (FWHM) of the XRD rocking curves for (111) and (2$\bar{2}$0) NiO reflections as a function of Ar-ion fluence (F). (b) Resistivity of the films plotted as a function of F. Inset shows the current-voltage characteristic profile obtained for sample irradiated with 1×10^{14} ions/cm^2, suggesting the ohmic nature of Ag contact.

decrease in resistivity can be attributed to the increase in the density of Ni-vacancy-related defects that act as shallow acceptor states in NiO. It is to be noted that NiO often exhibits p-type conductivity, which is attributed to Ni-vacancy-related defects [2]. To obtain the carrier concentrations and mobilities in these layers, field effect transistor (FET) structures with Al_2O_3 top gate are fabricated with these samples. The analysis is currently underway.

References:

1. Bhabani P. Sahu, Poonam Sharma, Alok Shukla and Subhabrata Dhar, *J. Phys. D: Appl. Phys.* **58**, 085302 (2025).
2. Dawson J. A., Guo Y., and Robertson J., *Appl. Phys. Lett.* **107**, 122110 (2015).

5.2.2 Low energy ion irradiation induced Au/Ag multilayer nanostructured substrates for SERS-based molecular sensing

Om Prakash[1], Abhijith T[2,3], G. R. Umapathy[4], Supravat Karak[2], Udai B. Singh[5], Santanu Ghosh[1]

[1] *Nanostech Laboratory, Department of Physics, Indian Institute of Technology Delhi, New Delhi 110016, India*
[2] *Organic and Hybrid Electronic Device Laboratory, Deptt. of Energy Science and Engineering, IIT Delhi, New Delhi 110016, India*
[3] *Department of Nanoscience and Technology, PSG Institute of Advanced Studies, Peelamedu, Coimbatore, 641004, India*
[4] *Inter-University Accelerator Centre, Aruna Asaf Ali Marg, New Delhi 110067, India*
[5] *Department of Physics, Deendayal Upadhyay Gorakhpur University, Gorakhpur 273009, India*

Au and Ag are the most prominent plasmonic materials used in Surface-Enhanced Raman Spectroscopy (SERS) due to their wide tunability of localized surface plasmon resonance across a broad wavelength range [1]. In this study, nanostructures of Au single-layer, Au/Ag bi-layer, and Au/Ag/Au/Ag four-layer thin films were fabricated on silicon substrates and irradiated with low energy Kr^{++} ions at fluences of 1×10^{15} and 3×10^{15} ions/cm^2. These nanostructured films were employed for dye molecule detection.

Surface morphology and microstructural analyses, conducted via atomic force microscopy (AFM) and field emission scanning electron microscopy (FESEM), revealed formation of distinct nanostructures depending on ion fluence. Rutherford backscattering spectrometry (RBS) confirmed film thickness reduction post-irradiation due to surface atom sputtering.

Among the different samples, the bi-layer Au–Ag substrate exhibited the highest enhancement in Raman signal of Rhodamine 6G (R6G), achieving an enhancement factor of 4.78×10^6 at the 1516 cm^{-1} SERS peak. Additionally, trace detection of Coumarin 343 demonstrated the substrate's sensitivity. Finite-difference time-domain (FDTD) simulations supported experimental SERS data by highlighting the localized field enhancement or 'hot-spots' arising from the nanostructures [3].

References:

1. K. H. Rieder *et al.*, Probing Single Molecules and Single Nanoparticles by Surface-Enhanced Raman Scattering, Springer (1994).
2. H. Liu *et al.*, Single molecule detection from a large-scale SERS-active $Au_{79}Ag_{21}$ substrate, *Sci. Rep.* 1 (2011).
3. Y. Jing *et al.*, *Adv. Compos. Hybrid Mater.* **4**, 885 (2021).

5.2.3 Structural and microscopic studies of ion-irradiated NASICON ($Na_3Zr_2Si_2PO_{12}$) ceramics

Ramcharan Meena[1] and Rajendra Singh Dhaka[2]

[1] *Material Science Group, Inter-University Accelerator Center, Aruna Asaf Ali Marg, New Delhi 110067, India*
[2] *Department of Physics, Indian Institute of Technology Delhi, New Delhi 110016*

The NASICON samples having the chemical composition of $Na_{1+x}Zr_2Si_xP_{3-x}O_{12}$ ($0 < x < 3$) are of great interest due to their potential application as a solid-state electrolyte material in Na-ion-based solid-state batteries. The highest conductivity is observed for the $Na_3Zr_2Si_2PO_{12}$ ($x = 2$) bulk ceramics [1]. Conductivity and other physical properties explained in the literature are mainly related to the structural arrangements. Hence, structural stability must be checked for all practical applications in different environments, including irradiation environments.

In this work, the ion-irradiation response of $Na_3Zr_2Si_2PO_{12}$ was checked using the high-energy ions of Au, Ag (100 MeV), and O (90 MeV) in the fluence range of 5×10^{11} to 5×10^{13} ions/cm^2. The crystal structure before and after irradiation was checked using the GIXRD (glancing angle X-ray diffraction) and electron diffraction (ED). The microscopic imaging was performed using a transmission electron microscope (TEM) in bright field mode.

The bulk NASICON, with a chemical composition of $Na_3Zr_2Si_2PO_{12}$, was prepared using the solid-state reaction method. For microstructural analysis, the colloidal suspension of NASICON was deposited onto Cu grids covered with amorphous carbon (200 mesh) by drop-casting. Ion irradiation was performed at the Inter-University Accelerator Center (IUAC), New Delhi, using the 15 UD Pelletron accelerator at the material science beamline (Phase-1). The electronic (Se) and nuclear (Sn) energy losses were calculated using SRIM-2013 software in full damage cascades mode [2]. It was found that for selected energies, the dominant energy loss mechanism was electronic excitation. The calculated Se and Sn values are shown in Table 5.1.

Table 5.1: Comparison of electronic (Se) and nuclear energy loss (Sn) for Au, Ag, and O ions in NASICON.

Ion and energy	Se (keV/nm)	Sn (keV/nm)	Range (μm)
Au (100 MeV)	16.72	0.315	11.38
Ag (100 MeV)	14.41	0.075	11.93
O (90 MeV)	0.99	0.0005	63.50

The XRD analysis shows no additional peak formation upon irradiation, excluding new phase formation. However, peak intensity decreases and broadening increases with increasing ion fluence. Au and Ag-irradiated samples exhibit amorphization above 5×10^{12} ions/cm^2, while the crystal structure remains intact for O-irradiated samples. The damage is explained by Coulomb explosion or thermal spike models [3,4]. Strain analysis from XRD (Figure 1(b)) shows that O-ion irradiation produces nearly constant strain across all fluences, whereas Au and Ag irradiation induces increasing strain with fluence, leading to amorphization. Swelling-type effects due to Au and Ag irradiation were also observed [5].

TEM micrographs of irradiated samples confirm damage through visible track formation in Au and Ag cases. Electron diffraction confirms the preserved crystalline nature of O-irradiated samples.

References:

1. Kushal Singh, Anjan Chakraborty, Raghunayakula Thirupathi and Shobit Omar, Ionics **28**, 5289 (2022).
2. James F. Ziegler, M.D. Ziegler and J.P. Biersack, Nucl. Instrum. Methods Phys. Res. B **268**, 1818 (2010).
3. W.J. Weber, Nucl. Instrum. Methods Phys. Res. B **166**, 98 (2000).
4. M. Toulemonde and C. Dufour, Phys. Rev. B **46**, 14362 (1992).
5. Parswajit Kalita et al., J. Appl. Phys. **122**, 025902 (2017).

5.2.4 Systematic study of oxygen incorporation in iron pyrite thin film using O^- implantation

Rudra Narayan Chakraborty[1], Kshetrimayum Devarani Devi[2], Debdulal Kabiraj[2] and Kasilingam Senthilkumar[1]

[1] *Department of Physics, National Institute of Technology Meghalaya, Cherrapunji 793108, India*
[2] *Inter-University Accelerator Centre, Aruna Asaf Ali Marg, New Delhi 110067, India*

Despite its appealing optoelectronic properties, the electrical behavior of FeS_2 remains a subject of active investigation. While bulk FeS_2 is reported to exhibit n-type conductivity, several studies on thin films have observed p-type behavior. The origin of this unexpected p-type conductivity in FeS_2 thin films remains unclear. However, it is often linked to the unintentional incorporation of impurities (O, P, As, Sb, Co, and Ni) during film growth. Among these, oxygen has been frequently suggested as a possible contributor. Understanding the role of oxygen incorporation could provide valuable insight into the conductivity behavior of FeS_2 thin films.

However, achieving controlled oxygen doping in FeS_2 thin films remains a significant challenge. Because of higher electronegativity compared to sulfur, the creation of Fe-O is more favorable than Fe-S. This often leads to excessive incorporation and distortion of the desired stoichiometry. Therefore, a more precise method is required to explore the influence of oxygen on the electrical properties of FeS_2. Low-energy oxygen ion implantation presents a promising strategy, as it enables controlled incorporation of oxygen atoms without causing major damage to the crystal structure. Furthermore, the use of negatively charged oxygen ions is particularly advantageous, as it eliminates surface charging effects typically associated with positive ion implantation. This will allow more uniform implantation and accurate investigation of oxygen-induced modifications in FeS_2 thin films.

Phase-pure iron pyrite thin films, deposited using sputtering, were implanted with singly negatively charged oxygen ions at an energy of 120 keV. The implantation was carried out at the Negative Ion Implanter Beam Facility (NIIBF) at the Inter-University Accelerator Centre (IUAC), New Delhi. The ion doses were varied between 9×10^{14} and 1×10^{16} ions cm^{-2}. The progressive broadening of the Raman peaks can be seen in Fig. 5.13, suggesting crystal damage. The strain caused by the implantation also causes the blue shift of the A_{1g} mode (S–S in-phase stretch, 377.4 cm^{-1}). The Raman spectrum of the 1×10^{16} ions cm^{-2} dose reveals the existence of the Fe_3O_4 phase (694.2 cm^{-1}). The structural and electrical transport properties of these thin films are currently under investigation to reveal the effects of systematic oxygen doping on the behavior of iron pyrite thin films.

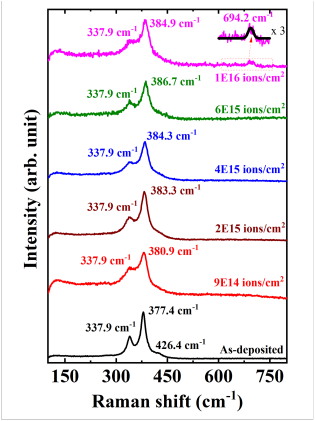

Figure 5.13: Raman spectra.

References:

1. R. Sun, M. K. Y. Chan, S. Kang and G. Ceder, Phys. Rev. B **84**, 035212 (2011).
2. J. Hu, Y. Zhang, M. Law and R. Wu, Phys. Rev. B **85**, 085203 (2012).
3. R. N. Chakraborty, D. S. Mahanta, S. Mazumder and K. Senthilkumar, Phys. Scr. **99**, 055953 (2024).

5.2.5 Role of ion beams in dye sensitized solar cells

Allwin Rajesh Somu[1], Ragavendran Venkatesan[1], Jayanthinath Mayandi[1] and Indra Sulania[2]

[1] *Department of Materials Science, School of Chemistry, Madurai Kamaraj University, Madurai 625021, India*
[2] *Inter-University Accelerator Centre, Aruna Asif Ali Marg, New Delhi 110067, India*

Ion beam irradiation has emerged as a promising technique to enhance the performance of titanium dioxide (TiO_2) in dye-sensitized solar cells (DSSCs) by introducing controlled defects and modifying surface morphology and electronic properties [1]. In this study, TiO_2 films were modified via low energy silver (Ag) ion beam irradiation to enhance their performance as photoanodes in DSSCs. Ag ions were implanted at different fluences to investigate their influence on the structural, optical properties, and photovoltaic device performance of irradiated TiO_2 films [2].

After performing post-treatment, the films were irradiated with 100 keV Ag^+ ions using a low-energy ion beam at three different fluences: 1×10^{14} ions/cm^2, 5×10^{14} ions/cm^2 and 5×10^{15} ions/cm^2 at the NEIB facility at IUAC.

X-ray diffraction (XRD), scanning electron microscopy (SEM), and energy dispersive X-ray spectroscopy (EDAX) were employed to characterize both pure and Ag ion-irradiated TiO_2 films. The results indicated enhanced crystallinity, increased surface roughness, and the presence of silver ions in the irradiated samples. From Fig. 5.14(a), XRD analysis shows that the anatase phase of pure TiO_2 remains unchanged after irradiation, indicating that Ag ion irradiation did not significantly alter the crystal structure. SEM micrographs show well-defined microspheres in pristine TiO_2, which became agglomerated after irradiation. EDAX confirmed the presence of silver, thereby verifying successful ion implantation.

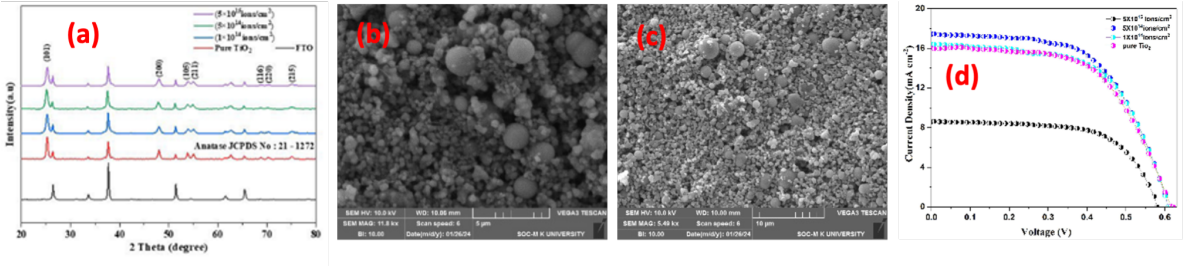

Figure 5.14: (a) XRD pattern of pure and irradiated TiO_2 thin films at different fluences, (b) and (c) SEM images of Ag ion-irradiated TiO_2 microspheres and (d) I-V characteristics of pure and Ag-irradiated devices.

DSSCs fabricated with Ag-irradiated TiO_2 exhibited a significant increase in power conversion efficiency compared to pristine TiO_2-based cells. This improvement is attributed to reduced charge recombination and enhanced electron mobility. These findings suggest that silver ion beam irradiation is a promising strategy for optimizing TiO_2 photoanodes in next-generation DSSCs.

References:

1. Vinodhini, J., Mayandi, J., Atchudan, R., Jayabal, P., Sasirekha, V., and Pearce, J. M., Ceramics International **45**, 4667 (2019).
2. Selvapriya, R., Sasirekha, V., Vajeeston, P., Pearce, J., and Mayandi, J. (2021), Ceramics International **47**, 8094 (2012).

5.2.6 Effect of 150 keV Ar irradiation on Cu-alloy and ceramic

Sejal Shah[1,2], Prashant Sharma[1], S Lakshmi Kanth Konuru[1], Indra Sulania[3] and S. A. Khan[3]

[1] *ITER-India, Institute for Plasma Research, Gandhinagar, India*
[2] *Homi Bhabha National Institute, Anushakti Nagar, Mumbai, India*
[3] *Inter-University Accelerator Centre, Aruna Asaf Ali Marg, New Delhi, India*

The Argon-ion irradiation experiments were carried out at the Low Energy Ion Beam Facility of IUAC. The aim was to study the effects of ion irradiation on materials for reactor applications, focusing on their mechanical, morphological, damage, and structural properties. Argon ions (Ar^{2+}) with an energy of 150 keV were used for irradiation, with beam currents between 500 nA and 1 μA. The fluence / exposure time was varied to assess irradiation effects on material properties.

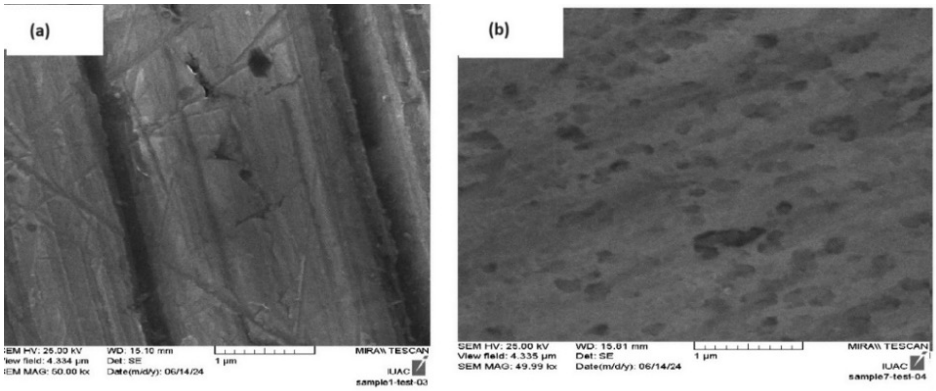

Figure 5.15: SEM micrographs of (a) pristine CuCrZr and (b) irradiated CuCrZr.

Irradiation was conducted on Cu alloys and Al_2O_3 and its composites using a 1 µA current for the fluence ranging from 5×10^{13} to 3.6×10^{16} ions/cm^2. Post irradiation, scanning electron microscopy (SEM) analyses of CuCrZr alloy revealed significant surface modifications. This analysis was performed at IUAC, New Delhi. The results are shown in the figure below. Further, SEM of neutron-irradiated samples was also carried out. Further analysis of these samples is ongoing and will be reported in future work. GIXRD was performed at UGC-DAE-CSR, Indore to understand phase stability of alumina composites post irradiation. CuCrZr XRD

data showed clear signs of strain accumulation with increasing fluence, highlighting the material's evolving microstructure under irradiation.

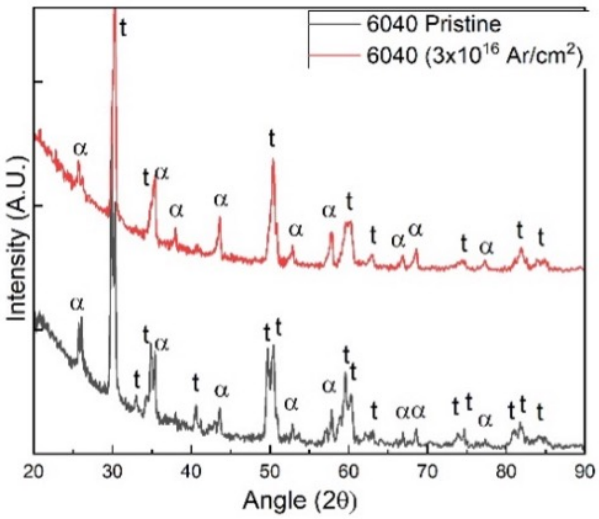

Figure 5.16: XRD graph of 6040 composite.

These findings underscore the complex interplay between ion fluence and material composition in determining radiation response. The accumulation of heavy strain in the lattice due to energy deposition by ion irradiation is evidenced by the variation in FWHM of the XRD peaks with fluence.

References:

1. S. Lakshmi Kanth Konuru, Prashant Sharma, Anil Tyagi, M Abhangi *et al.* (submitted).

5.2.7 Tuning the thermoelectric properties of metal chalcogenides based thin films by low energy ion beam irradiation

Kachhara Chetan[1], Sharma Pradeep Kumar[2], Asakho[1] and Kedia Sanjay[3]

[1] *Department of Physics, Kohima Science College, Jotsoma, Kohima 797002, India*
[2] *Department of Physics, Shyam Lal College, University of Delhi, Delhi 110032, India*
[3] *Inter-University Accelerator Centre, Aruna Asaf Ali Marg, New Delhi 110067, India*

Thermoelectric energy harvesting has emerged as a clean and environmentally friendly technique in the last decade to capture the waste heat and convert it into useful electric energy. The thermoelectric energy conversion efficiency of thermoelectric materials is positively related to the dimensionless figure of merit (zT), which in turn reflects a complex interrelated dependency of thermoelectric parameters, namely the Seebeck coefficient, electrical conductivity, and electronic thermal conductivity. Motivated by the successful decoupling of these parameters in nanostructured materials, we attempted to enhance the thermoelectric properties in metal-chalcogenides-based materials using low energy ion beam irradiation.

High-quality thin films of Bi_2Te_3 and Sb_2Te_3 having variable thicknesses (100–200 nm) have been successfully deposited using RF sputtering. The deposited thin films have been irradiated with low energy Argon (120 keV), Helium (100 keV), and Nitrogen (220 keV) ions with fluences ranging from 10^{14}–10^{16} ions/cm^2 for different durations, focusing on their transport and structural properties.

X-ray diffraction (XRD), Scanning Electron Microscopy (SEM), and Transmission Electron Microscopy (TEM) analyses have been performed on both pristine and ion beam irradiated thin films to investigate the effects of phase and microstructure on charge transport properties. The XRD studies revealed that the thin films are polycrystalline and exhibit notable structural modifications upon irradiation.

References:

1. P. J. McWhorter and P. S. Winokur, Appl. Phys. Lett. **48**, 133 (1986).

5.2.8 Optically stimulated luminescence studies in $NaLi_2PO_4$:X Phosphor irradiated with γ-rays and high energy C^{6+} ion beam for applications in radiation-hadron therapy

Martina Saran[1], P. D. Sahare[2] and Ambuj Tripathi[1]

[1] *Inter-University Accelerator Centre, Aruna Asaf Ali Marg, New Delhi 110067, India*
[2] *Department of Physics and Astrophysics, University of Delhi, Delhi 110070, India*

Optically stimulated luminescent detectors (OSLDs) have a number of advantages over thermoluminescence detectors (TLDs) in radiation dosimetry, making them excellent dosimeters for quality assurance and patient dose verification. Although OSLDs have been investigated in several modalities, relatively little work has been done in examining them for use in clinical beams [1]. This study examines the characteristics of OSLD response in clinical hadron therapy. There is a continuous need to find better dosimetric materials, as Al_2O_3:C is currently the only commercially available OSL dosimeter. The optical nature of the phosphate-based OSLD readout process allows the use of dosimeter samples in various physical forms (chips, fibres, powders, thin films, etc.) [2]. This, combined with the material's intrinsic high sensitivity, enables applications in personal, environmental, medical, and space dosimetry.

The objective of this work is to demonstrate that synthesized $NaLi_2PO_4$:X OSL dosimetric materials (pellet and film forms) exhibit excellent response for hadron therapy dosimetry, with minimal reduction in luminescence detector efficiency under particle beam exposure. Hadron beams used in radiotherapy (protons, neutrons, helium, carbon, oxygen, and neon ions) offer physical and radiobiological advantages over conventional photon beams and are already being used in countries such as the UK, USA, and Russia for cancer treatment [3]. Given the shortcomings of Al_2O_3:C, there is a pressing need to develop alternative OSLDs with features like linear dose response, minimal fading, and high saturation levels.

The synthesized $NaLi_2PO_4$:X phosphor, optimized with 0.0X mol% cerium nitrate doping and annealed at 400°C for 1 hour, was prepared via a solid-state diffusion method. XRD characterization confirmed single-phase formation with an orthorhombic structure (space group Pnma, JCPDF #98-006-9967). Dosimetric evaluation using CW-OSL with blue light stimulation ($\lambda \approx 470$ nm) shows high sensitivity—6 times greater with gamma rays and 9 times greater with C^{6+} beams—than Al_2O_3:C over a linear dose range of 0.1 Gy – 1 kGy (gamma) and fluence of 1×10^{10} – 1×10^{12} (C^{6+}, 80 MeV).

The material exhibits favorable properties such as simple synthesis, tissue equivalence ($Z_{eff} \approx 10.8$), wide dose and fluence range (0.1 Gy – 32 kGy; 1×10^{10} – 1×10^{13}), and suitability for photon and hadron therapy dosimetry. Further comparative studies on dose-response, fading, and reusability were conducted under gamma and high-energy ion beam (C^{6+}) irradiation. A theoretical CW-OSL curve fitting was used to analyze decay constants and photo-ionization cross-sections, relevant for personal dosimetry applications. The high sensitivity and low Z_{eff} value make this material suitable for compact online dosimetry using optical fiber and small photodetectors in cancer radiotherapy applications involving gamma, proton, or hadron beams [4].

References:

1. Radiation Protection Dosimetry (2004), Vol. 109, No. 4, pp. 269–276.
2. Med. Phys. **39**, (2012).
3. Eur. J. Cancer **34**, 459 (1998).
4. J. Lumin. **238**, 118207 (2021).

5.2.9 Comparative analysis of the radiation hardness of PM6 and PTB7-Th for space application in organic solar cell

Anuradha[1], Kshetrimayum Devrani Devi[2], Fouran Singh[2] and Rahul Singhal[1]

[1] *Department of Physics, Malaviya National Institute of Technology, Jaipur, Rajasthan, India*
[2] *Inter-University Accelerator Centre, Aruna Asaf Ali Marg, New Delhi 110067, India*

In this experiment, the solutions of PM6 and PTB7-Th were first prepared. 5 mg of PM6 was dissolved in 2.5 mL of chlorobenzene, with thorough mixing achieved using an ultrasonic bath. The dissolution was completed within 15 minutes, resulting in a homogeneous solution. A similar procedure was followed for PTB7-Th, with 5 mg of the material dissolved in chlorobenzene using the ultrasonic bath. The thin films were then spin-coated onto glass substrates. The spin coating was performed using an NXG-m1 spin coater,

applying the materials at four different rotational speeds: 600 rpm, 800 rpm, 1500 rpm, and 3000 rpm, onto 1 cm by 1 cm substrates. Both PM6 and PTB7-Th were coated at these speeds to investigate their film quality and properties under varying spin coating conditions. After preparing the thin films, we subjected them to ion beam irradiation. The films were irradiated with Au ions at a fluence of 1×10^{13} ions/cm^2 at an energy of 70 keV, using the ion implanter accelerator facility at IUAC. This step aimed to induce changes in the structural and electronic properties of the films.

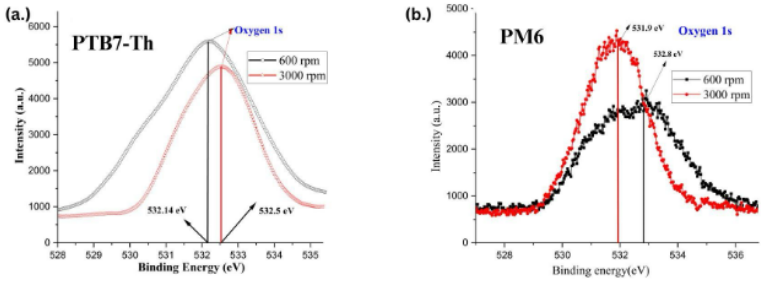

Figure 6: Effect of ion beam on oxygen element present in PTB7-Th and PM6 studied with help of X-ray photoelectron spectroscopy (XPS)

Figure 5.17: Effect of ion beam on oxygen element present in PTB7-Th and PM6 studied with the help of X-ray photoelectron spectroscopy.

To characterize the irradiated samples, we employed several techniques. The excitation source was a 532 nm laser operating at 15 mW, allowing us to observe the PL spectra of all irradiated samples.Similarly, we studied the Raman spectra of the samples using the same high-resolution spectrometer, with a 532 nm laser operated at 25 mW as the excitation source. The absorption spectra of the irradiated PM6 and PTB7-Th thin films were recorded using a UV-Visible spectrometer to assess their optical properties. Furthermore, we utilized X-ray photoelectron spectroscopy (XPS) to investigate the elemental composition and oxidation states of the materials. To analyze the morphological properties of the thin films, we employed Atomic Force Microscopy (AFM), which provided detailed insights into the surface topography of the films. This comprehensive set of experimental procedures and characterization techniques allowed us to thoroughly study the properties and behaviors of the PM6 and PTB7-Th materials after irradiation, contributing to a better understanding of their potential for use in space applications.

We have reported that both PM6 and PTB7-Th exhibit nearly identical modifications in optical properties, as observed through UV-visible, Photoluminescence, and Raman spectroscopy. However, upon irradiation, we found that the absorption and photoluminescence spectra shifted closer to the UV region, which is beneficial for organic solar cells intended for space applications. The Raman spectra showed minimal shifts, indicating slower vibrational modes, suggesting improved lifetime and stability in space. While no significant differences were observed in the optical and vibrational properties, we noticed notable morphological differences in AFM and SPM images, with PTB7-Th being less affected by 70 keV radiation. Furthermore, XPS spectra revealed that PTB7-Th has a more robust chemical structure, particularly due to the attachment of oxygen to a single carbon chain and the presence of only one fluorine atom.

References:

1. Kumari, N., Meena, S., Singhal, R. et al., J. Mater Sci: Mater Electron **35**, 1164 (2024).
2. Gupta, D., Kumari, R., Singhal, R., Sahoo, P.K., Aggarwal, S., Applied Surface Science Advances, (2024).

5.2.10 Correlation between structural, morphological, and electrical transport properties of nano-dimensional Tellurium thin film by KeV ion impact

Santanu Ghosh[1], Sanjay Kumar Kedia[2] and Pankaj Srivastava[2]

[1] *Nanostech Laboratory, Department of Physics, Indian Institute of Technology Delhi, New Delhi 110016, India*
[2] *Material Science Group, Inter-University Acceleration Centre, New Delhi 110067, India*

Low-dimensional Tellurium (Te) [2] films (16 nm) are deposited on Si substrates by physical vapour deposition technique. The films are irradiated with a 400 keV Kr^{2+} ion beam of varying fluence of 1×10^{13},

5×10^{13}, and 1×10^{14} ions cm^{-2}. The present study investigates the structural, morphological, and transport properties of Te thin film after ion irradiation. The X-ray diffraction analysis reveals the retention of the hexagonal phase of Te even at higher fluences with degradation of crystallinity. A red shift in the Raman spectra of the irradiated sample compared to the pristine sample also supports the XRD findings. AFM analysis indicates morphological evolution at various fluence levels. The critical investigation of this measurement describes the semiconducting behaviour of all films. This work demonstrates low energy ion irradiation as a viable method for tailoring the properties of semiconducting Te thin film.

References:

1. Bordoloi, U., Ghosh, S., Kedia, S. K., and Srivastava, P. Materials Science and Engineering: B, **305**, 117399 (2024).
2. Zhu, Z., Cai, X., Yi, S., Chen, J. *et al.*, Phys. Rev. Lett. **119**, 106101 (2017).

5.2.11 Green biosynthesis of silver nanoparticles utilizing Monstera deliciosa leaf extract and estimation of its antimicrobial characteristics

Janvi Shirsul[1], Ambuj Tripathi[2] and Balaprasad Ankamwar[1]

[1] *Bio-Inspired Materials Research Lab., Dept. of Chemistry, Savitribai Phule Pune University, Ganeshkhind, Pune 411007, India*
[2] *Inter-University Accelerator Centre, Aruna Asaf Ali Marg, New Delhi 110067, India*

Herein, single step biosynthesis of silver nanoparticles (AgNPs) is reported by using $AgNO_3$ and *Monstera deliciosa* (MD) leaf extract. Spherical AgNPs are obtained with difference in particle sizes and antibacterial activities using two sets of MD leaf extract having different heating periods 5 and 10 min. They are characterized by UV–vis spectroscopy, X-ray diffraction (XRD), Zeta potential, Attenuated Total Reflectance Infrared Spectroscopy (ATR-IR), and Field Emission Scanning Electron Microscopy (FE-SEM). Dynamic Light Scattering (DLS) studies propose two types of AgNPs have hydrodynamic diameters of 104 and 80 nm. Nuclear Magnetic Resonance (NMR), Gas Chromatography-Mass Spectrometry (GC-MS), and High Resolution–Mass Spectrometry (HR-MS) studies, which reveal the presence of various phytochemicals found in MD leaf extract. These biomolecules play a vital role as stabilizing and reducing agents to fabricate stable AgNPs. These AgNPs exhibit strong antibacterial activities having effective zone of inhibition for both Gram-positive (*Staphylococcus aureus*, *Bacillus subtilis*) and Gram-negative (*Escherichia coli*, *Pseudomonas aeruginosa*) microorganisms, nonetheless AgNPs against different fungi (*Penicillium* sp., *Aspergillus flavus*, *Fusarium oxysporum*, *Rhizoctonia solani*) show non-antifungal characteristics because of their inert nature. This study suggests that AgNPs can be used in treating bacterial infections and drug delivery also for several therapeutic and diagnostic applications.

References:

1. Janvi Shirsul, Ambuj Tripathi and Balaprasad Ankamwar, Particle & Particle Systems Characterization **41**, 2400043 (2024).

5.2.12 Investigation of SHI irradiation on the quaternary Se-Te-Sn-Ag thin films

Karthikeyan Kandhasamy[1], Matheswaran Palanisamy[1*], Gokul Bangaru[1], K. Asokan[2] and Ramcharan Meena[3]

[1] *Thin film and Nanotechnology Lab., Dept. of Physics, Kongunadu Arts and Science College, Coimbatore 641029, India*
[2] *Dept. of Physics & Center for Interdisciplinary Research, University of Petroleum and Energy Studies, Dehradun 248007, India*
[3] *Inter University-Accelerator Center, Aruna Asaf Ali Marg, New Delhi 110067, India*

Thin films of the quaternary metal chalcogenide have recently gained attention due to their improved electrical, optical, thermal, and structural properties for various applications. In order to investigate the as-deposited thin film's structural, thermal, morphological, optical, and electrical properties of Ag-modified novel quaternary Se-Te-Sn-Ag thin film systems; we synthesized Se-Te-Sn-Ag thin films via melt quenching and thermal evaporation (PVD) methods. The impact of Ag incorporation of Se-Te-Sn-Ag thin film on the structural, optical, electrical, and morphological properties was investigated via various characterization techniques such as X-ray diffraction, UV-Vis-NIR spectroscopy, I-V, Hall, Seebeck, FESEM, AFM, etc. This primary investigation ensured the as-deposited properties of Se-Te-Sn-Ag thin films (for details, see Ref. [1]).

To investigate the effect of swift heavy ion (SHI) irradiations on structural, optical, electrical, and morphological properties of the as-deposited thin films, the as-deposited samples are subjected to irradiation with 100 MeV Au^{8+} and Ni^{8+} ions at three different ion fluencies (5×10^{11} ions/cm^2, 1×10^{12} ions/cm^2, and

5×10^{12} ions/cm^2) with a current of 1 pA (particle nano ampere), using the 15 UD Pelletron Tandem accelerator at IUAC. Remarkable structural phase transition has been observed with SHI irradiation by varying ion fluence and choice of ion. Surface topography was highly influenced by the choice of ion. The transport properties of SHI-irradiated samples infer that the material will be highly suitable for thermoelectric and phase-change memory applications. Rest of the analysis such as Temperature gradient GI-XRD, DSC and XPS are under progress.

References:
1. K. Kandhasamy, M. Palanisamy, S. Hari, S. Suman *et al.*,Mater. Sci. Semicond. Process. **171**, 108037 (2024).

5.2.13 Influence of argon ion irradiation and silver ion implantation on properties of nanocrystalline ZnO

V. V. Siva Kumar[1]

[1] *Materials Science Group, Inter-University Accelerator Centre, New Delhi 110067, India*

To study the changes in the structural, surface as well as transport properties caused by coupled effects of intermediate energy argon ions, highly c-axis oriented nanocrystalline ZnO thin films were deposited on Si substrates using rf sputtering method. 1.8 MeV Argon ion irradiation of these films was performed at fluences of 1×10^{15} ions/cm^2, 3×10^{15} ions/cm^2, 5×10^{15} ions/cm^2 and 7×10^{15} ions/cm^2 using Low energy ion beam facility (LEIBF). The changes in structural, surface and transport properties of these ZnO thin films due to irradiation was investigated [1] using various characterization techniques such as X-ray diffraction, Fourier Transform Infrared spectroscopy, Atomic force microscopy and I-V measurements.

To study the effects of 80 keV Silver (Ag) ion implantation on the structural and optical properties, nanocrystalline ZnO thin films were deposited on quartz substrates using rf sputtering method. The distance between the target and substrate was adjusted at 5 cm and the rf power during the deposition was 150 watts with a self bias voltage of -300 V. These films have been deposited at a pressure of 80 mTorr for 60 minutes. Implantation with 80 keV Ag ions was performed, using Negative energy ion beam facility (NEIBF), at two different ion fluences i.e. 8×10^{15} ions/cm^2 and 2×10^{16} ions/cm^2 with a current of 400 nA (nanoampere). The films were fixed to the target ladder which was placed inside the high vacuum chamber. Implantation was performed in a high vacuum of $\sim10^{-6}$ torr, in the direction perpendicular to the sample surface. The Ag ion beam was scanned over an area of 1.5 $\times$ 1.5 cm^2 using magnetic scanner to cover the complete sample surface for uniform implantation. To investigate the structural and optical changes caused by the Ag ion implantation, XRD and UV-Vis spectrophotometry measurements were performed on the pristine and implanted thin films. Plan for 60 keV Al ion implantation, other measurements and analysis are under process.

References:
1. V. V. Siva Kumar, J. Mater. Sci.: Mater. Electron. (under review).

5.2.14 Swift heavy ion induced effects on the structural and magnetic properties of Sb and Sm doped Co_3O_4 thin Films

Jisna Rahman[1,2], Manish Chandra Joshi[3], R. C. Meena[4], Asokan K.[5], Ranjith Ramadurai[3] and Rajeevan N. E.[1,2]

[1] *Department of Physics, Farook Autonomous College, Calicut, Kerala 673632, India*
[2] *University of Calicut, Calicut, Kerala, India*
[3] *Department of Materials Science and Metallurgical Engineering, IIT Hyderabad, Hyderabad 502285, India*
[4] *Inter-University Accelerator Centre, New Delhi 110067, India*
[5] *Department of Physics & Centre for Interdisciplinary Research, University of Petroleum and Energy Studies, Dehradun India*

The effect of swift heavy ion (SHI) irradiation on Sb and Sm doped Co_3O_4 thin films grown by PLD, was carried out. The structural modifications of thin films were analyzed using X-ray diffraction and Raman studies. The films were irradiated using the 15UD Pelletron tandem accelerator at IUAC with 140 MeV Ag^{11+} ions at three different ion fluences i.e. 1×10^{11}, 5×10^{12} and 1×10^{13} ions/cm^2 with a current of 1 pnA. Irradiation was performed in the direction perpendicular to the sample surface.

The structural, electrical, magnetic, and magnetoelectric properties of these oxides were studied at IIT Hyderabad, IUAC New Delhi, and UGC-DAE Indore. The intensity and peak position of the XRD peaks

(Fig. 5.18(a)) shifted with irradiation. The increase in intensity with irradiation is due to the improved crystallinity within the material, and the shift in the peak is due to the defect created by stress. It is found that the structure of the $Co_{3-x}Sb_xO_4$ (x=0, 0.1 and 0.2) thin films are sensitive to the Ag^{11+} ion irradiation. The modification of the crystalline structure is due to the defect formation and strain produced by irradiation. SHI irradiation causes a thermal spike in the material as an impact of large electronic energy loss resulting in local heating followed by rapid quenching. It leads to localized modification in the thin film. The localized changes in crystal and the creation of point/clusters of defects followed by the defect-induced strain are responsible for the modification of different properties of the material.

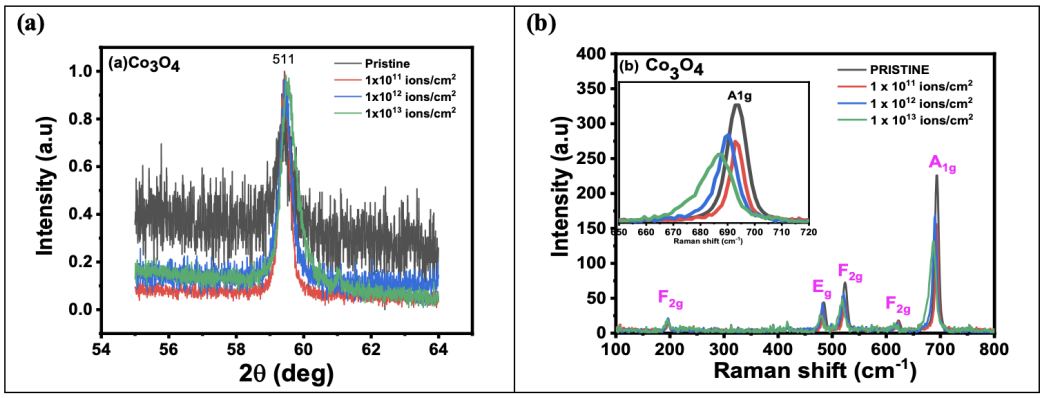

Figure 5.18: (a) XRD spectra and (b) Raman spectra of Co_3O_4 thin films, pristine and irradiated with different fluences.

Raman scattering measurements (Fig. 5.18(b)) have been performed for pristine and irradiated thin film samples. The prominent Raman active peaks are observed in the 100–800 cm^{-1} range. The pristine sample shows the normal spinel structure and possesses five Raman active modes: F_{2g} (188 cm^{-1}), E_g (466 cm^{-1}), F_{2g} (508 cm^{-1}), F_{2g} (603 cm^{-1}), and A_{1g} (670 cm^{-1}). The left shift in F_{2g}, E_g, and A_{1g} peak positions indicates the change in the crystal lattice due to the modification of strain by irradiation.

The surface morphology of both pristine and irradiated $Co_{2.8}Sb_{0.2}O_4$ thin films was studied using field emission scanning microscopy. The morphology of the thin film is drastically changed with irradiation. The irradiated samples show radiation-induced densification. The magnetoelectric coupling shows an increase with irradiation.

The impact of SHI was observed in the ferrimagnetic properties of the thin film studied for different temperatures from 20 K to 300 K. The results indicate that the irradiation with Ag^{11+} ions changes the properties. The overall magnetism of the material changes with the SHI irradiation. The influences of SHI irradiation on thin films depend on the ion, fluence, energy of ion, and the material properties. All the pristine and irradiated thin films show a ferromagnetic hysteresis loop at all the measured temperatures.

References:

1. N. E. Rajeevan, Ravi Kumar, D. K. Shukla, P. Thakur and P. P. Pradyumnan, Key Engineering Materials **547**, 71 (2013).
2. Ravi Kumar, M. W. Khan, J. P. Shrivastava, S. K. Arora *et al.*, J. Appl. Phys. **100**, 033703 (2006).
3. Anjana Dogra, M. Singh, V. V. Siva Kumar, N. Kumar and Ravi Kumar, Nucl. Instrum. Methods B **212**, 184 (2003).

5.2.15 Effect of ion irradiation on morphological, structural, and electrical properties of $Ge_2Sb_2Te_5$

Puspender Singh Beniwal[1], Indra Sulania[2], Sanjay Kumar Kedia[2] and Yogita Batra[1]

[1] *Department of Physics, J. C. Bose University of Science and Technology, YMCA, Faridabad 121006, India*
[2] *Inter-University Accelerator Centre, Aruna Asaf Ali Marg, New Delhi 110067, India*

$Ge_2Sb_2Te_5$ (GST) thin films were synthesized on a silicon substrate using a DC magnetron sputtering system. Thin films of ternary compound GST composed of germanium, antimony, and tellurium alloyed in atomic ratios of 2, 2, and 5, respectively, were irradiated using Ag^{11+} ion irradiation of 140 MeV. The melting point of GST alloy is 600°C (873K), and its crystallization temperature ranges from 100 to 150°C [1]. For this reason, GST is a suitable material for energy harvesting as a thermoelectric. Electrical energy transformation

in thermoelectric materials is determined by the thermoelectric figure of merit $ZT = S^2\sigma T/(\kappa_e+\kappa_{ph})$, where S, σ, κ_e, κ_{ph}, and T are the Seebeck coefficient, electrical conductivity, thermal conductivity, phononic component of thermal conductivity, and operating temperature respectively [2]. The thermoelectric performance, including the performance factor (PF = $S^2\sigma$) and ZT, can be improved by modifying carrier concentration through doping or alloying with aliovalent elements. The change in carrier concentration can be achieved by creating defects and vacancies through ion irradiation. Improved electrical properties are attributed to the ionization radiation-enhanced crystallinity, which increases the electrical conductivity of the materials. Ion irradiation of Te-based materials is a promising approach for improving the performance and stability of these materials. The crystal structure can be modified by bombarding these materials with ions, reducing thermal conductivity while maintaining high electrical conductivity [3].

For this purpose, the deposited films were irradiated using a high-energy beam of Ag^{11+} ions of 140 MeV produced by a 15 UD pelletron accelerator based on tandem electrostatic acceleration. The irradiation experiments were conducted at the material science beamline (Beam Hall-I) of IUAC, with different ion fluences, at room temperature, and with a chamber pressure of 10^{-6} mbar. For ion fluences of 1×10^{12}, 5×10^{12}, 1×10^{13}, and 3×10^{13} ions/cm^2, 0.6–0.7 particle nanoampere (pnA) beam current was employed for irradiation to reduce target charging and overheating. Then, pristine and irradiated thin films were characterized to study structural and electrical transport properties. An X-ray source-based Bruker D8-Advance X-ray diffractometer with Cu Kα ($\lambda = 1.54$ Å) was used to record the XRD patterns. A scintillator detector with a scan rate of 2°/min was used to record XRD patterns from 15° to 60° using an X-ray source operated at 40 keV and 40 mA. SEM (TESCAN MIRA II LMH) was used to capture surface images of the GST film using 25 keV electron energy, for the pristine and the irradiated samples. This was for the same set of samples as used for the XRD analysis. Also, the selected area energy dispersive spectroscopy (EDAX) was done simultaneously for these samples. The topography of the surface of GST thin films (pristine and irradiated) was analyzed using the tapping mode of a Digital Instruments Nanoscope-III AFM. To study the electrical transport behaviour, a Hall effect measurement system (Ecopia HMS-300) was used. The studies and analysis of structural, morphological, and electrical transport properties through these characterization techniques explore the possibility of optimizing GST thin films by means of regulated ion irradiation.

References:

1. Boschker J. E. and Calarco R., Adv. Phys. X **2**, 675 (2017).
2. Kang S. -H., Jella V., Pammi S. V. N., Eom J. -H. *et al.*, Curr. Appl. Phys. **17**, 744 (2017).
3. Bux S. K., Fleurial J. -P. and Kaner R. B., Chem. Commun. **46**, 8311 (2010).

5.2.16 Tuning of electrical properties through field effects for manganite based n-n Junctions: Role of swift heavy ion irradiation

Mayur Parmar[1], P. S. Solanki[1], Ambuj Tripathi[2] and N. A. Shah[1]

[1] *Department of Physics, Saurashtra University, Rajkot 360005, Gujarat, India*
[2] *Inter-University Accelerator Centre, Aruna Asaf Ali Marg, New Delhi 110067, India*

The ongoing work is focused on the fabrication and detailed characterizations of manganite-based n-n heterojunctions, specifically focused on the CdO/GSMO/STO (CGS Series) and CdO/LSMO/STO (CLS-Series) systems. These bilayered heterojunctions were prepared by simple, cost-effective spin coating chemical solution deposition (CSD) technique. Structural, microstructural and surface properties were investigated using performing X-Ray Diffraction (XRD) and Atomic Force Microscopy (AFM) measurements, confirming the formation of high purity, polycrystalline films with well distribution of grain structure. During present work, the primary objective is to study the light-dependent electrical properties of CGS-PRI [i.e. CGS-Series without any irradiation (Pristine)] sample under various modes i.e. normal, dark and light modes. These electrical measurements provide the baseline for understanding the intrinsic behaviour of the sample, which will be essential for interpreting the future modifications resulting from swift heavy ion (SHI) irradiation in different samples.

Firstly, the charge transport properties have been examined using current-voltage (I-V) characteristics (Fig. 5.19) under normal, dark and light (intensity: 35 mW/cm^2) modes. Significant modifications in the properties have been observed under different modes, highlighting the influence of light on the charge transport properties of the GS-PRI sample.

To understand the electrical nature of the thin film heterojunction, a.c. conductivity and impedance spectroscopy were performed over a frequency range of 20 Hz to 2 MHz under different modes of action (i.e. normal, dark and light modes). Fig. 5.20(a) represents the frequency-dependent a.c. conductivity

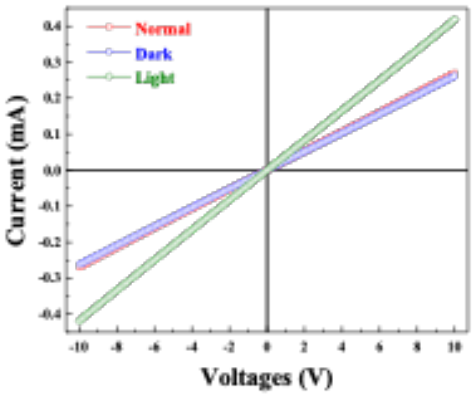

Figure 5.19: current-voltage (I-V) characteristics of light dependent CGS-PRI thin film sample at normal, dark and light modes.

measurements, which shows the notable changes under different modes with variation in frequencies. a.c. conductivity data have been theoretically fitted using Jonscher's power law using the equation [1];

$$\sigma_{ac} = \sigma_{dc} \times A\omega^{\eta},$$

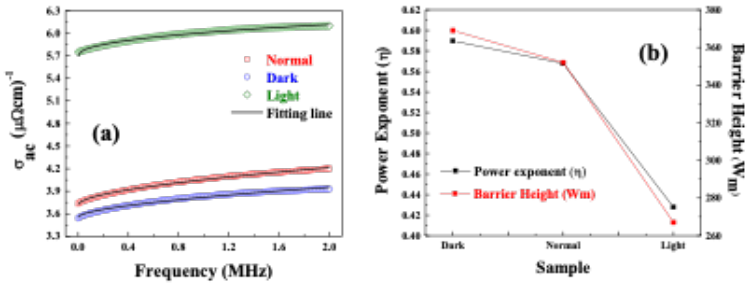

Figure 5.20: (a) Jonscher's power law fitted a.c. Conductivity plots for dark/light dependent and (b) obtained parameters for GS-PRI thin film sample.

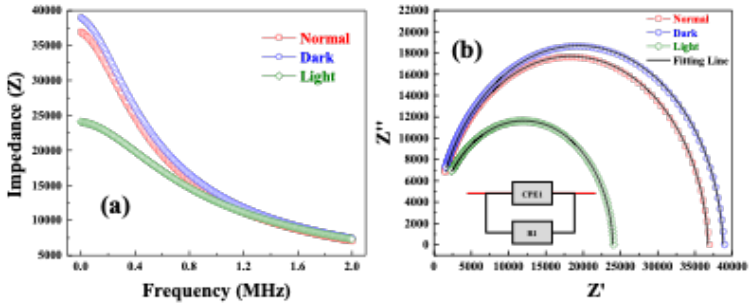

Figure 5.21: Impedance spectroscopy studies (a) real impedance and (b) Nyquist plot for GS-PRI thin film sample.

where σ_{dc} is the dc conductivity, A is the power law exponent or constant (which varies with the material) and η is the power exponent. Additionally, the maximum barrier height has been calculated using the formula [2]:

$$W_m = \frac{6k_BT}{1-\eta},$$

where k_B is the Boltzmann constant, T is the temperature, and η is the power exponent. The obtained

parameters, including the power exponent (η) and barrier height (W_m), are shown in Fig. 5.20(b).

Subsequently, the resistive nature of the sample has been evaluated through impedance spectroscopy under different measurement modes. Fig. 5.21(a) shows the impedance spectroscopy response in normal, dark and light modes, where distinct variations in impedance behaviors can be observed. To analyze these responses in more detail, Nyquist plots have been generated and fitted using an equivalent circuit model, as illustrated in the inset of Fig. 5.21(b). The fitting results confirm the changes in the sample's resistance and capacitive behaviour under different modes of action.

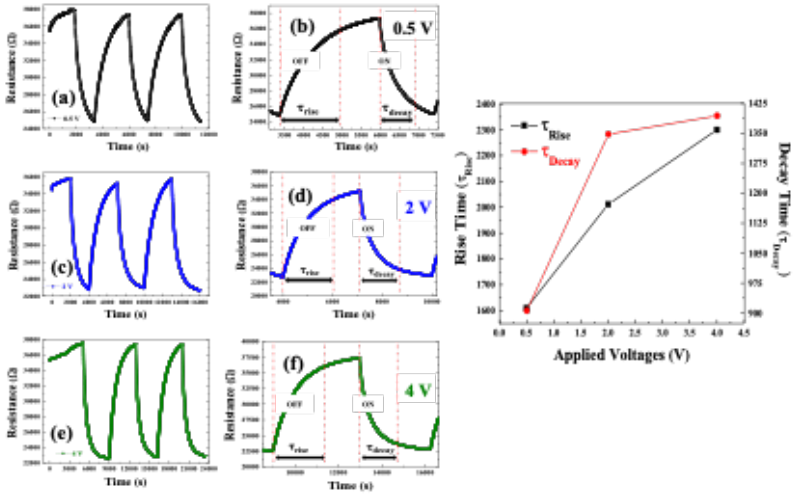

Figure 5.22: R-t plots under different voltages and light ON/OFF states (left) and change in rise time (τ_{rise}) and decay time (τ_{decay}) (right).

The stability of the GS-PRI device sample was examined through resistance vs time (R-t) measurements under the application of different voltages (0.5 V, 2 V and 4 V) with altering light under ON/OFF conditions. As shown in Fig 5.22 (left) the device exhibits a clear and repeatable switching behaviour under influence of light, demonstrating distinct resistance state with good rise and decay times. The corresponding rise time (τ_{rise}) and decay time (τ_{decay}) under influence of light for different applied voltages are presented in the Fig. 5.22 (right), indicating a wide resistance window and stable performance across multiple cycles.

To understand the energy matter involved (as released by the energetic heavy ions during irradiation) in the governance of opto-electrical behaviors of different manganite-based n-n junctions, the SRIM (Stopping and Range of Ions in Matter) software were utilized in the present project work [3]. SHI irradiation of the CGS and CLS systems, were recently carried out (April-2025) for all the prepared samples. To further understand ion-material interaction, TRIM (Transport of Ions in Matter) was performed wherein, it estimates how ions move through the material and how damage have been caused with SHI and where the energy gets deposited.

Based on the findings of SRIM and TRIM simulations, it is believed that the selected 120 MeV Ag^{+9} ion energy demonstrates suitable penetration depth and energy deposition within the film layers of the manganite-based n-n heterojunctions. These results support the use of swift heavy ion (SHI) irradiation with 120 MeV Ag^{+9} ions to induce controlled modifications in the material. Therefore, in the upcoming sanctioned year of research project (i.e., 2025-26 for two months fellowship only). The properties such as the structural, microstructural, electrical and transport characteristics of the heterojunctions will be repeated as done for CGS-PRI sample. Furthermore, all the irradiated samples will be thoroughly characterized and the outcomes will serve the foundation of the preparation of research manuscript, which will subsequently be communicated to reputed international journals for publications.

References:

1. A. K. Jonscher, Nature **267**, 673 (1977).
2. Akram Krichene, W. Boujelben, K. N. Rathod, Keval Gadani, N. A. Shah and P. S. Solanki,J. Electro. Mater. **49**, 5244 (2020).
3. P. Biersack and L.G. Haggmark, Nucl. Instrum. Methods **174**, 257 (1980).

5.3 AMS and geochronology

S. Ojha

Radionuclides play a crucial role in studying the paleo-environment and its processes by providing a chronological framework for associated events. Cosmogenic radionuclides such as ^{10}Be, ^{14}C and ^{26}Al, measured using the AMS facility at IUAC, have been widely applied in various scientific domains. These include assessing the paleo-behavior of glacial and periglacial landscapes across the Indian Himalaya, estimating denudation rates, conducting paleo-climatic and paleo-monsoon studies, tracing the sources of atmospheric CO_2 and archaeological investigations. Isotopic measurements conducted with mass spectrometers (HR-ICPMS & HR-SIMS) have been applied for establishing U-Pb Zircon geochronology and evolution conditions for metallogeny during the development phases of NE and NW Himalaya. Elemental analysis with Q-ICPMS and other ancillary instruments have been widely applied in geochemical investigation, understanding the heavy metal pollution in soil, water, plants etc.

5.3.1 Assessing event chronology in the glacial and periglacial landscape of Lahaul and Spiti, Northwest Himalaya

Milap C. Sharma[1], Chakraborty Elora[1], Das Soumik[1] , Malik Chandan[1], Kumar Pankaj[2] and Kumar Pavitra V.[2]

[1] *Centre for the Study of Regional Development, Jawaharlal Nehru University, New Delhi 110067, India*
[2] *National Geochronology Facility, Inter-University Accelerator Centre, New Delhi 110067, India*

In order to build a continuous chain of glacial and periglacial events in the Northwest Himalaya we have focused on a multiproxy methodology using ^{14}C AMS dating, ^{10}Be TCN dating. Exposure samples were brought in from the heavily glaciated valley of Miyar and Sonapani. These two valleys contribute to the Chandrabhaga river, a major tributary of the Indus catchment. The northwestern Himalayan region has historically experienced a complicated accumulation regime owing to the activity of two climatic systems, namely the Mid Latitude Westerlies (MLW) and the Indian Summer Monsoon (ISM). Studies suggest Lahaul has served as the northernmost boundary of the Palaeo-monsoon in the region. Available researches showcase ages obtained through several different absolute dating methods in the South Western Himalayan Tibetan System (SWHTS) encompassing the study area. Researches explain glacial advances in the study area prior to ∼35 ka as a result of the event of intensified Indian Summer Monsoon (ISM) and advances post ∼35 ka as a result of weaker Mid Latitude Westerly intensification (MLW)[1]. Calibrated ^{14}C AMS dates from bulk sediments (processed with Acid-Base-Acid protocol at IUAC, New Delhi) at the Gumba thermokarst formation reveal initiation of periglacial activities prior to ∼23,000 yrs Cal BP. The available ^{14}C AMS dates from a core at Gumba thermokarst (∼23,000-3500 yrs Cal BP) located on top of an older glaciolacustrine formation places Miyar Valley glaciation to before ∼35 ka (OSL date).

In the arid Trans Himalayan Spiti, Permafrost is a major contributor to the region's fresh water needs. The Spiti valley has not experienced extensive glaciation since the Local Last Glacial Maximum (LLGM) contemporaneous with the Chandra stage of glaciation (∼30-80 ka) [2] . The upper Spiti catchment has experienced rapid changes in the landscape due to paraglacial activities and post LLGM enhanced because of the local lithology and frequent seismic events. Much of the paraglacial debris has been rendered as vast reservoirs of permafrost in the entire upper Spiti watershed. Calibrated ^{14}C AMS dates for bulk sediments from bogs amidst hummocky ground yielded dates between ∼7,300-3,300 yrs Cal BP from a core collected at an elevation of 4561 masl. A separate core at a lower altitude of 4532 masl yielded dates between ∼18,000-9,500 yrs Cal BP and at an elevation of 4548 masl a core yielded date between ∼16,000-6,500 yrs Cal BP. These processed dates help estimate a timeline for climatic amelioration leading to accumulation of ancient carbon due to periglacial geomorphological processes. However, a reduced sedimentation rate in the typically permafrost landscape bearing no evidences of prior extensive glaciation, has been noted between the years 12,000-9,500 yrs Cal BP. These dates may be a proxy for climatic cooling during this period where further rejuvenation of the permafrost may have occurred.

References:

1. Dortch, Jason M., Lewis A. Owen, and Marc W. Caffee, Quaternary Science Reviews **78**, 188 (2013).
2. Owen, L.A., L. Gualtieri, R.C. Finkel, M.W. Caffee, D.I. Benn, and M.C. Sharma, Journal of Quaternary Sciences **16**, 555 (2001).

5.3.2 Late Quaternary Landscape Denudation in the lateritic badlands of Garbeta, West Bengal

Dasgupta R.[1], Murari, M.K.[2], Patel, P.P.[1], Das, S.K.[3], Gupta, H[4], Kumar, P.[2] and Kumar, P.V[2]

[1] *Department of Geography, Presidency University, Kolkata 700073, India*
[2] *National Geochronology Facility, Inter-University Accelerator Centre, New Delhi 110067, India*
[3] *Department of Geology, Presidency University, Kolkata 700073, India*
[4] *Department of Civil Engineering, Osmania University, Hyderabad 500007, India*

Uplift and denudation (chemical weathering + erosion) of rocks release minerals, which have variable residence times within the weathering zone. Depending upon specific weathering pathways, they can alter denudation rates and also either sequester or release carbon dioxide. Although such changes in denudation rates are the fastest in active orogens, cratonic areas can experience epeirogenic upheavals, which can accelerate the weathering and erosion of the ambient rocks and sediments. Under such circumstances, silicate weathering can sequester carbon dioxide at rates equal to or other higher than in orogens [1]. Therefore, estimation of landscape denudation rates in cratonic areas is essential. In this study, weathering and denudation rates in the Rarh region of West Bengal are being estimated using cosmogenic radionuclides and major ion geochemistry of river water and solutes collected from selected small catchments within the region, with a special focus on the Garbeta badlands.

The Rarh region is a transition zone between the Chotanagpur Plateau in the west and the Ganga delta to the each. Geologically, it is part of the Stable Shelf province of the Bengal basin with a series of NW-SE trending faults and lineaments traversing the region. It is composed of a Precambrian basement with mixtures of igneous and sedimentary rocks, Plio-Pleistocene clays and Holocene alluvium. Six major river systems and their tributaries flow across the region from West to East. Twenty small river catchments (including one gully catchment), ranging in size from 09 to 150 sq. km. were selected from this region. The catchments were selected based on the lithology over which they flow and distance from major anthropogenic perturbations such as dams/check dams across the catchment. For each catchment, water samples were collected at the catchment outlet and filtered through nylon filters. These were used for cation and anion analysis. Sediment samples (2-3 kg) were collected from river bed or stable sand bars for cosmogenic radionuclide (^{10}Be) analysis.

The water samples were analysed using Ion Chromatography for cations (Na, K, Ca and Mg) and anions (Cl, F, NO_3, SO_4, PO_4 and HCO_3) at the National Geophysical Research Institute, Hyderabad. Although detailed analyses of the results obtained are still ongoing, preliminary results suggest that HCO_3 is the major anion (80-90%) in all the samples, while carbonates (Ca and Mg) account for a significant portion (30-45%) of the cations. This is despite the lack of major carbonate rocks in the area but is consistent with previous studies in the Ganga-Brahmaputra systems [2,3].

Twenty sediment sample were processed of ^{10}Be extraction at National Geochronology Facility, IUAC. This involves physical and chemical treatment of sediment to extract pure quartz from the sediment with grain size (250-500 μm). To enrich the purity of quartz, Isodynamic Magnetic Separation was used to separated other minerals and further purity of sample was verified by measuring ^{27}Al with Q-ICP-MS and samples were rejected which have contamination. In this purification process only 10 sample yielded measurable quartz to process for the extraction of ^{10}Be. Our samples ^{10}Be/^{9}Be ratio have been measured on AMS facility National Geochronology Facility, IUAC. Recently, we got data and working on analyses to obtain ^{10}Be denudation rates

References:

1. Y. Godderis, Y. Donnadieu, M. Tombozafy and C. Dessert, Geoderma **145**, 439 (2008).
2. M. M. Sarin, S. Krishnaswami, K. Dilli, B. L. K. Somayajulu and W. S. Moore, Geoch. Cosmochim. Acta **53**, 997 (1989).
3. D. K. Datta and V. Subramanian, J. Hydrol. **198**, 196 (1997).

5.3.3 Paleoclimate reconstruction using peat-based proxy and understanding peat dynamics from climatically distinct regions in the Indian sub-continent

Anchana P.[1] and Debajyoti Paul[1]

[1] *Department of Earth Sciences, Indian Institute of Technology Kanpur, Kanpur 208016, India*

Peatlands are vital wetland ecosystems that store large amounts of atmospheric carbon, significantly contributing to the global carbon cycle [1,2]. Peat accumulates under waterlogged, oxygen-poor conditions due to the incomplete decomposition of plant material [3]. When left undisturbed, these ecosystems function

as important terrestrial carbon sinks [4]. However, when disturbed events such as forest fires influenced by climate change and human activity, peatlands can shift from carbon sinks to carbon sources, releasing substantial amounts of CO into the atmosphere. Although several studies have been carried out using peat samples from temperate regions in this regard, tropical peats have been less studied. Peat as a proxy for paleoclimate reconstruction has not been utilized significantly in the Indian subcontinent and the peat formation and accumulation in climatically distinct regions need to be explored. This study presents a comparative analysis of peat from four climatically diverse regions in India, namely, Kerala, Tamil Nadu, Himachal Pradesh and Sikkim, with an emphasis on their formation processes and potential use as proxies for reconstructing past climate conditions.

The peat core collected from these locations were divided into 2 and subsampled at an interval of 1 cm for radiocarbon dating, stable carbon and nitrogen isotope and other geochemical analyses. The samples were dried, powdered, and cleaned by removing materials such as rootlets. Total 17 -sample were selected for radiocarbon measurement at Accelerator Mass Spectrometer (AMS) facility of National Geochronology Facility, IUAC. Prior to analysis, the samples underwent an Acid-Base-Acid (ABA) pretreatment with 1M HCl and 0.1M NaOH to eliminate carbonates and humic acids. Following pretreatment, the samples were freeze-dried and graphitized using an Automated Graphitization Equipment (AGE) coupled with an Elemental Analyzer (EA). The resulting graphite was then analyzed using the AMS to determine the radiocarbon (^{14}C) ages of the samples [5].

The obtained ^{14}C dates were calibrated in the Calib software by using the IntCal20 calibration curve [6]. The stable C and N isotope analyses have been done for all the locations and the remaining geochemical analyses are ongoing for the peat samples to achieve a clear understanding of the paleoclimate in the study area.

References:

1. Silva, A.C., Barbosa, M.S., Barral, U.M., Silva, B.P.C. *et al.*, Catena **180**, 69 (2019).
2. Yu, Z., Loisel, J., Brosseau, D.P., Beilman, D.W. and Hunt, S.J., Geophysical Research Letters **37**, 13 (2010).
3. Charman, D., Peatlands and environmental change. Chichester, West Sussex, England: J. Wiley. (2002).
4. Page, S.E. *et al.*, Tropical Peatland Fires in Southeast Asia. Tropical Fire Ecology, Springer, 263 (2009).
5. Sharma, R., Umapathy, G.R., Kumar, P., Ojha, S. *et al.*, Nucl. Instrum. Methods B **438**, 124 (2019).
6. Reimer, P., Austin, W., Bard, E., Bayliss, A., Blackwell, P., Bronk Ramsey, C., Talamo, S., Radiocarbon **62**, 725 (2020).

5.3.4 Reconstruction of past seasonality using chemical proxies in gastropod remains at Tigrana, Haryana

Ritvik Chaturvedi[1], Narender Parmar[2], Anil K Pokharia[3], Pankaj Kumar[4], Rajveer Sharma[4] and Prosenjit Ghosh[1]

[1] *Centre for Earth Sciences, Indian Institute of Science, CV Raman Avenue, Bengaluru 560012, India*
[2] *Department of History and Archaeology, Central University of Haryana, Mahendergarh, Haryana 123029, India*
[3] *Birbal Sahni Institute of Palaeosciences, 53 University Road, Lucknow, Uttar Pradesh 226007, India*
[4] *National Geochronology Facility, Inter-University Accelerator Centre, New Delhi 110067, India*

Underr BTR 76403, 22 molluscan aragonite and 8 wood charcoal samples from the archaeological site of Tigrana, Haryana (Mature/Late Harappan phase – 5000-3800 BP), were graphitised and radiocarbon dated at the National Geochronology Facility, IUAC New Delhi. Radiogenic isotope dating establishes the chronological framework for interpreting δ^{18}O and δ^{18}C signatures in mollusc aragonite. Since shell biomineralization occurs in equilibrium with surrounding water, the δ^{18}O signature reflects the temperature at the time of formation. The δ^{18}O record from the sites full chronological sequence aims to reconstruct continuous changes in temperature and/or evaporation–precipitation regimes between 4000 and 3800 BP. To our knowledge, this is the first study to reconstruct past environments using stable isotopes from in situ mollusc shells at an Indus Valley Civilisation site. Other palaeoclimate reconstructions for this period using molluscan biominerals have relied on lake cores located some distance from archaeological sites [1,2]. Earlier work highlights both similarities and differences between the δ^{18}O record from Tigrana molluscs and nearby lakes such as Karsandi and Kotla Daha.

One, Lake Karsandi, being a large reservoir, shows a rather muted signature. This is because large reservoirs collect water from multiple precipitation events through long timescales (months, even years) and provide a more 'averaged-out' signal. There are some striking similarities at certain points (a) The period at ~4400 BP shows a marked shift towards heavier values (warmer conditions); (b) There is again a shift towards slightly humid conditions around ~4175 BP, then (c) another similar shift between 4100 to 4000 BP. Both the archaeological site of Tigrana and Lake Karsandi, being in the upper riparian of River Saraswati, likely experienced similar hydrological regimes. In contrast, Lake Kotla Dahar does not follow

the shifts observed at Lake Karsandi or Tigrana, instead showing a consistent trend toward drier conditions. Being considerably distant from the Saraswati River watershed, Lake Kotla Dahar was likely influenced by a different hydrological regime, shaped more by the eastern river systems due to its proximity to the Yamuna River.

Our interpretation was constrained by the absence of continuous data covering the entire depth sequence of the site. Previous research, conducted as part of BTR 73229, primarily focused on samples retrieved from Trench ZA1; however, even these records were incomplete as samples from other trenches/strata were, at that time, unavailable. Additionally, radiocarbon ages associated with Trench ZA1 did not consistently increase with depth and some horizons/strata showed age inversions, necessitating further investigation. To address these limitations and construct a more robust temporal framework, we have incorporated wood charcoal (organic matter), alongside molluscan aragonite. The integration of age data derived from multiple proxies within the same depth or stratum enhances the credibility of chronological assessments (see [3] for a comparison).

Recent excavations uncovered new trenches capturing the site's full chrono-stratigraphic history. To address potential anthropogenic disturbances, their bio-archaeological records were incorporated, offering a more comprehensive and nuanced understanding of the site's temporal and stratigraphic dynamics. Under BTR 76403, we analyzed mollusc shells from newly excavated horizons, dated wood charcoal, and revisited layers with previously anomalous radiocarbon ages. This integrated approach aims to provide a clearer understanding of the site's depositional history and past environmental conditions.

References:

1. Dixit Y, Hodell DA, Giesche A, Tandon SK *et al.*, Scientific Reports **8**, 4225 (2018).
2. Dixit Y, Hodell DA and Petrie CA, Geology **42** 339 (2014).
3. Tripathi D, Pokharia AK, Parmar N, Kumar P, Srivastava A and Sharma R., Current Science **122**, 1126 (2022).

5.3.5 Holocene climate variability deciphered from Chilika Lagoon sediments: Implication to anthropogenic activity or paleocyclones?

Barnita Banerjee[1,2], Monalisa Mallick[1,2], Mohd Amir[3,4], Abdul Hameed[5], Luan Ozelim[6], Nihar Ranjan Kar[1], E.V.S.S.K Babu[1,2], Venkatesham, K[1], Venkateshwarulu, M[1,2], Tanveer Hassan[1], Vireswar Samanta[1], Prem Chand Kisku[1], Debajyoti Paul[3], Pankaj Kumar[7] and Aurovinda Panda[1]

[1] *CSIR-National Geophysical Research Institute, Uppal Road, Hyderabad 500007, India*
[2] *Academy of Scientific and Innovative Research, CSIR-National Geophysical Research Institute, Hyderabad 500007, India*
3*Department of Earth Sciences, Indian Institute of Technology Kanpur, Kanpur 208016, India*
[4] *Department of Oceanography, National Sun Yat-sen University, Kaohsiung 804, Taiwan*
[5] *Department of Geology, University of Delhi, Delhi 110007, India*
[6] *Department of Civil and Environmental Engineering, University of Brasilia, Brazil*
[7] *National Geochronology Facility, Inter-University Accelerator Centre, New Delhi 110067, India*

Coastal lagoons, acting as a link between land and sea, serve as valuable archives for past climate variations, human activities, and paleo-cyclonic events. In this study, we employ a multi-proxy approach to analyze sedimentary records and uncover climatic shifts influenced by both monsoonal and non-monsoonal factors. Our analysis incorporates sediment characteristics such as grain size, magnetic susceptibility (MS), and clay mineralogy to infer high-energy conditions within the Chilika Lagoon. Additionally, we utilize Rock-Eval pyrolysis and deconvolution of Flame Ionization Detector (FID) signals to determine the type of organic matter (OM) present.

Findings reveal that during the Early Holocene, a high sand percentage and elevated MS indicate an intensified monsoon, coinciding with a dominance of terrestrial OM. However, as monsoonal intensity declined after the Early Holocene, marine OM became more prevalent, likely linked to the formation of an estuary around ~7.7 ka. Despite a weakening monsoon around ~4 ka, MS values remained high, possibly due to increased aeolian input, which transported titanomagnetite, contributing to elevated MS in the sediment record. After ~4 ka, the sedimentary record indicates a greater influx of terrestrial OM, likely due to the formation of a barrier spit that limited marine influence. From this period onward, monsoonal intensity gradually increased, peaking around ~1.1 ka, coinciding with the Medieval Warm Period.

Following ~1.1 ka, sedimentation rates rose, accompanied by low magnetic susceptibility (MS) and high sand content. This phase also shows an increase in both terrestrial and marine OM, along with higher $CaCO_3$ and illite concentrations (analyzed at IUAC, New Delhi), suggesting the impact of high-energy events, possibly cyclones. The intensification of cyclonic activity after ~1.1 ka may be associated with a weakening of El Niño–Southern Oscillation (ENSO) intensity during this period [1].

For better understanding, high resolution work involves analysis of 900+ sediment samples from both Chilika and Pulicat Lagoon. A Total 30 samples from both lagoons have been processed at National Geochronology Facility, IUAC for radiocarbon dating. The dates, which are crucial for the ongoing investigation and subsequent publications, are pending.

References:

1. Banerjee, B., Mallick, M., Amir, M., Hameed, A. *et al.*, Geosystems and Geoenvironment, p.100390 (2025).

5.3.6 Paleomonsoonal studies using multi-proxy data from marine and continental archives

Gupta Anil Kumar[1], Kaushik Arun[2], Sengupta Sreya[1], Palar Biswajit[2], Santra Abhijeet[1], Parhi Arpita[1], Ghosh Mainak[1], Verma Yachna[1] and Kumar Pankaj[3]

[1] *Department of Geology and Geophysics, Indian Institute of Technology Kharagpur, Kharagpur 721302, India*
[2] *Centre for Ocean, River, Atmosphere and Land Sciences, Indian Institute of Technology Kharagpur, Kharagpur 721302, India*
[3] *National Geochronology Facility, Inter-University Accelerator Center, New Delhi 110067*

The Indian Summer Monsoon (ISM) is a complex atmospheric phenomenon, brings about 80% of the yearly precipitation to large parts of the Indian landmass, controlling the agriculture-based economy and livelihoods of more than a billion people [2]. The paleoclimate proxies provide indirect clues about past climatic various geologic records viz. lacustrine, marine, speleothems, tree rings, and ice cores. To understand past variability and intensity of the ISM over the Indian subcontinent, sediment cores were collected from eleven lakes in eastern and northern India. Total fourteen cores of length 5.10 m, 3.5 m, 1.06 m, 1.36 m, 1.12 m, 4.88 m, 6.30 m, 5.11 m, 5.94 m, 5.02 m, 0.85 m, 0.35 m, 1.44 m and 0.38 m were obtained from Hansadanga, Nowpara, Sartola, Karajgram, Mathura Beel, Duma Baor and Panchita- Chanda lakes, respectively. These lakes are located in the Nadia, Burdwan and North 24 Pragana districts of West Bengal. Six cores of length 7.17 m, 14.64 m, 9 m, 11.7 m, 7.8 m, and 7.5 m were obtained from Chilika, Anshupa, and Tampara lakes in Ganjam and Cuttack districts of Odisha using the gravity and auger drilling methods. By trenching, samples were also collected from Sahaswan Lake, Budaun District, Uttar Pradesh, with a total length of 2.15 m and 3.30 m. The samples are sub-sampled at 5 mm, 10 mm, and 2 cm intervals. The age of 80 approved samples (including bulk sediments, gastropods, and Bivalvia) from different lakes and marine sediments was determined at the AMS radiocarbon system of National Geochronology Facility (NGF), IUAC, New Delhi.

Before AMS ^{14}C measurement, samples were finely crushed using a mortar and pestle and sieved to remove the detrital materials and plant roots. Afterward, sediment samples were pre-treated in the Graphitization laboratory of NGF, IUAC using acid-base-acid treatment, and the ages were determined using the techniques after [1]. A few coarse grain sediment samples were low on carbon and could not be measured by AMS, sent elsewhere for OSL dating.

The West Bengal lakes are mostly oxbow lakes of the Lower Ganga plain system, mainly formed in the Holocene period. Hence, these lakes are a good indicator of extreme events like floods and droughts, and are also used for paleogeographical study. Hansadanga Lake has a bottom age of ca. 12 ka cal yr BP. Radiocarbon dates of Chilika Lake sedimentary cores have provided an age range of nearly 25 ka cal yr BP, whereas the coastal lake Tampara goes up to 10 ka cal yr BP. The Fluvial freshwater lake Anshupa provides an age range of 5.8 ka cal yr BP to Present. Radiocarbon ages of these lakes helped in identifying several climate events like the Dark Ages Cold Period (DACP), Medieval Climate Anomaly (MCA), Little Ice Age (LIA), 4.2 ka and 8.2 ka events, Younger Dryas, and the Last Glacial Maximum. The grain size and XRF analyses of these lakes have been completed. Magnetic and biomarker studies of some lakes have also been completed. To reconstruct the past climate and environments, samples are prepared for other proxy records, including TOC, Pollen, and Stable isotope study (e.g., ^{13}C and ^{15}N). To study the effects on benthic foraminifera due to gas hydrate occurrences along the Chilean margin, an age- depth model for the concerned site (ODP Leg 202 Site 1235A) was required. For the present study, the radiocarbon dating was done at NGF, IUAC and the ages obtained so far go up to 29 ka. Further, Speleothem samples from different carbonate caves were analyzed for AMS dating to determine the age of the deposition, including Mawsmai, Akanagama, and Deogiri caves. These records cover the age ranges of the Holocene period. Total 85 samples were approved for AMS measurement, which are currently being processed at NGF, IUAC.

References:
1. Sharma, R., Umapathy, G.R., Kumar, P., Ojha, S. *et al.*, Nucl. Instrum. Methods B **438**, 124 (2019).
2. Gadgil, S., Annual Review of Earth and Planetary Sciences **31**, 429 (2003).

5.3.7 Uranium-bearing quartz used in the synthesis of soda-lime-silica glasses having antifungal properties

Pati Jayanta Kumar[1,2], Singh Anuj Kumar[1], Dwivedi Shivanshu[1], Dwivedi Mrigank Mauli[2], Kumar Pankaj[3], Kapindar[1], Sarkar Sneha[4], Chaprana Parveen[1], Sharma Aishanya[1] and and Mishra Shivam[1]

[1] *Department of Earth and Planetary Sciences, University of Allahabad, Prayagraj 211002, India*
[2] *National Centre of Experimental Mineralogy and Petrology, University of Allahabad, Prayagraj 211002, India*
[3] *National Geochronology Facility, Inter-University Accelerator Centre, New Delhi 110067, India*
[4] *Department of Geological Sciences, Jadavpur University, Kolkata 700032, India*

Quartz crystals sourced from agates of the Dhala impact structure (Shivpuri district, Madhya Pradesh) show green fluorescence under SW-UV light using a UVGL-25 Compact UV Lamp (Upland, CA, USA) with wavelength ranges of 254 nm (SW) and 365 nm (LW). These green fluorescence in quartz agate samples attributed mainly due to presence of uranyl ion. In this study, fluorescent quartz is visually classified into three categories: dark green, moderate green, and light green. To investigate the uranium (U) content in green, fluorescent quartz within agates as a function of UV intensity, 10 samples were selected with varied green fluorescence for analysis. The elemental analysis was done at Q-ICP-MS facility at National Geochronology Facility, IUAC, New Delhi. Q-ICP-MS results showed the U concentration between 114 ppb and 1446 ppb. The quartz samples from agates, after fine powdering, were integrated into soda-lime-silica glass matrices through controlled melting and quenching processes. Preliminary microbiological experiments indicate that some of the glass compositions exhibit notable antifungal and antibacterial activity. These promising observations open new avenues for the development of specialty glasses with inherent bioactive properties, particularly valuable in healthcare and environmental applications.

This study is currently under the process of patent filing, detailed descriptions of the experimental procedures, glass compositions, and specific biological assay results are intentionally withheld from this abstract. Further investigations are ongoing to study the material properties and fully understand the mechanisms underlying the observed bioactivity.

5.3.8 Paleoseismological evidence for segmentation of the Main Himalayan Thrust in the Darjeeling-Sikkim Himalaya

Atul Brice[1,2], R. Jayangondaperumal[1], Rao Singh Priyanka[3], Pandey Arjun[1], Mishra Rajeeb Lochan[1], Ishwar Singh[1], Madhusudan Sati[2], Kumar Pankaj[4] and Dash Sandipta Prasad[1]

[1] *Wadia Institute of Himalayan Geology, Dehradun, Uttarakhand, India*
[2] *Department of Geology, HNBGU, Srinagar, Uttarakhand, India*
[3] *Department of Geology, University of Delhi, Delhi, India*
[4] *National Geochronology Facility, Inter-University Accelerator Centre, New Delhi, India*

The potential for the Main Himalayan Thrust (MHT)—the primary plate boundary fault accommodating the convergence between the Indian and Eurasian plates—to generate a single, exceptionally large earthquake with surface rupture extending over 700 km remains a matter of ongoing scientific debate [1, 2]. Such an event, if proven possible, would represent one of the most extensive surface-rupturing earthquakes in a continental setting. Paleoseismological investigations conducted in the Darjeeling-Sikkim Himalaya (DSH), a tectonically active region in the eastern Himalaya, have previously identified geomorphic and stratigraphic evidence for large, medieval earthquakes [3]. These events have been tentatively correlated with the historically documented earthquakes that occurred in Nepal and Bhutan during the 11^{th} to 13^{th} centuries CE, suggesting the possibility of a single, enormous rupture that extended across multiple segments of the Himalayan arc, potentially exceeding 700 km in total length.

However, this interpretation is challenged by a notable absence of surface rupture evidence in the DSH from two more recent and well-documented great earthquakes: the 1714 Bhutan earthquake and the 1934 Bihar–Nepal earthquake. Despite their magnitude and regional impact, neither event appears to have produced discernible surface faulting in the DSH segment, based on current paleoseismological data. This lack of

continuity in surface rupture signatures introduces uncertainty about whether great Himalayan earthquakes rupture across multiple segments in a single event or are confined to shorter, independent segments.

To clarify this issue, a detailed paleoseismological trench investigation was carried out at Chenga village in the DSH. The study focused on a ∼10 m high fault scarp along the Himalayan Frontal Thrust (HFT), which represents the surface expression of the MHT. Trench excavations and stratigraphic analysis at this site revealed compelling evidence of a major surface-faulting earthquake that occurred between 1313 and 395 BCE—well before the medieval period events previously considered. This discovery not only challenges the notion that the DSH participated in the 11^{th}–13^{th} century ruptures, but also suggests a longer recurrence interval for major earthquakes in this segment.

Based on these findings, it is proposed that the DSH behaves as an independent seismic segment approximately 150 km in length. This segment appears to be structurally bounded by a transverse ridge and a lateral fault, which may act as barriers to rupture propagation during major earthquakes. The recurrence interval for large surface-rupturing earthquakes in the DSH is estimated to be between 949 and 1963 years—significantly longer than the recurrence intervals observed in neighbouring segments such as the central Nepal Himalaya (∼700–900 years) and the Bhutan Himalaya (∼339–761 years). These differences highlight the heterogeneous nature of seismic behaviour along the Himalayan arc and underscore the importance of segment-specific studies for assessing seismic hazard in this tectonically complex region. This study is published [4].

References:

1. Nakata, T., The Science Reports of the Toboku University, VII series. Geography **22**, 39 (1972).
2. Jayangondaperumal, R. *et al.*, Active Tectonics of Kumaun and Garhwal Himalaya, Springer Singapore, (2018).
3. Pandey, A. *et al.*, Sci. Rep. **11**, 879 (2021).
4. Atul Brice, R. Jayangondaperumal, Rao Singh Priyanka, Arjun Pandey *et al.*, Sci. Rep. **14**, 14537 (2024).

5.3.9 Estimation of fossil fuel CO_2 in Delhi city using radiocarbon measurements

Rajveer Sharma[1], Ravi Kumar Kunchala[2], Sunil Ojha[1], Pankaj Kumar[1], Satinath Gargari[1] and Sundeep Chopra[1]

[1] *National Geochronology Facility, Inter-University Accelerator Centre, New Delhi 110067, India*
[2] *Centre for Atmospheric Sciences, Indian Institute of Technology Delhi, New Delhi, India*

Global warming is one of the most burning issue of the world. Continuous rise in CO_2 concentrations in the atmosphere has a greatest effect on the global warming as it has the highest impact on the overall radiative forcing. The primary source of this increase in CO_2 is the combustion of fossil fuel. Traditionally, fossil fuel emissions are estimated using two approaches: bottom up and top down. The bottom-up approach estimates emissions using the fossil fuel utilization data while in top-down approach uses CO_2 observations from a network of sites. However, it is difficult to infer source information using CO_2 observations alone.

As an alternative method, atmospheric tracer such as ^{14}C, CO, SF_6 etc. are utilized for this purpose. Among these, radiocarbon is a particularly effective tracer for fossil fuel-derived CO_2. Radiocarbon (^{14}C), with a half-life of 5,730 years, is absent in fossil fuels due to its complete decay over millions of years. Consequently, the release of CO_2 from fossil fuel combustion not only increases the atmospheric CO_2 concentration but also reduces the $^{14}C/^{12}C$ isotopic ratio. Atmospheric $^{14}CO_2$ can be reported as Δ^{14}C, the per mil deviation from the absolute radiocarbon reference standard corrected for isotopic fractionation and for radiocarbon decay. Radiocarbon measurements using Accelerator Mass Spectrometry at the National Geochronology Facility, IUAC, helped us to determine the temporal variations in fossil fuel $CO_2(CO_{2ff})$ in Delhi city. We have also analysed annual and seasonal variations of CO_{2ff} over the study region. Additionally, we analyzed the correlations between air pollutants and CO_{2ff}, calculated the emission ratios R_{CO} and R_{NOx} for Delhi, and assessed the impact of COVID-19 lockdowns on CO_{2ff} levels. A manuscript based on these results has been communicated for the publication.

5.3.10 Tracing element mobility during Serpentinization: A case study from Indian Tethyan Ophiolites

Nayak Bikash Ranjan[1] and Ovung Thungyani N[1]

[1] *Department of Earth and Atmospheric Sciences, National Institute of Technology, Rourkela 769001, Odisha, India*

Serpentinization is a geological process in which ultramafic rocks react with water to create a series of exothermic chemical reactions that lead to the formation of serpentine minerals and release of molecular hydrogen and methane. The process not only reconstitutes mineralogical assemblages but also substantially modifies the geochemical composition of the rock [2]. Whole-rock trace and REE data of the Naga Hills and Spongtang ophiolites yield insight into element mobility during serpentinization. Transition elements like chromium (Cr), nickel (Ni), cobalt (Co), and vanadium (V) behave differently during serpentinization. Cr is usually resident in spinel is relatively immobile and ends up being generally enriched in serpentinites via volume loss and redistribution. Ni, which is predominantly present in olivine, displays both enrichment and depletion patterns, with serpentinite contents varying between ~1200 and & 2000 ppm, presumably indicating the extent of breakdown of olivine and partitioning of Ni into secondary serpentine or sulfide minerals. Co is quite immobile, while V shows slight depletion or is preserved based on fluid composition and redox conditions. Fluid-mobile elements such as Sr, Ba, Rb, Cs, Pb, and U are greatly changed. Sr and Ba contents are highly increased in serpentinites (e.g., Sr from 1–3 ppm in peridotites to 5–21 ppm in serpentinites), which suggests incorporation of external fluids, perhaps seawater or subduction-related fluids. Likewise, Rb and Cs, although trace in peridotites, are enriched in serpentinites, as expected by their high fluid mobility [5]. Pb and U are enriched too, particularly in Spongtang serpentinites, which indicate interaction with oxidizing, potentially sediment-controlled fluids [3]. Rare Earth Element (REE) patterns indicate subtle but significant variations. Peridotites show strongly depleted LREEs and relatively flat HREEs indicative of residual mantle signatures. The serpentinites, on the other hand, display mild enrichment of LREEs (e.g., La, Ce) and elevated concentrations of MREEs, supporting REE gain from fluid sources during alteration. HREEs like Yb and Lu hardly change, signaling minimal mobility of these elements [1, 4]. High Field Strength Elements (HFSEs) such as Zr, Nb, Hf, andTa are in general immobile, but localized enrichment in certain serpentinites indicates mobilization under certain fluid conditions. Chalcophile elements Cu and As also exhibit mixed behavior; Cu can be subtracted or supplemented based on the stability of sulfides, whereas As is enriched in serpentinites, pointing towards oxidizing alteration conditions. In general, the geochemical signatures of the Naga Hills and Spongtang serpentinites are indicative of a complex interplay between conservative and non-conservative behavior during serpentinization. Immobile elements (Cr, Co, HREEs) are juxtaposed with the addition of fluid-mobile elements (Sr, Ba, Pb, U, LREEs), which indicate the role of external fluids. These trends are in accordance with serpentinization in a marine hydrothermal or subduction zone environment, where seawater-derived or slab-related fluids are the key to metasomatism. For this study Samples were measured using ICP-MS at the National Geochronology Facility, IUAC.

References:

1. Deschamps, F., Godard, M., Guillot, S., Chauvel, C. *et al.*, Chemical Geology **312–313**, 93 (2012).
2. Hattori, K. H., & Guillot, S., Geochemistry, Geophysics, Geosystems **8**, Q09010 (2007)
3. Peters, D., Bretscher, A., John, T., Scambelluri, M., & Pettke, T., Chemical Geology **466**, 654 (2017).
4. Raia, N. H., Whitney, D. L., Teyssier, C., & Lesimple, S., Geochemistry, Geophysics, Geosystems **23**, e2022GC010395 (2022).
5. Ressico, F., Cannaò, E., Olivieri, O. S., Pastore, Z. *et al.*, Chemical Geology **662**, 122228 (2024).

5.3.11 Biospheric CO_2 flux at a suburban site (Sonipat) in the Indo-Gangetic Plain using radiocarbon measurements

Vimal Jose Vazhathara[1], Ravi Kumar Kunchala[1], Sajeev Philip[1] and Rajveer Sharma[1,2]

[1] *Centre for Atmospheric Sciences, Indian Institute of Technology Delhi, New Delhi*
[2] *National Geochronology Facility, Inter-University Accelerator Centre, New Delhi*

To investigate biospheric CO_2 fluxes over Sonipat in the Indo-Gangetic Plain (IGP), the study will integrate radiocarbon ($^{14}CO_2$) analysis with continuous CO_2 monitoring, following methodologies refined in urban and suburban settings globally [1-3]. Air samples were collected biweekly from April 2024 to March 2025 at 14:00 IST from a rooftop intake at IIT Delhi's Sonipat campus, ensuring sampling during well-mixed atmospheric conditions to minimise local emissions. Continuous CO_2 mole fractions were measured using a Picarro G2301 analyser. For $^{14}CO_2$ analysis, 10 L air samples were collected in chemically inert bags and graphitised in graphitization laboratory at the National Geochronology Facility, IUAC. Radiocarbon in these graphite will be measured using accelerator mass spectrometry (AMS) of National Geochronology Facility to quantify the fossil fuel-derived CO_2 (CO_{2ff}) component, as demonstrated in other studies worldwide [1,2]. Background CO_2 levels, determined using the Adaptive Diurnal Variational Selection (ADVS) method, which identifies the daily minimum (5th percentile) have been used to represent regional baseline air, a technique validated in the Beromünster tall tower study [3].

The CO_{2ff} time series will be calculated by combining $^{14}CO_2$ -derived fossil fractions within situ CO_2 data and biospheric CO_2 will be isolated by subtracting CO_{2ff} and background CO_2 from the total observed CO_2. Seasonal and diurnal variations will be analysed to differentiate photosynthetic uptake and respiratory emissions, with boundary-layer dynamics assessed using meteorological data. Results will be validated against regional emission databases and global models, ensuring alignment with methodologies that have exposed underestimated fossil emissions in complex urban environments. This dual-tracer strategy aims to provide a replicable template for quantifying biospheric fluxes in rapidly urbanising regions like the IGP.

References:

1. Basu, S., Lehman, S. J., Miller, J. B., Andrews *et al.*, Proc. of the National Academy of Sciences **117**, 13300 (2020).
2. Berhanu, T. A., Szidat, S., Brunner, D., Satar, E. *et al.*, Atmospheric Chemistry and Physics **17**, 10753 (2017).
3. Zazzeri, G., Graven, H., Xu, X., Saboya, E. *et al.*, Geophysical Research Letters **50**, e2023GL103834 (2023).

5.3.12 Scientific and chronological investigation of ancient construction practices of UNESCO World Heritage Sites of Nalanda Mahavihara

Anand N.J.[1], Singhal V.[1] and Kumar P.[2]

[1] *Department of Civil and Environmental Engineering, Indian Institute of Technology Patna, Patna 801103, India*
[2] *National Geochronology Facility, Inter-University Accelerator Centre, New Delhi 110067, India*

Nalanda Mahavihara showcases the majestic structural and engineering advancements achieved by an ancient Indian civilization. As a well-planned university, it is believed to have started during the Gupta rule, i.e., the 4th century CE. Thereafter, its expansion was carried out by successive dynasties until the 13th century CE. The excavation carried out on more than 48 acres of land has exposed 16 large structures, and these structures in total show seven levels of construction phases. Despite its recognition as a UNESCO World Heritage Site, Nalanda Mahavihara lacks a systematic chronological study aimed at understanding the construction practices and techniques employed in its development. This investigation seeks to establish a detailed construction chronology by examining the evolution of materials used in the manufacturing of brick and mortar. A comprehensive site survey was conducted which yielded three charcoal samples, one half burned rice grain, seven brick samples and 14 lime mortar samples. These samples are being dated with radiocarbon (^{14}C) using Accelerator Mass Spectrometry (AMS) facility at National Geochronology Facility, IUAC. The methodology of AMS radiocarbon dating has been discussed [1,2]. All the sample were graphitized which converts CO_2 into graphite (elemental carbon). Laboratory analyses, including chemical and microstructural characterization, will be performed on the dated samples to gain insights into ancient construction methods at Indian Institute of Technology Patna [3]. The outcomes will contribute to both the historical understanding of building techniques and the development of compatible materials for conservation interventions.

References:

1. T. Jull, G. S. Burr, and G. W. Hodgins, Quatern. Int., **64**, 299 (2013).
2. R. Sharma, G. R. Umapathy, P. Kumar, S. Ojha *et al.*, Nucl. Instrum. Methods B **438**, 124 (2019).
3. N. J. Anand, V. Singhal, and S. Manohar, Case Stud. Constr. Mater. **22**, e04412 (2025).

5.3.13 A comprehensive analysis of presence of heavy and trace elements in tumor cells suggesting the importance of personalized medicine

Mudasir Ashraf Shah[1], Afzal Anees[2], Mohammad Jaseem Hassan[3], Mohd. Azhar Aziz[4] , Pavitra V. Kumar[5] and Pankaj Kumar[5]

[1] *Radiological Physics, Department of Diagnosis, Faculty of Medicine, Aligarh Muslim University, Aligarh*
[2] *Departments of Surgery, Faculty of Medicine, Aligarh Muslim University, Aligarh*
[3] *Department of Pathology, Faculty of Medicine, Aligarh Muslim University, Aligarh*
[4] *Interdisciplinary Nanotechnology Center, Aligarh Muslim University, Aligarh*
[5] *National Geochronology Facility, Inter-University Accelerator Centre, Aruna Asaf Ali Marg, New Delhi*

Cancer, a complex disease, causes about 10 million global deaths yearly, posing challenges in diagnosis and treatment. Factors like trace elements, heavy metals, and metalloids play crucial roles in cancer development. Investigating these micronutrients could help understand cancer progression. The significance of trace element anomalies in the context of cancer has sparked increasing interest since they have been linked to carcinogenesis and tumor progression. The millions of cancer cells implanted in a microenvironment warped by neoplastic alterations make up tumors. The striking heterogeneity of the cells that make up the tumor microenvironment and cancer cells contributes to the advancement of the disease and resistance to

therapy. Therefore, enhancing clinical outcomes requires a deeper comprehension of the cellular, molecular, and geographical heterogeneity present in cancers as well as the application of this information to therapy design. The present study is aimed to determine the elemental concentrations in tumor cells with Quadrupole Inductively Coupled Plasma – Mass Spectroscopy (Q-ICP-MS).

A total of 10 specimens, each of paired tumorous and normal tissue were obtained from surgical excision with confirmed diagnosis of malignancy. The normal tissue was taken from regions of the organs defined by the safety margins from the same patients. The paired sample methodology adopted in this study was to avoid the demographic uncertainties which may arise due to difference in age, diet, sexual orientation, hormonal status, medication, genetics and other environmental factors. The Collected normal and malignant tissue fixed in formaldehyde solution were subjected to histopathology study by the senior pathologist of our institution to confirm that the normal tissue is normal only and the malignant tissue comprises of at least 50% atypical cancer cells. The tissue samples submerged in ethanol were utilized for Quadrupole Inductively Coupled Plasma Mass Spectrometry (QICPMS) after drying, approximately 1 mg of finely grounded sample were digested in strong nitric acid (HNO_3) fallowed by hydrogen peroxide (H_2O_2) treatment at 60°C. The dried residue was dissolved in 1% HNO_3 acid and filtered to remove any insoluble component present in the sample. The analysis was carried out with iCAP-Q ICP-MS from Thermo Scientific at the National Geochronology Facility (NGF), IUAC. The kinetic energy discrimination (KED) mode was employed for removal of spectral interferences. For calibration, multi-element standard from Inorganic Ventures and single element (for Hg) standard from Merck was used. The acquired data was analyzed using QTEGRA ISDS software. For data validation, a known concentration (25 ppb) of multi-element standard and mercury (Hg) standard (10 ppb) was run as secondary standard and the observed offset of measured values were less than 5% from reference values. The reported values are average of three runs carried out during one sample acquisition. Further, in order to measure the quantitatively changes in trace element levels for the two tissue classes fold change was computed. The student's t-test was performed to compare the means of normal and tumor tissue for each element at 95% level of significance and to estimate the element-wise variation in the logarithm of fold change. The Euclidean hierarchical heatmap clustering analysis (Euclidean distance) of all the trace elements was plotted to illustrate the in normal and tumor tissues. The preparation of final manuscript is under process.

References:

1. Jahankhani K., Taghipour N., Mashhadi Rafiee M. *et al.*, Food Chem. Toxicol. **179**, 113983 (2023).
2. Sravani, A.B., Ghate, V. & Lewis, S., Biol. Trace Elem. Res. **201**, 1026 (2023).
3. Institute of Medicine, Food and Nutrition Board. Dietary Reference Intakes for Vitamin A, Vitamin K, Arsenic, Boron, Chromium, Copper, Iodine, Iron, Manganese, Molybdenum, Nickel, Silicon, Vanadium and Zinc Washington, DC: National Academy Press, (2001).

5.3.14 The production of low carbon steel at the Vikramshila Mahavihara

Eshan Harit[1], Prof. Sukanya Sharma[1] and Rajveer Sharma[2]

[1] *Department of Humanities and Social Sciences, Indian Institute of Technology, Guwahati, 781039, India*
[2] *National Geochronology Facility, Inter-University Accelerator Center, New Delhi 110067, India*

More than 1,000 iron objects have been recovered from the Vikramshila Mahavihara, comprising 28 different types including weapons (daggers, javelins, arrowheads), tools (chisels, needles, nails), and ornaments (bangles, rings, beads)[1]. This diversity points to an advanced metallurgical tradition. Explorations around the monastery reveal a long, continuous history of iron production in the surrounding landscape. Approximately 20 iron production sites have been identified, providing strong evidence of sustained and extensive ironworking activities throughout the medieval period.

Samples were collected from the identified iron production sites, including tap and body slags. These samples were brought under study using petrography, XRD, and SEM-EDS analysis. Under reflected light, the slag exhibited evidence of wüstite, fayalite, and magnetite. EDS analysis confirmed the presence of 30-50% oxygen, 20-30% iron, and 8-10% silica, among other minerals. These studies provide insights into the provenance, firing range, and production techniques of these artifacts. A total of eight samples—two iron and six slags—were submitted for AMS carbon dating at National Geochronology Facility (NGF), IUAC. It was suggested that the carbide present in the sample could be a potential source of carbon extraction. To prevent modern contamination, the samples were powdered using titanium nitrate-coated drill bits. The powdered samples were then weighed and stored in centrifuge tubes. During the graphitization process, the

carbon percentage in the slag samples was analyzed. The two iron samples showed carbon content of 0.3% and 0.34%. The presence of 0.3% carbon in one of the iron samples confirms its identity as low carbon steel. The slag samples exhibited carbon content ranging from 0.33% to 0.06%, indicating that the slag also traps some carbon during the firing process. However, the carbon content in the slag varies, suggesting that additional samples may be required for further analysis.

The study confirms that the iron was produced using a bloom in a cylindrical furnace. Evidence of such furnace parts has been found in the Vikramshila landscape. Based on the presence of wüstite, magnetite, and fayalite, it is suggested that the slag was fired at a temperature range of 1000^{o}C to 1200^{o}C. This temperature range allows for the coexistence of magnetite and fayalite, while wüstite remains stable within this range, especially with the use of human-driven bellows. Carbon dating of the samples will provide a date range for the production of iron, offering insights into the continuity of iron production knowledge across millennia in the Vikramshila landscape.

References:

1. Verma B.S., Antichak-2, Archaeological Survey of India, Janpath, New Delhi p-261 (2011).

5.3.15 Oral traditions of the Lepchas: An archaeological enquiry in Sikkim

Sukanya Sharma[1] and Upasna Chettri[1]

[1] *Department of Humanities and Social Sciences, Indian Institute of Technology Guwahati, North Guwahati, Assam 781039*

The limited availability of absolute dates within the archaeological context of the region has resulted in Sikkim remaining a significant gap in the archaeological record, both spatially and temporally. To address this gap, five charcoal samples retrieved from various stratigraphic depths. These samples were measured for radiocarbon dating with the help of Accelerator Mass Spectrometry (AMS) housed at National Geochronology Facility (NGF), IUAC.

The radiocarbon dates obtained were calibrated using the OxCal 4.4 application, an online tool for refining radiocarbon age estimates. The radiocarbon dates and their calibrated range is given in Table 5.2.

The results of the analysis are partially published [1].

Table 5.2: Radiocarbon ages, calibrated age of charcoal samples.

Sl. no.	Sample name) (IUAC code)	Sample depth) (cm)	Radiocarbon date (BP)	Calibrated date range (BCE / CE)
1	DRD C.1(23C6558)	30	980 ± 36	1016 CE - 1159 CE
2	DRD C.2(23C6559)	42	357 ± 26	1547 CE - 1635 CE
3	DRD C.3(23C6560)	78	345 ± 33	1468 CE - 1638 CE
4	DRD C.4(23C6561)	97	2107 ± 30	199 BCE - 45 BCE
5	DRD C.5(23C6562)	100	330 ± 31	1479 CE - 1640 CE

References:

1. U. Chettri and S. Sharma, Space and Culture, India **12**, 83 (2024).

5.3.16 Trace metal analysis in atmospheric aerosols (PM_{10}) in the cities of Bihar, India

Nisha Verma[1] and Ningombam Linthoingambi Devi[1]

[1] *Department of Environmental Science, Central University of South Bihar, Gaya 824236, Bihar*

Atmospheric particulate matter (PM) pollution is a major environmental concern due to its potential health impacts and ability to transport toxic trace metals over long distances [1-3]. Among the various constituents of PM, heavy metals are of particular concern due to their toxicity, persistence, and bioaccumulative nature. Bihar, located in the Indo-Gangetic Plain, frequently experiences poor air quality, yet systematic assessments of metal content in PM are limited. To investigate seasonal variations and sources of trace metal pollution in atmospheric aerosols, coarse particulate matter (PM_{10}) samples were collected from

seven cities in Bihar: Patna, Gaya, Muzaffarpur, Hajipur, Sonpur, Samastipur, and Aurangabad. The Q-ICPMS facility at the National Geochronology Facility (NGF), IUAC, provided high-sensitivity and accurate metal quantification, which is crucial for understanding trace metal pollution dynamics in the region.

For analyzing heavy metals in PM_{10}, samples were digested using a HNO_3 and HF mixture and analyzed using the Q-ICPMS. The study quantified concentrations of metals such as Mg, Cr, Mn, Fe, Ni, Cu, Zn, As, Sr, Cd, Ba, Hg, Pb, and U. Furthermore, the work aims to perform health risk assessments and source apportionment using receptor models such as PCA and PMF. The experimental part, sample collection, digestion, and Q-ICPMS analysis have been completed. The raw data has been obtained and is currently being processed for statistical interpretation. The results, including detailed data analysis and risk assessments, will be included in a forthcoming manuscript.

References:

1. Allen, A. G., Nemitz, E., Shi, J. P., Harrison, R. M., and Greenwood, J. C., Atmospheric Environment **35**, 4581 (2001).
2. Attri, P., Mani, D., Satyanarayanan, M., Reddy, D. V., Kumar, D., Sarkar, S., and Hegde, P., Heliyon **10**, e26746 (2024).
3. Rawat, B., Sharma, C. M., Tripathee, L., Wan, X., Cong, Z., Paudyal, R., and Zhang, Q, Environ. Pollut. **344**, 123359 (2024).

5.4 Atomic and molecular physics

5.4.1 Charge state distribution for 1.78–3.93 MeV/u Si projectiles passing through 10 μg/cm^2 carbon foil

D. K. Swami[1], Sarvesh Kumar[2], Sunil Ojha[1] and R. K. Karn[3]

[1] *Inter-University Accelerator Centre, New Delhi 110067, India*
[2] *Chemical Science Division, Lawrence Berkeley National Laboratory, Berkeley, CA, 94720, USA*
[3] *Jam. Cooperative College, Jamshedpur, Kolhan University, Chaibasa, Jharkhand India*

The charge state distribution of Si projectiles with energies ranging from 1.78 to 3.93 MeV/u, and initial charge states Si^{p+} (p=4-10), was investigated after traversing a 10 μg/cm^2 carbon foil (schematic of the experimental set up shown in Fig. 5.23). This study was focused on determining the relevant parameters of the outgoing projectile such as the charge state distribution fraction (F_q), the mean charge state (q_m), distribution width (w), and asymmetric/skewness parameter (s). These parameters were then compared with predictions from the Fermi gas model [1] and ETACHA4 [2]. Notably, a significant disparity was observed between the experimental measurements and the theoretical calculations, with the latter overestimating the former. This overestimation was attributed to non-radiative electron capture (NREC) occurring at the exit surface[3], influenced by the wake and dynamic screening effects [1]. Understanding and accurately determining the charge state distribution parameters hold immense importance in various scientific applications including in the field of plasma studies, these fractions of charge states are directly utilized to tackle complex problems and facilitate the detection of superheavy ions. Furthermore, these parameters play a vital role in enhancing our understanding of ion behavior, collision dynamics, and plasma characteristics. The insight observed from such parameters may be used to refine the theoretical models for accurate predictions and in planning of experiments involving ion interactions.

A thorough comparison of experimental data with ETACHA4 and F-G-M predictions for mean charge state, shown in Fig. 5.24 reveals that these models overestimate the experimental values, indicating that the exit surface might play a significant role in changing the charge state due to the non radiative electron capture at the exit surface of the target. Therefore, we find that there is a need to consider the effect of exit surface to be included in the current theoretical models. Experimentally there is a need to study the effect of the bulk and the exit surface of the target by performing a thorough study of CSD by varying the target and projectile parameters. Further, we purpose that the coincidence experiments between the characteristic x-ray emitted from a target and the outgoing projectile charge states may also be performed to elucidate the presence of capture of electrons at the exit surface of the target.

References:

1. W. Brandit, R. Laubert, M. Mourino, *Phys. Rev. Lett* **30**, 358 (1973).
2. E. Lamour, P. D. Fainstein, M. Galassi, C. Prigent *et al.*, *Phys. Rev. A* **92**, 42703 (2015).
3. M. Kaur, S. Kumar and T. Nandi, *Phys. Rev A* **108**, 052817 (2023).

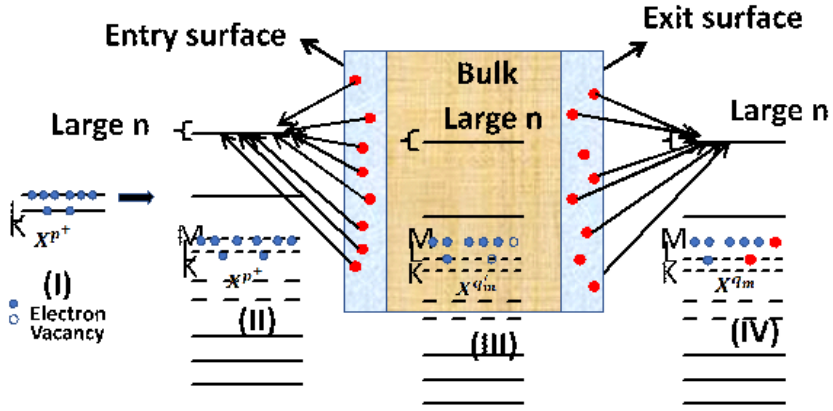

Figure 5.23: Schematic of the experimental setup where X^{p+} denotes the incoming projectile and $X^{(q\pm n)+}$ represent the CSD of the outgoing projectile after traversing the C-foil (a) electron capture processes occurring at the entrance and exit target surface during the passage of the projectile ions X^{p+} through a target medium. $X^{q'_m}$ and X^{q_m} denote the mean charge state of the projectile inside the target and after traversing through target, respectively (b).

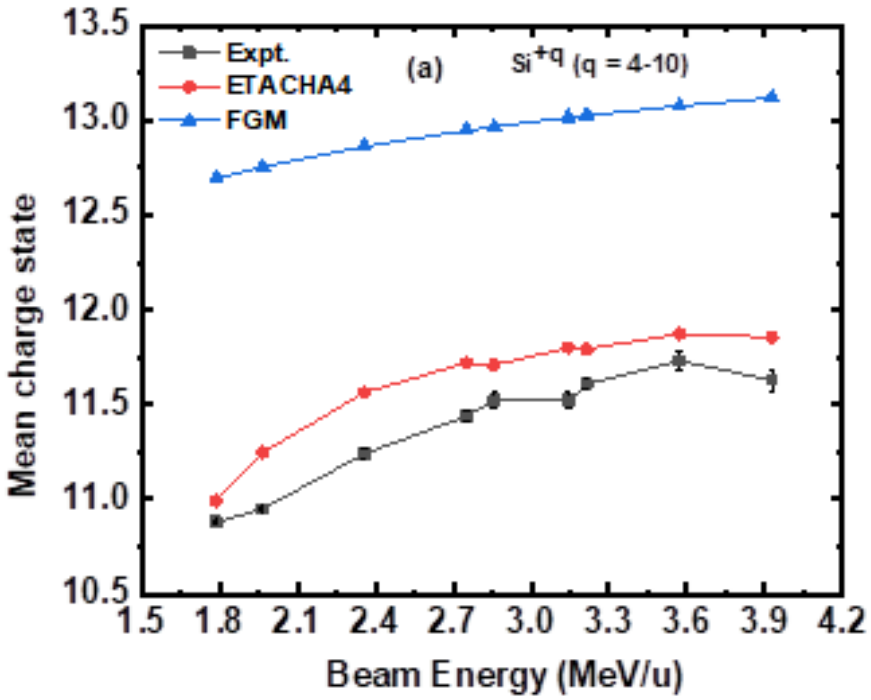

Figure 5.24: Mean charge state (q) versus Beam Energy (MeV/u): (a) Comparison between experimental, ETACHA4 and F-G-M mean charge state for ^{28}Si on C

5.4.2 Measurement of Ar^{q+} ion induced tungsten M x-ray relative intensity ratio with energy dependence

D. K. Swami[1,4], B. Singh[2], S. Kaur[3] and R. K. Karn[5]

[1] *Inter-University Accelerator Centre, Aruna Asaf Ali Marg, New Delhi 110067, India*
[2] *Department of Physics, Punjabi University, Patiala, Punjab, India*
[3] *Department of Physics, Akal University, Bathinda, Punjab, India*
[4] *Department of Physics, Kolhan University, Chaibasa, Jharkhand, India*
[5] *Jam. Cooperative College, Jamshedpur, Kolhan University, Chaibasa, Jharkhand, India*

The measurement of M-shell x-ray production from $_{74}$W under energetic highly charged ion Ar^{q+} impact has been reported. The intensity ratios, $I_{Mk}/I_{M\alpha\beta}$, (where $k = \epsilon, \gamma, \delta, m1, m2$) for Tungsten induced by 875-2100 keV Ar^{q+} (q=7,8) ions have been measured. These intensity ratios have been compared with estimated intensity ratios based on ECPSSR and ECUSAR models [1-5]. Significant difference have been observed between measured and estimated intensity ratios. However, no significant effect of the mean charge state or projectile vacancy configuration is found on the theoretical intensity ratios. For present measurements, natural ^{74}W targets of 230 μg/cm^2 thickness, deposited on a very thin carbon backing of 12 μg/cm^2 thickness, have been fabricated in ultra-high vacuum environment (Fig. 5.25) by the evaporation method using 8 kW electron beam. The targets have been characterized by X-ray Diffractometry, Scanning Electron Microscopy, and Energy Dispersive X-ray Spectroscopy (Fig. 5.26). The thicknesses of the targets have been measured using the Rutherford Backscattering Spectrometry (Fig. 5.27).

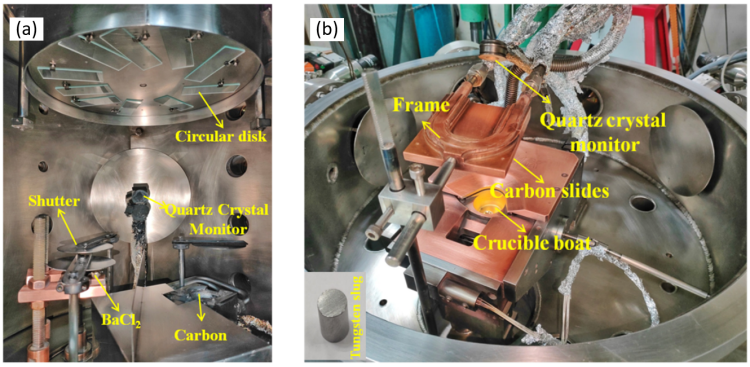

Figure 5.25: (a) Dedicated evaporation chamber for the fabrication of Carbon. (b) Evaporation chamber for the fabrication of Tungsten target.

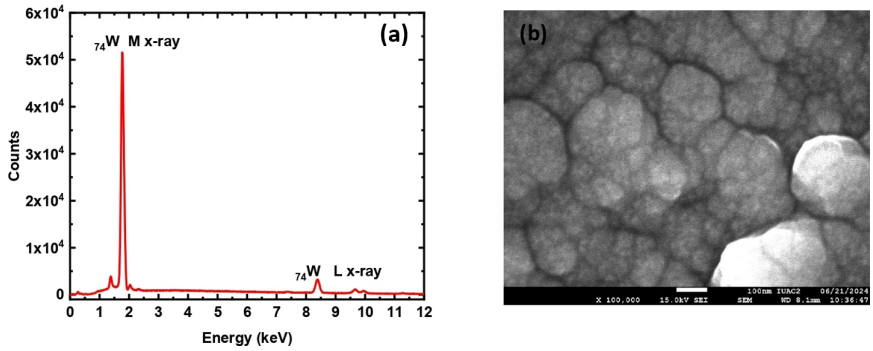

Figure 5.26: (a) EDS characterization of natural $_{74}$W target films to determine the elemental composition of the films. (b) SEM images of $_{74}$W targets at a magnification of 100K.

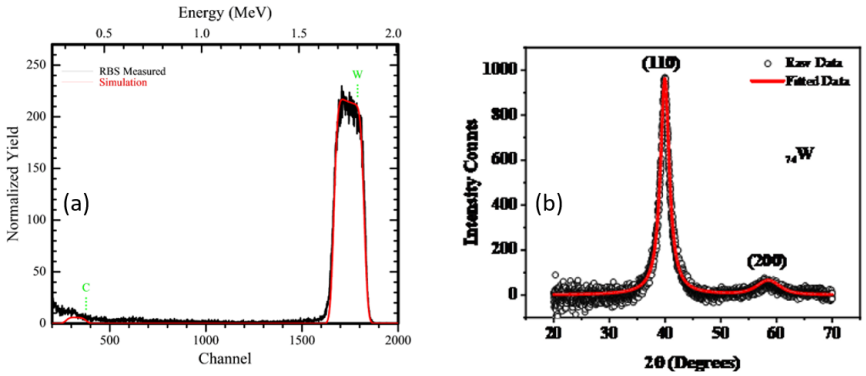

Figure 5.27: (a) The RBS spectrum of $_{74}$W. The simulation have been performed using SIMNRA software. (b) The GIXRD pattern of the deposited Tungsten thin film. The solid red line is the fit using Fityk.

X-ray measurements on $_{74}$W: The experiment was performed using the Low Energy Ion Beam Facility (LEIBF) [6] at IUAC. Ar^{q+} energies from 875 keV to 2100 keV were chosen for the experiment. A tungsten target was mounted on a 10 mm diameter target holder ladder, which can be moved linearly using a linear motion feedthrough.

The HCI induced x-rays produced from the Tungsten target have been obtained (Fig. 5.28) and the intensity ratios of various M-shell x-ray components have been measured for the first time. These intensity ratios are compared with the theoretical ECPSSR and ECUSAR models. Upon comparison, there is significant difference between theoretical estimation and experimental findings. However, for ratio $\frac{I_{M_{\alpha\beta}}}{I_{M_{total}}}$, the experimental and theoretical results agree within the experimental uncertainties. Both the theoretical models ECPSSR and ECUSAR show no significant difference for the initial and mean charge states of the incident projectile. However, the experimental intensity ratios show varying trend when compared to these models. We suggest that by considering the electron capture processes along with the DCI+MI processes in the theoretical models may reduce the discrepancy with the experimental data.

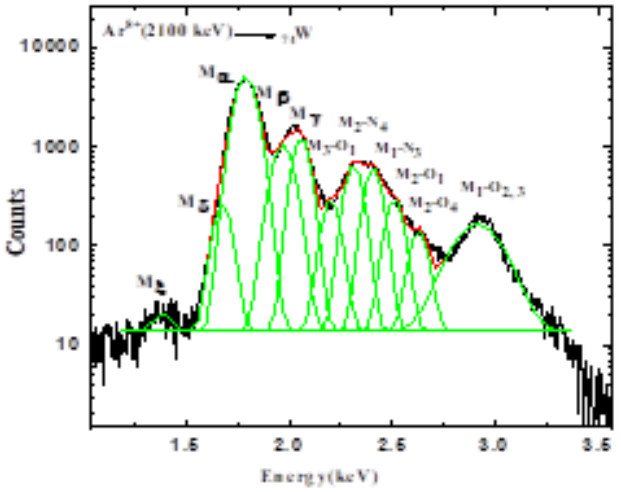

Figure 5.28: M shell x-ray spectrum for $_{74}$W induced by 2100 keV Ar^{8+} ion beam with fitted using multi Gaussian function.

References:

1. Z. Liu and S. J. Cipolla, *C*omput. Phys. Commun. **97**, 315 (1996).
2. Z. Liu and S. J. Cipolla, *C*omput. Phys. Commun. **1**82, 2439 (2011).
3. Z. Liu and S. J. Cipolla, *C*omput. Phys. Commun. **1**80, 1716 (2009).
4. S. J. Cipolla, *C*omput. Phys. Commun. **1**76, 157 (2007).
5. S.J. Cipolla, *N*ucl. Instrum. Methods B **2**61, 142 (2007).
6. D. Kanjilal, T. Madhu, G. O. Rodrigues, U. K. Rao, C. P. Safvan and A. Roy, *I*nd. J. Pure Appl. Phys. **3**9, 25 (2001).

5.4.3 Equilibrium and non equilibrium charge state distribution of fast Ti^{+p} ions in carbon target

D. K. Swami[1,4], P. Bhatt[1], S. Ojha[1], Veena C. P.[1], K. K. Pal[1], A. Kumar[1], B. Singh[2], M. Verma[3] and R. K. Karn[5]

[1] *Inter-University Accelerator Centre, Aruna Asaf Ali Marg, New Delhi 110067, India*
[2] *Department of Physics, Punjabi University, Patiala, Punjab, India*
[3] *Department of Physics, University of Rajasthan, Rajasthan, India*
[4] *Department of Physics, Kolhan University, Chaibasa, Jharkhand, India*

[5] *Jam. Cooperative College, Jamshedpur, Kolhan University, Chaibasa, Jharkhand, India*

The equilibrium and non equilibrium charge state distribution of Ti^{+p} (p = 3-7) passing through carbon foils of varying thicknesses have been measured (Fig. 5.29) across an energy range 0.83 - 2 MeV/u. Key parameters of outgoing projectile, such as charge state fractions F_q, mean charge state q_m, distribution width d, and skewness s have been determined and compared with predictions from the ETACHA4 code [1]. Equilibration is achieved with carbon foils of 20 $\mu g/cm^2$ and thicker throughout the energy range studied. The Fermi Gas Model [2] has been employed to estimate the mean charge state inside the target, and these values are compared with the experimental equilibrium mean charge states. A notable discrepancy has been observed between experimental findings and Fermi Gas Model estimations, which is attributed to non radiative electron capture occurring at the target's exit surface, influenced by wake effect and dynamic screening [2]. Furthermore, a comparison of the experimental mean charge state with empirical models indicates that the Shima-Ishihara-Mikumo model [3] provides a more accurate fit to the experimental data.

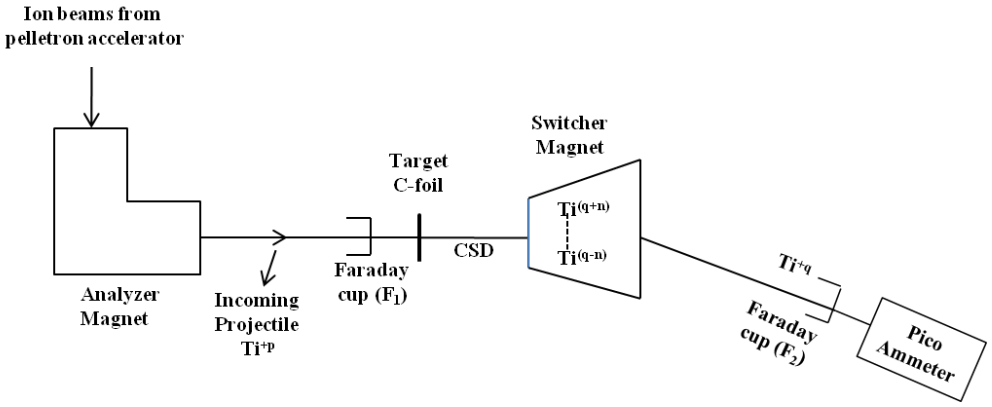

Figure 5.29: Schematic of the experimental setup.

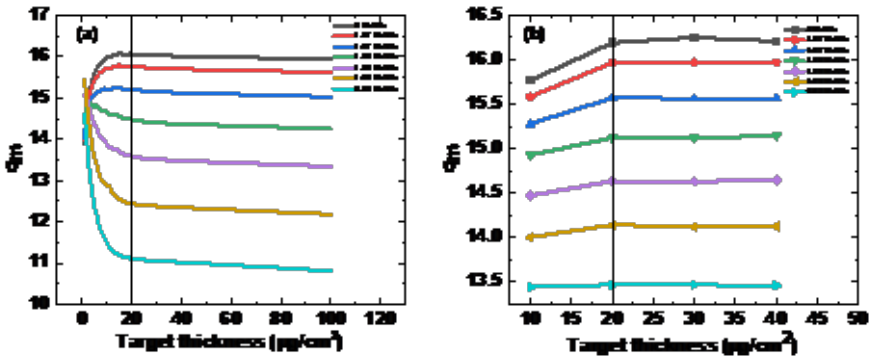

Figure 5.30: Mean charge state q_m versus carbon target thicknesses for Ti^{+p} (p=3-7) ions with energy range 0.83 - 2 MeV/u. (a) ETACHA4 calculations and (b) experimental results.

We observed that at higher energies, the ETACHA4 code exhibits good agreement with experimental data within the uncertainties (Fig. 5.30). However, at low energies, significant discrepancy arises due to large distortion. While ETACHA4 [1] is an extended version of the earlier ETACHA code towards low energy side (0.5 - 30 MeV/u), it still shows notable deviations from experimental data in this regime. Therefore, it is concluded that there is a need for further theoretical refinements to improve its accuracy at lower energies. The experimentally determined equilibrium thickness is 20 $\mu g/cm^2$ and above, which shows good agreement with ETACHA4 predictions.

Furthermore, the experimental results have been compared with empirical models, including Shima et al. (SIM) [3], Nikolaev and Dmitriev (N&D) [4] and SGM [5]. The comparison indicates that the SIM model provides a more accurate fit to the experimental data compared to the N&D and SGM models. Additionally,

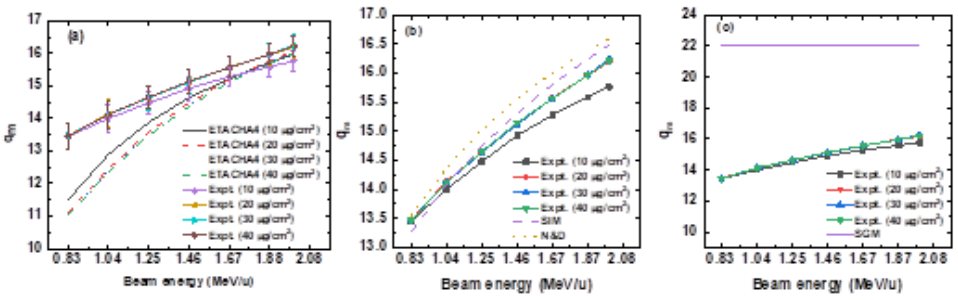

Figure 5.31: Mean charge state q_m versus beam energy with energy range 0.83 - 2 MeV/u for 20-40 μg/cm^2 thicknesses. Comparison between experimental data and Fermi gas model (FGM) estimations. Solid lines are for guiding the eye.

we calculated the mean charge state inside the target using Fermi Gas Model (FGM) [2] and compared it with experimental data (Fig. 5.31). The results show that the FGM overestimates the experimental values, indicating that the mean charge state inside the target is higher than that at its exit. This suggests that the exit surface of the target plays a crucial role in charge-changing processes.

References:
1. E. Lamour, P. D. Fainstein, M. Galassi, C. Prigent *et al.*, Phys. Rev. A **92**, 42703 (2015).
2. W. Brandit, R. Laubert and M. Mourino, Phys. Rev. Lett **30**, 358 (1973).
3. K. Shima, T. Ishihara, T. Miyoshi and T. Mikumo, Phys. Rev. A **28**, 2162 (1983).
4. V. Nikolaev and I. Dmitriev, Phys. Lett. A **28**, 277 (1968).
5. G. Schiwietz, K. Czerski, M. Roth, F. Staufenbiel and P. Grande, Nucl. Instrum. Methods B **225**, 4 (2004).

5.4.4 L- shell X-ray production cross sections for Au and Bi induced by 30 MeV to 75 MeV boron ions

Balwinder Singh[1], Shehla[2], Anil Kumar[1], D. K. Swami[3], Ajay Kumar[4] and Sanjeev Puri[1]

[1] *Department of Physics, Punjabi University, Patiala, Punjab, India*
[2] *Department of Physics, Govt Mohindra College, Patiala, India*
[3] *Inter-University Accelerator Centre, Aruna Asaf Ali Marg, New Delhi 110067, India*
[4] *Nuclear Physics Division, Bhabha Atomic Research Centre, Trombay, Mumbai 400085, India*

Ion atom collisions can lead to the creation of atomic L-shell vacancies through two main processes: direct Coulomb ionization (DCI) or the capture of a target electron by the projectile. These ionized atoms then undergo relaxation either via radiative transitions, resulting in the emission of characteristic X-rays, or via non-radiative transitions, leading to the emission of Auger electrons. Precise and reliable data on L-shell X-ray production (XRP) cross sections are important for a wide range of applications [1, 2], such as plasma diagnostics, astronomical X-ray studies, ion implantation, radiation shielding, dosimetry, and elemental analysis using the Particle Induced X-ray Emission (PIXE) technique.

To determine the XRP cross sections for a specific element and ion beam, key theoretical parameters are required. These include the ionization cross sections (ICS), X-ray emission rates, and fluorescence and Coster–Kronig (CK) yields. The ICS values for a given target-projectile combination can be calculated using various theoretical models such as the Semi-Classical Approximation (SCA) [3], the Plane Wave Born Approximation (PWBA) [4], and more advanced models like ECPSSR [5] and its United Atom variant, ECPSSR-UA [6]. The computer code "ISICS" [7–11] is commonly used to compute the ICS values for K-, Lp (p = 1–3), and Mj (j = 1–5) subshells based on the ECPSSR and ECPSSR-UA models, for various combinations of target and projectile.

Other required parameters such as X-ray emission rates, fluorescence yields, and CK yields are typically estimated using models based on the Independent Particle Approximation (IPA) [12, 13]. A detailed review of the available physical parameters for L- and M-shells has been provided in the literature [14].

In this work, Au and Bi targets were bombarded with B^{+q} ions (q = 3, 4, 5) in the energy range of 30–75 MeV to study the dependence of L-shell X-ray emission on projectile energy and the effect of multiple ionization. The experimental XRP cross sections obtained were compared with theoretical predictions, which

were computed using fundamental parameters reported in the literature [4, 6, 7, 15, 16]. In addition, the fluorescence yields, which play a significant role in X-ray production, were calculated for the studied elements to improve the interpretation of the results. These calculations help quantify the efficiency of X-ray emission following ionization and allow for meaningful comparison with theoretical results, such as those derived from ISICS [7–11]. The accuracy of these cross-section analyses depends strongly on reliable fluorescence yield values.

The measured L_r XRP cross sections and average fluorescence yields for boron ion-induced emissions in Au and Bi targets were found to be significantly higher than the theoretical estimates, as shown in Fig. 5.32. It is well known that charged particles can cause substantial simultaneous multiple ionization in both outer and inner shells, which in turn can affect X-ray emission rates as well as fluorescence and CK yields. In this study, fluorescence and CK yields corrected for multiple ionization were determined using the procedure proposed by Lapicki [17]. When these corrected yields were used, the calculated L_r XRP cross sections differed by up to 8% compared to those obtained using single-vacancy yields.

However, the large discrepancies observed between experimental and calculated XRP cross sections could not be fully explained by the multiple ionization corrections based on Lapicki's formalism [17]. This suggests that the models used for evaluating charged particle-induced inner-shell ionization may need to include additional effects such as multiple ionization, many-body interactions, and solid-state effects in order to account for the observed differences between experimental data and theoretical predictions.

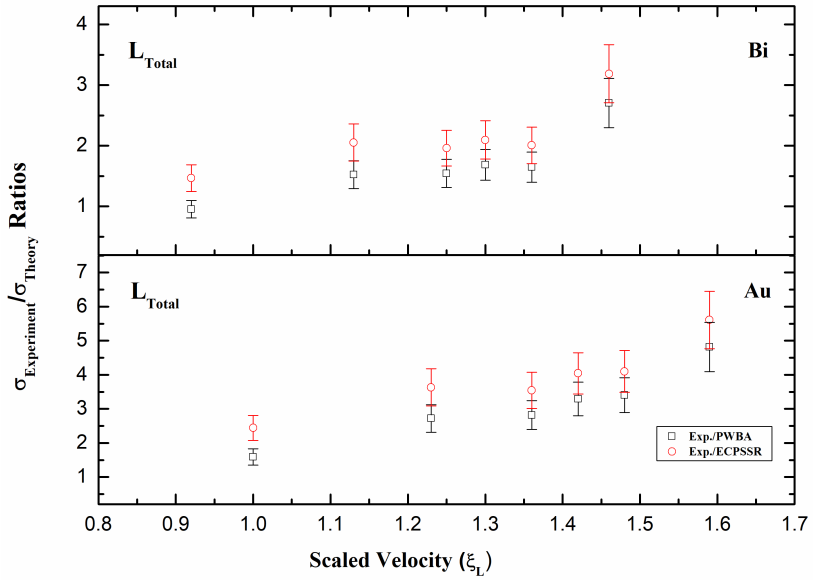

Figure 5.32: A plot of ratios of measured σ_k^X (k = L_{Total}) σ_k^X (PWBA) and σ_k^X (ECPSSR) for Au and Bi as a function of scaled velocity (ξL).

References:

1. J. H. Hubbell, Report NISTIR 89 (1989).
2. J. H. Hubbell, Radiat. Research **70**, 58 (1977).
3. J. M. Hansteen, O. M. Johnson and L. Kobach, J. Phys. B. **7**, L271 (1974).
4. E. Merzbacher and H. W. Lewis, Encyclopedia of Phys. Ed. S. Flugge **34**, 166 (1958).
5. W. Brandt and G. Lapicki, Phys. Rev. A **23**, 1717 (1981).
6. G. Lapicki, Nucl. Instrum. Methods B **189**, 8 (2002).
7. S. J. Cipolla, Comput. Phys. Commun. **176**, 157 (2007).
8. S. J. Cipolla, Nucl. Instrum. Methods B **261**, 142 (2007).
9. Z. Liu and S. J. Cipolla, Comput. Phys. Commun. **97**, 315 (1996).
10. Z. Liu and S. J. Cipolla, Comput. Phys. Commun. **180**, 1716 (2009).
11. Z. Liu, and S. J. Cipolla, Comput. Phys. Commun. **182**, 2439 (2011) 2439.
12. J. H. Scofield, Lawerence Livermore University Report no UCRL 51326 (1973).
13. B. Crasemann, Eds., Atomic inner-shell Ionization Processes, Part A, Academic Press, New York, (1985).
14. Shehla and S. Puri, Rad. Phys. Chem. **127**, 194 (2016).
15. J. L.Campbell and J. X. Wang, At. Data Nuc. Data Tables **43**, 279 (1989).
16. S. Puri, D. Mehta, B. Chand, N. Singh and P. N. Trehan, X-Ray Spectrometry **22**, 358 (1993).
17. G. Lapicki, R. Mehta, J. L. Duggan, P. Kocur, J. Price and F. D. McDaniel, Phys. Rev. A **34**, 3813 (1986).

5.4.5 Multiple neutral emissions from ionic forms of small hydrocarbons

Jyoti Rajput[1], Pooja Kumari[1], Aakash Dixit[1], Jatin Yadav[1] and C. P. Safvan[2]

[1] *Department of Physics and Astrophysics, University of Delhi, Delhi 110007, India*
[2] *Inter-University Accelerator Center, Aruna Asaf Ali Marg, New Delhi 110067, India*

The emission of neutral fragments, an H-atom or H_2 molecule or C_2H_2 molecule, is one of the efficient ways in which ionized linear hydrocarbon molecules dissipate their excess energy [1,2]. In our recent experiments, we investigated the fragmentation patterns of ionic forms of small hydrocarbons (C_3H_6 and C_4H_6) formed by ion-impact ionization of neutral hydrocarbon molecules. These ion-molecule collision experiments were carried out at the Low Energy Ion Beam Facility (LEIBF) of IUAC, under single-collision conditions. The experimental setup used for the purpose was a "recoil ion momentum spectrometer". Data was collected on the charged fragments produced in the ion-molecule collision process using coincidence time-of-flight technique. Doubly charged hydrocarbon molecules are populated through various ionization processes (direct double ionization, auto-ionizing double capture, and transfer ionization) and several of them subsequently break into singly charged fragments with or without emission of neutral fragments. In our experiments, the start trigger for the data acquisition (DAQ) was taken from the ejected electrons, so we are sensitive to only those processes where an electron gets free during such ion-molecule interaction. The detection of fragment ions in coincidence enables us to reconstruct the dissociation pathways and investigate neutral particle loss preceding Coulomb explosion (CE). In our data, we saw prominent signatures of hydrogen scrambling and neutral particle emissions in these molecular dications. Our study not only enriches our understanding of fragmentation dynamics in small hydrocarbon dications but is likely to be useful for the broad area of astrophysical chemistry. Such small hydrocarbons have been detected in extra-terrestrial environments e.g. in the Taurus molecular cloud (TMC-1) [3,4].

Our key findings show that there is a high tendency of these hydrocarbon dications to emit neutral fragments- mainly H, H_2, and/or -C_2H_2 before undergoing a two-body Coulomb explosion into singly charged fragments. Experimental data suggest that neutral emissions and subsequent hydrogen scrambling lead to a variety of daughter dications, highlighting the complex reorganization of hydrogen atoms within the molecule. Propene molecules and ions are likely to be directly involved in chemical reactions resulting in the formation of larger hydrocarbon molecules in the interstellar medium, or also occur as intermediates in astrophysical chemistry. 1,3-Butadiene is a key precursor to aromatic compounds may undergo extensive neutral emission and hydrogen scrambling under the extreme conditions. From the smaller propene molecule, significant neutral particle emission has been recorded. This could influence the hydrogen abundances and the chemical evolution of interstellar clouds where the presence of such hydrocarbons is relatively high. The intense dehydrogenation pathways and multiple rearrangements suggest a rich, complex chemistry for unsaturated hydrocarbons exposed to ionizing radiation. The analysis of the acquired data is underway and few publications are likely to come in near future.

References:

1. J. Rajput *et al.*, *J. Chem. Phys.* **159**, 184303 (2023).
2. S. Oghbaie *et al.*, *J. Chem. Phys.* **143**, 114309 (2015).
3. I. R. Cooke *et al.*, *Astrophys. J.* **948**, 133 (2023).
4. N. Marcelino *et al.*, *Astrophys. J.* **665**, L127 (2007).